MOUNTAIN-PLAINS CONSORTIUM

MPC 19-403 | Z. Lin, H. Pan, X. Wang and M. Li

Improved Element-Level Bridge Inspection Criteria for Better Bridge Management and Preservation

MOUNTAIN-PLAINS CONSORTIUM REGION 8

A University Transportation Center sponsored by the U.S. Department of Transportation serving the Mountain-Plains Region. Consortium members:

Colorado State University
North Dakota State University
South Dakota State University
University of Colorado Denver
University of Denver
University of Utah
Utah State University
University of Wyoming

Improved Element-Level Bridge Inspection Criteria for Better Bridge Management and Preservation

Dr. Zhibin Lin, Associate Professor
Hong Pan, Postdoc
Xingyu Wang, PhD student
Mingli Li, PhD student

Department of Civil and Environmental Engineering
North Dakota State University

December 2019

Acknowledgements

The authors gratefully acknowledge the financial support provided by North Dakota State University and the Mountain-Plains Consortium, a University Transportation Center funded by the U.S. Department of Transportation. The authors also acknowledge the support from Director Dr. Denver Tolliver, Dr. Kimberly Vachal, and the other staff at the Transportation Center, and the support from the Department of Civil and Environmental Engineering, North Dakota State University. The authors appreciated contributions from Dr. Lin's group members, including Fei Yan, Muhammad Metla, Mohsen Azimi, Qusay Al-Kaseasbeh, and Matthew Pearson.

ABSTRACT

Bridge inspection data is an essential step in the bridge asset management operation and the bridge management system. As such, a reliability-based, holistic framework was proposed to effectively collect reliable data and perform data fusion and information fusion of sensory data used for element-level inspection and conditional assessment. A comprehensive literature review was conducted to better understand the current state of the research of and practice in the bridge element inspection.

To overcome the limitations of the visual inspection used in the routine bridge inspections, an unmanned aerial vehicle (UAV) was used to supplement the traditional visual inspection data by providing high quality, real-time, reliable data. Moreover, effective data fusion and information process methods were proposed to enhance the features extraction for sensor data for in-depth/special/damage inspections. This study explored the new data fusion methods based on three representative feature extraction techniques, while the kernel function-based support vector machine (SVM) was used to facilitate pattern recognition and improve identification. The effectiveness of these methods was verified even in conditions with high levels of noise interference.

In addition, this study attempted to unveil and reduce the structural uncertainty experienced in in-depth/special/damage inspection. The DBBN was herein used to extract statistical representation from vast amount of structural data, for probabilistically determining structural condition and health state for decision making.

TABLE OF CONTENTS

LIST OF FIGURES

LIST OF TABLES

EXECUTIVE SUMMARY

The reliability-based holistic framework was proposed to effectively collect reliable data and perform data fusion and information fusion of sensory data used for element-level inspection and conditional assessment.

A comprehensive literature review revealed that the quality bridge element inspection data and consistency of bridge element inspection were related to critical factors, including structural importance factor, material vulnerability, aging effects, and others. The study demonstrated that we could consider different condition rating by integrating these critical factors in the element-level inspection.

To overcome some challenges associated with different weather and environmental conditions, the use of UAV as enhanced visual inspection dramatically impact data collection to avoid subjective judgement or reaching those inaccessible locations.

Moreover, three representative feature extraction techniques were explored to provide effective data fusion and information process for in-depth/special/damage inspections. Results confirmed that these data-driven techniques exhibited high accuracy to allow distinguishing between undamaged and damaged cases, even when there are certain noise interferences as well as operational conditions. Moreover, the data-driven classification methods in this study could effectively address the major factors of interest, including effects of damage level, damage location, sensor location, and moving load.

Furthermore, this study proposed the new deep learning methods for the enhanced structural condition assessment for better decision making in in-depth/special/damage inspection for structures with uncertainties. The new deep Bayesian belief network (DBBN) was highly accurate for structural diagnostics, but it can be further improved by tailoring the layers and their architecture to account for higher-order and highly non-linear statistical structural information, as experienced by a complex structure under high uncertainties and variability of interest. As such, timely information of bridge conditions obtained during the inspection will be used for determining needed maintenance and repairs, for prioritizing rehabilitations and replacements, for allocating resources, and for evaluating and improving the design of new bridges.

1. INTRODUCTION

1.1 Background

The over 600,000 bridges in the United States are a critical component of the transportation network for both economic and societal needs. Assessing bridge conditions and timely maintenance are critical for ensuring bridge health, as well as for enabling cost-effective decision making for preservation activities. Successful bridge-inspection programs nationwide are an important element of assessing bridge conditions and ultimately extending the service life of bridges.

Bridge owners nationwide recognize the benefits of detailed condition assessments using raw inspection information, expanded performance measures, and bridge management system deterioration forecasting and evaluation, which are covered in the 2013 new American Association of State Highway and Transportation Officials (AASHTO) Manual for Bridge Element Inspection.

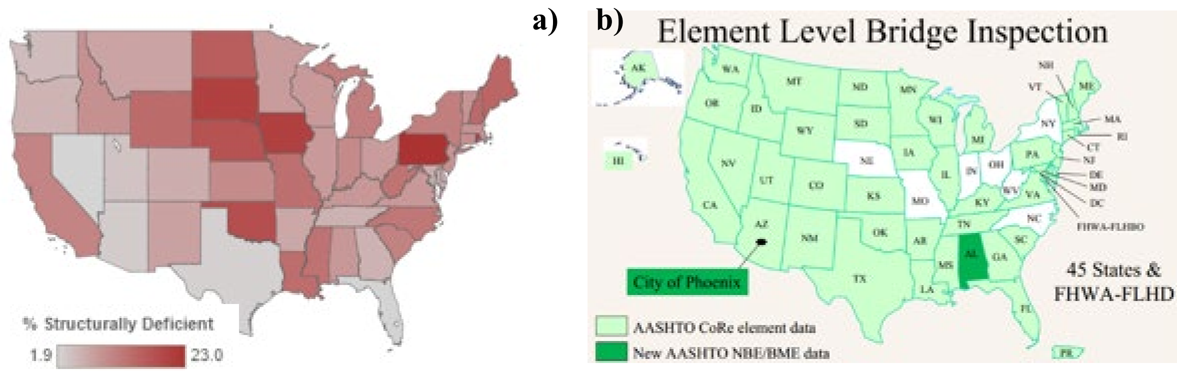

Figure 1.1 Maps of a) bridge condition ratings (after 2013 U.S. Federal Highway Administration (FHWA), National Bridge Inventory) and b) implementation of element-level bridge inspection in the United States (after O'Donnell, 2013)

The current bridge condition rating system in the United States, illustrated in Figure 1.1a, is based on the National Bridge Inventory (NBI) data for national highway bridges (2013). Historically, bridge owners and stakeholders have assessed bridge conditions and made decision based upon the NBI data. As clearly illustrated in Figure 1.1b, the vast majority of states have employed element-level inspections for more than a decade based on the Commonly Recognized Structural Elements (CoRe) guide. The new 2013 American Association of State Highway and Transportation Officials (AASHTO) manual define frequency of inspections, element definitions, qualifications of inspection personnel, defeat descriptions, and inspection reporting, more detailed information as compared to initial CoRe guide. Accordingly, different states provide more complementary information to help region engineers to capture information. Such differences may cause inconsistencies in data collection. Ultimately, this will affect the quality of the element-level data that are reported to the National Bridge Inventory (NBI) by the different states. In addition, as newer bridge types become more common, the demand for a new set of guidelines for inspection ratings is needed to improve the uniformity and consistency of inspections.

To improve the bridge management system, it is necessary to establish a consistent scale for assessing bridge element conditions, which in turn will help establish accurate levels for evaluating bridges and for forecasting bridge deterioration. In order to do this, several challenges must be addressed scientifically and systematically. It is essential that the application of high-quality, element-level bridge inspections are done nationwide using more comprehensive, reliable, and accurate levels for element conditions and defect types than those that are currently being used. Although the 2013 AASHTO element-level inspection manual for data collection provides the criteria for the bridge element condition rating and for the bridge defect descriptions, they are done without reliability-based calibration. The reliability-based calibrations adjust for factors that may affect the quality and consistency of data collection which can lead to high variability. Thus, reliability-based indices that account for the correlation between the levels of element conditions and critical factors (i.e. environmental, inspector qualification, structural importance, material vulnerability, defect type/location, and bridge age) are necessary. Finally, although existing manuals introduce material distress for condition rating, they overlook bridge element conditions that contribute to bridge performance and may indicate the probability of the risk of failure and actual failure of the bridge. Consequently, the guidelines set forth by these manuals cannot guarantee the desired performance of the bridge; therefore, new guidelines should be established that address these concerns.

To meet the requirements of the "Moving Ahead for Progress in the 21st Century Act (MAP-21)" legislation and to ensure the safety of the motoring public, a methodology to improve the quality of the element-level bridge inspection data and enhanced bridge management for assisting bridge inspectors and bridge owners is needed. Significant effort from practicing engineers, bridge inspectors, and inspection trainers, as well as local and state DOT bridge owners is required to develop the guidelines which will promote consistency in reliable data collection that will support bridge asset management practices. The proposed research will address these important technical needs by characterizing the quality of element-level data, generating a reliability-based correlation between levels of element conditions and critical factors, and developing new data-driven based guidelines.

1.2 Objectives

Bridge inspection data is an essential step in the bridge asset management operation and the bridge management system. The main objective of this research is to develop a reliability-based, holistic framework that will improve the quality of element-level data collection for better bridge management and bridge preservation. The specific research goals of the project are as follows:

- To identify the key factors that affect the quality and consistency of bridge element inspection and the corresponding bridge asset management
- To explore the enhancement of the visual inspection in routine inspections
- To develop a fusion process for data and information that will allow for an in-depth/special/damage inspections
- To unveil and reduce structural uncertainty in in-depth/special/damage inspections by extracting structural information and then probabilistically determine bridges with uncertain structural conditions.

1.3 Organization of the Report

This report is organized into eight chapters. Chapters 1 and 2 include the introduction and background information about element-level bridge inspections nationwide and worldwide. A review of existing practices and new element-level inspection practices being used for bridge inspection and ratings are also provided in Chapter 2. The reliability-based holistic framework is proposed in Chapter 3. Chapter 4 is focused on understanding the critical factors affecting visual inspections in routine inspections, while Chapter 5 explores the enhancement of visual inspections in routine bridge inspections. Chapter 6 discusses the enhancement of data fusion and information processing in in-depth/special/damage inspections. Chapter 7 unveils the process through which structural uncertainty in in-depth/special/damage inspection can be reduced by extracting structural information, and then probabilistically determining the bridges that have uncertain structural conditions. Conclusions and future work are summarized in Chapter 8.

2. LITERATURE REVIEW

2.1 Background

Bridge inspection data is an essential step in the bridge asset management operation and the bridge management system. Timely information of bridge conditions obtained during inspections are used for determining needed maintenance and repairs, for prioritizing rehabilitations and replacements, for allocating resources, and for evaluating and improving designs for new bridges. The accuracy and consistency of the inspection, documentation, and levels-of-element conditions are vital because they not only impact bridge funding appropriations, but also affects public safety.

To better understand the current state of research and practice in the bridge element inspection practices, the review provided below included national and international published manuals along with articles and reports. It will provide critical information for understanding the current state of element-level inspection knowledge, what the characteristics are of quality, bridge element inspection data, and how various factors affect the quality and consistency of element-level bridge inspections.

2.2 Overview of Element-Level Inspection

2.2.1 Worldwide Specification and Guidelines

Element-level bridge inspection have been widely used as an important protocol for assessing bridge safety and preservation activities, and are currently accepted in bridge inspection manuals in many countries, including the United States, Canada, Europe, Australia, and Japan. An element-level bridge inspection is performed in such a way that a bridge is broken into elements, and then data are collected from measurable quantities and pieces of the elements. The new element-level inspection of bridges provides more specific and quantitative condition levels, as well as a more precise condition assessment of the bridges, thus leading to enhanced bridge safety and timely information for maintenance decision-making. A comparison of the United States and international bridge inspection practices, illustrated in Table 2.1, shows that there are many similar concepts used by the different countries.

Table 2.1 Nationwide and international manuals (after Oshiro et al. 2012; Atkins 2009)

<table>
<tr><th>Name</th><th>Frequency of inspection</th><th>Inspection method</th><th>Element descriptions</th><th>Quantity calculations</th><th>Condition state system</th></tr>
<tr><td>US*</td><td>Every 2 years (2~5 years**)</td><td rowspan="11">Direct visual</td><td rowspan="10">Element level</td><td rowspan="2">Length, area, each (record individual state and total quantity)</td><td>4 levels: 1 to 4 (good, fair, poor, severe)</td></tr>
<tr><td>Canada</td><td>Every 2 years (2~5 years**)</td><td>4 levels: 1 to 4 (excellent, good, fair, poor)</td></tr>
<tr><td>UK</td><td>1 year (6 years**)</td><td rowspan="8">Length, area, each</td><td rowspan="8">5 levels</td></tr>
<tr><td>Denmark</td><td>1 year (5.5 years**)</td></tr>
<tr><td>Finland</td><td>1 year (5 years**)</td></tr>
<tr><td>France</td><td>1 year (3~9 years**)</td></tr>
<tr><td>Sweden</td><td>1 year (10 years**)</td></tr>
<tr><td>German</td><td>3 years (6 years**)</td></tr>
<tr><td>Norway</td><td>1 year (5 years**)</td></tr>
<tr><td>Australia</td><td>half year (2 years**)</td></tr>
<tr><td>Japan</td><td>Every 5 years</td><td>Unit level</td><td>Length, area, each (record individual state only)</td><td>5 levels</td></tr>
</table>

*: AASHTO Manual for Bridge Element Inspection (2013)
**: detailed visual/instrumented inspection

In general, element descriptions are built upon each element from a bridge and quantified by measurable quantities and pieces of the elements. Japan, however, uses a more detailed unit level by dividing each element into additional units for element description. As such, the detailed condition and defects location can be identified over time for future repair and maintenance decision making. Most of the countries use direct visual examination the most frequently for routine inspection, yet there was great variance in the frequency of these inspections. The period for direct visual inspections ranged from 6 months in Australia to 3 years in Germany, while the detailed visual/instrumented inspection varied from 2 to 10 years between the different countries. The condition states for all countries for each element were defined at 4 or 5 levels, and these data were collected over time. The major difference from country to country was in the damage type description for condition states. Thus, the quality of data collection is dependent upon the frequency of inspection, defined condition states, and the corresponding treatment actions.

2.2.2 Specification or Guidelines used in United States

The bridge condition rating for the United States is based on the NBI data of national highway bridges (2013). Before using the concept of element-level inspection, Bridge owners and stakeholders used to assess bridge conditions and make decision based on the NBI data, which usually included the four major parts of condition assessment for a bridge: superstructure, substructure, deck, and culverts. The severity of the condition for each component was defined by rating it on a scale from 0-9. Studies have demonstrated that this level of detail was not sufficient enough to identify appropriate specific information, and thus made it hard to use the collected data for maintenance decision-making.

In an effort to improve the quality of the data collected for maintenance decision-making, the element-level inspection method was developed in the 1990s by the FHWA and the Subcommittee on Bridges and Structures (SCOBS). Instead of referring to the four components of bridges as had been done previously, this inspection method breaks the bridge into the CoRe elements. Each of these elements was assessed on a scale of condition states for each element ranging from 1-3 or 1-5. Since its development, this method has demonstrated its advantages over conventional, inspection technologies. Data collected from the element level bridge conditions are reported to the FHWA for the NBI data. The vast majority of the states in the United States use the element-level methods and apply the CoRe elements for the determination of bridge conditions in their manuals; however, some states like California, Texas and Florida have defined some of their own elements (Agency Developed Elements, ADE) to accommodate their needs.

2.2.2.1 AASHTO New Manual (2013)

(a) Bridge elements

The 2013 AASHTP manual lists 11 areas for its element-level inspection, but these are broken down further into subcategories for each element as shown in Table 2.2.

Table 2.2 Bridge element lists (based on Bridge Element-level inspection manual 2013)

Element Listings	Unit	ID
Deck		
ELEMENT		
Reinforced Concrete Deck	Area	12
Prestressed Concrete Deck	Area	13
Steel Deck - Open Grid	Area	28
Steek Deck - Concrete Filled Grid	Area	29
Steel Deck / Orthotropic	Area	31
Timber Deck	Area	31
Top Flange		
ELEMENT		
Prestressed Concrete Top Flange	Area	15
Reinforced Concrete Top Flange	Area	16
Other Slab	Area	65
Railing		
ELEMENT		
Metal Bridge Railing	Length	330
Reinforced Concrete Bridge	Length	331
Timber Bridge Railing	Length	332
Other Bridge Railing	Length	333
Masonry Bridge Railing	Length	334
Girder		
ELEMENT		
Steel Closed Web / Box Girder	Length	102
PC Closed Web/Box Girder	Length	104
RC Closed Web/Box Girder	Length	105
Other Closed Web/Box Girder	Length	106
Steel Open Girder/Beam	Length	107
PC Open Girder/Beam	Length	109
RC Open Girder/Beam	Length	110
Timber Open Girder	Length	111
Wearing & Protective Coating		
ELEMENT		
Wearing Surface	Area	510
Steel Protective Coating	Area	515
Reinforcing Steel Protective	Area	520
Concrete Protective Coating	Area	521

Bearing		
ELEMENT		
Elastomeric Bearing	Each	310
Moveable Bearing	Each	311
Enclosed/Concealed Bearing	Each	312
Fixed Bearing	Each	313
Pivot Beaing	Each	314
Disc Bearing	Each	315
Other Bearing	Each	316
Abutment		
ELEMENT		
Reinforced Concrete Abutment	Length	215
Timber Abutment	Length	216
Masonry Abutment	Length	217
Other Abutment	Length	218
Column		
ELEMENT		
Steel Column	Each	202
Other Column	Each	203
PC Column	Each	204
RC Column	Each	205
Timber Column	Each	206
Pier Cap		
ELEMENT		
Steel	Length	231
PC	Length	233
RC	Length	234
Timber	Length	235
Other	Length	236
Pier Wall		
ELEMENT		
RC	Length	210
Other	Length	211
Timber	Length	212
Masonry	Length	213
Pile Cap/Footing		
ELEMENT		
RC Pile Cap/Footing	Each	220

Depending on the state manuals that are developed, the different elements that are defined could from different sources in an attempt to meet the specific needs for each state. These elements could be categories such as: (a) national bridge elements (NBEs); (b) bridge management elements (BMEs); and (c) agency developed elements (ADEs), including ADE-NBE or ADE-BME, and ADE alone. An example of this method's major elements (e.g., NBEs, BMEs) are listed in Table 2.3.

Table 2.3 Some ADE-NBE and ADE-BME element lists

Element	Unit	I.D.
Parent: **Steel Open Girder/Beam**	Length	107
Children: **Steel Open Girder/Beam, Ends**	Length	**807**
Parent: **Prestressed Concrete Closed Web/Box Girder**	Length	104
Parent: **Prestressed Concrete Open Girder/Beam**	Length	109
Parent: **Prestressed Concrete Deck**	Length	13
Children: **Steel Tension Rods/Post-Tensioned Cables**	Each	**8165**
Parent: **Concrete Reinforcing Steel Protective System**	Area	520
Children: **Coated Reinforcing**	Area	8522
Children: **Stainless Steel Reinforcing**	Area	8523
Children: **Non-Metallic Reinforcing**	Area	8524
Parent: **Wearing Surfaces**	Area	510
Children: **AC Overlay**	Area	8511
Children: **AC Overlay & Membrane**	Area	8512
Children: **Thin Polymer Overlay**	Area	8513
Children: **Concrete Overlay**	Area	8514
Children: **Polyester Concrete Overlay**	Area	8515

As such, the bridge components are, as illustrated in Figure 2.1, labeled based on the I.D. number and quantity (length, or area, or each) to better classify potential degradation/damage/defects experienced in the element in detail for bridge management.

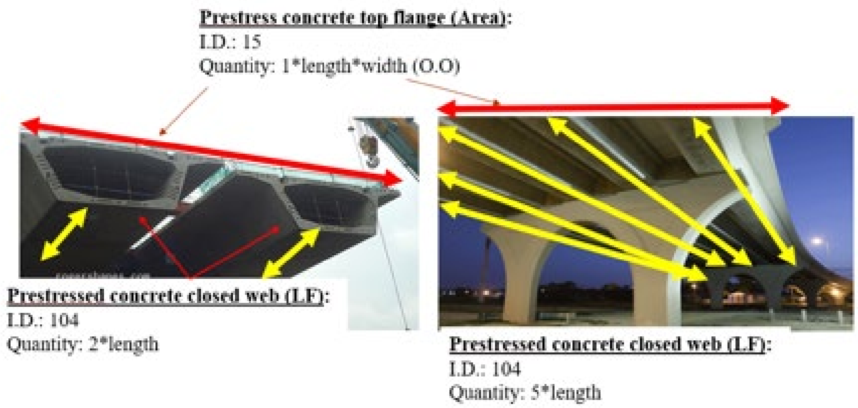

(a) Top flange and girder elements

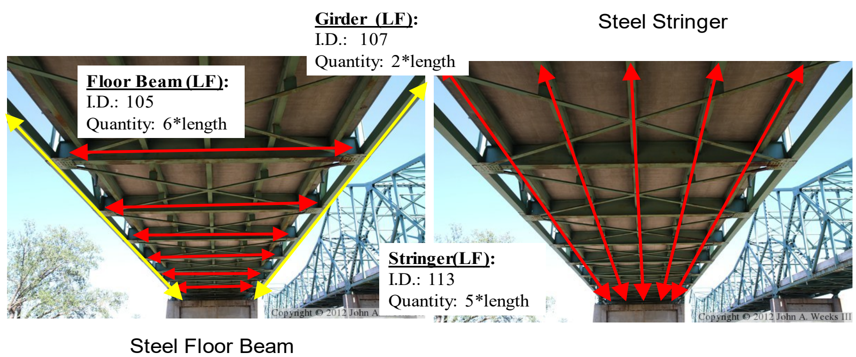

(b) floor beam, stringer, and girder elements

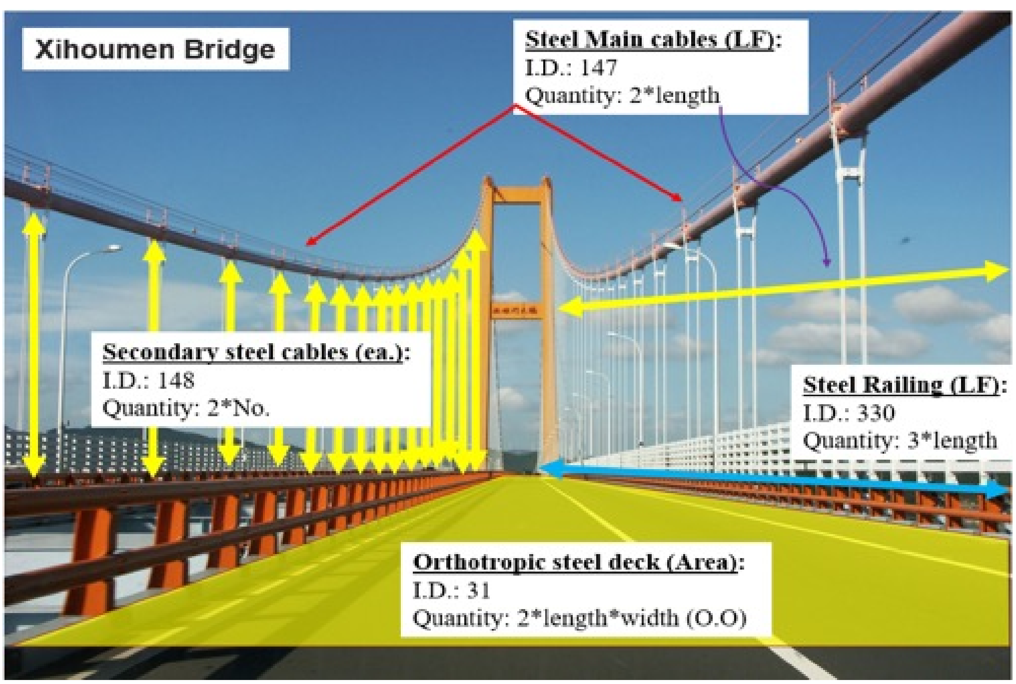

(c) steel deck, steel railing, main and secondary cable element

Figure 2.1 Typical bridge element identification and quantity: (a)-(c)

(b) Element-level condition state rating:

In the new element-level inspection manual, the bridge element is classified into four condition state rating, as shown in Figure 2.2.

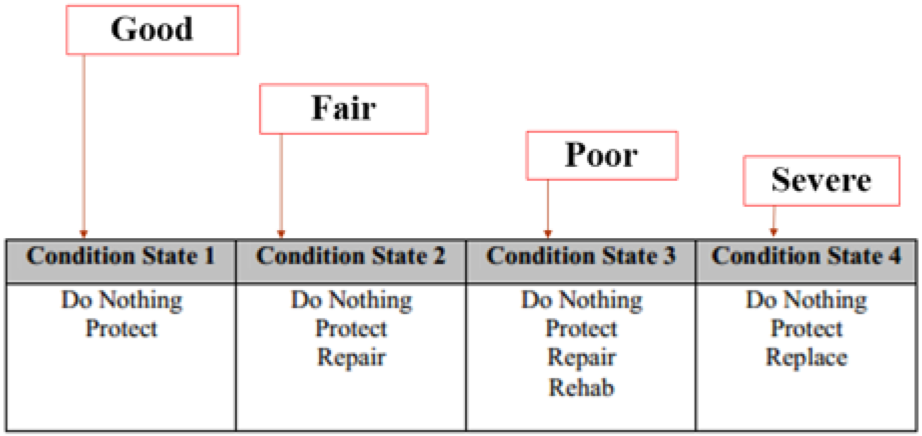

Figure 2.2 Four condition state rating (based on Bridge Element-level inspection manual 2013)

As shown in Figure 2.3 and Tables 2.4-2.10, defect codes are used to identify the defect and the condition state assignment.

Defect	CS 1 Good	CS 2 Fair	CS 3 Poor	CS 4 Severe
Delaminations/ Spalls/Patch Areas (1080)	None	Delaminated. Spall 1 in. or less deep or less than 6 in. diameter. Patched area that is sound.	Spall greater than 1 in. deep or greater than 6 in. diameter. Patched area that is unsound or showing distress. Does not warrant structural review.	The condition warrants a structural review to determine the effect on strength or serviceability of the element or bridge; OR a structural review has been completed and the defects impact strength or serviceability of the element or bridge.
Exposed Rebar (1090)	None	Present without measurable section loss.	Present with measureable section loss, but does not warrant structural review.	
Cracking (RC) (1130)	No cracks. Hairline cracks not requiring sealing, or cracks that have been sealed.	Unsealed cracks of narrow width, or unsealed minor to moderate pattern/map cracking. Where efflorescence is present, it's minor with no evidence of rust staining.	Unsealed cracks of medium to wide width, or extensive pattern map cracking. Where efflorescence is present, there is heavy build-up and/or rust staining.	
Abrasion/Wear (PSC/RC) (1190)	No abrasion	Abrasion has exposed coarse aggregate but the aggregate remains secure in the concrete.	Coarse aggregate is loose or has popped out of the concrete matrix due to abrasion.	
Chloride Concentration (8905)	Chloride concentration at level of rebar tested below the threshold for potential active corrosion.	Chloride concentration at level of rebar tested equal to or greater than the threshold for potential active steel corrosion. No visual signs of active corrosion exist.	Chloride concentration at level of rebar tested greater than the threshold for potential active steel corrosion. Testing methods (such as half-cell potential) have been used and have verified active steel corrosion.	Not used for this defect. Other reinforced or prestressed concrete defects control the Condition State over chloride concentrations (elevated levels of chloride concentrations may be cause of controlling defects).
Precast Concrete Connections (8906)	None	Minor cracking at the joints. Connection is functioning as intended.	Cracking and/or spalling at the joints. No displacement is evident.	Connection is failing or has failed. Condition warrants structural analysis.

Figure 2.3 RC condition state rating (Bridge Element-level inspection manual 2013)

Table 2.4 Defect I.D. and condition state for reinforced concrete

I.D.	Defeat	CS1	CS2	CS3	CS4
1080	Delamination / Spall / Patched Area				
1090	Exposed Rebar				
1120	Efflorescence / Rust Staining				
1130	Cracking (RC)				
1190	Abrasion / Wear (PSC/RC)				
1900	Distortion				
4000	Settlement				
6000	Scour				
7000	Damage				

Table 2.5 Defect I.D. and condition state for steel

I.D.	Defeat	CS1	CS2	CS3	CS4
1000	Corrosion				
1010	Cracking				
1020	Connection				
1900	Distortion				
4000	Settlement				
6000	Scour				
7000	Damage				

Table 2.6 Defect I.D. and condition state for prestressed concrete

I.D.	Defeat	CS1	CS2	CS3	CS4
1080	Delamination / Spall / Patched Area				
1090	Exposed Rebar				
1110	Exposed Prestressing				
1120	Efflorescence / Rust Staining				
1130	Cracking (PSC)				
1190	Abrasion / Wear (PSC/RC)				
1900	Distortion				
4000	Settlement				
6000	Scour				
7000	Damage				

Table 2.7 Defect I.D. and condition state for timber

I.D.	Defeat	CS1	CS2	CS3	CS4
1020	Connection				
1140	Decay/Section Loss				
1150	Check/Shake				
1160	Crack				
1170	Split/Delamination				
1180	Abrasion / Wear				
1900	Distortion				
4000	Settlement				
6000	Scour				
7000	Damage				

Table 2.8 Defect I.D. and condition state for masonry

I.D.	Defeat	CS1	CS2	CS3	CS4
1080	Delamination				
1120	Efflorescence / Rust Staining				
1610	Mortar Breakdown				
1160	Crack				
1620	Split/Spall				
1630	Patched Area				
1640	Masonry Displacement				
1900	Distortion				
4000	Settlement				
6000	Scour				
7000	Damage				

Table 2.9 Defect I.D. and condition state for bearings

I.D.	Defeat	CS1	CS2	CS3	CS4
1000	Corrosion				
1020	Connection				
2210	Movement				
2220	Alignment				
2230	Mortar Breakdown				
7000	Damage				

Table 2.10 Defect I.D. and condition state for joints

I.D.	Defeat	CS1	CS2	CS3	CS4
1000	Corrosion				
1020	Connection				
2310	Seal Adhesion				
2330	Seal Damage				
2340	Debris Impaction				
2360	Adjacent Deck or Header				
2370	Metal Deterioration or Damage				
7000	Damage				

Thus, the bridge component is labeled by element I.D. and quantity along with a detailed defect code, as shown in the example in Figure 2.4.

Element/ Str. Unit #	Env	Element/ Str. Unit Description	Total Qty	Units	Condition State Quantity			
					CS 1	CS 2	CS 3	CS 4
1		Span(s) - All						
DECK/SLAB								
12	3	RC Deck	8663	sq. ft.	8114	543	6	
1080		Delamination / Spall / Patched Area	39	sq. ft.		33	6	
1130		Cracking	510	sq. ft.		510		
16	3	RC Top Flange	7877	sq. ft.	7697	96	84	
1080		Delamination / Spall / Patched Area	114	sq. ft.		40	74	
1120		Efflorescence / Rust Staining	66	sq. ft.		56	10	

Figre 2.4 Typical bridge element classification and quantity (after Bridge Element-level inspection manual 2013)

2.2.2.2 Manuals Used in Various States

Critical information about the implementation of element-level inspection methods in several representative states is summarized in Table 2.11. California is a key proponent of collecting element-level bridge inspection data and has put forth great effort in helping to develop the AASHTO inspection manual. Their state element-level bridge inspection manual (2008) covers a relatively comprehensive set of Commonly Recognized Elements (CoRe) and California-specific elements to handle seismic-related elements. In particular, the detailed description of damage types with illustrations are valuable demonstrations for later AASHTO manuals. Florida, which has been inspecting bridges since 1998 with the CoRe elements for bridge inspections, and Texas are other key states that have put great effort into helping to develop the updated inspection manual. Similar to California, these states have specific elements that must be handled for inspection needs, such as movable bridges, high-mast light poles, overhead sign structures, and traffic-signal mast arms. As shown in Table 2.2, Florida and Ohio have updated the newest version of their inspection manual in accordance with the new 2013 AASHTO manual. Several states, such as Minnesota, South Dakota, and North Dakota, are updating the transition and training for inspectors that perform inspections using the new manual.

Table 2.2 Major contents in practices and guidelines in existing national manuals

Name	Element descriptions	Quantity calculations	Condition rating	Reporting process of data to FHWA
FHWA	Components: superstructure, substructure, deck and culverts	-	9 to 1 (excellent, very good, …failed)	-
AASHTO (CoRe)	CoRe elements	-	1 to 3, 1 to 4, or 1 to 5 (good, fair...)	-
AASHTO (2013)	NBE, BME, ADE	-	1 to 4 (good, fair..)	-
California (2008)	CoRe elements ADE	Length, area, each (record individual state and total quantity)	1 to 3, 1 to 4, or 1 to 5	a) NBI data (transition rating) b) Element-level data* (data from NBE, BME, NBE-ADE, BME-ADE)
Florida (2014)	NBE, BME, ADE		1 to 4	
Texas (2001)	CoRe elements ADE		1 to 3, 1 to 4, or 1 to 5	
Ohio (2014)	NBE, BME, ADE		1 to 4 (summary 9-0)	
Minnesota (2013)	CoRe elements		1 to 3, 1 to 4, or 1 to 5	
South Dakota (2008)	CoRe elements		1 to 3, 1 to 4, or 1 to 5	
North Dakota (2013)	CoRe elements		1 to 4 (summary is 9-0)	

*: FHWA will collect data starting April 1, 2015 and year thereafter

2.3 Overview of Bridge Asset Management

2.3.1 Overview of Inspection Data for Bridge Asset Management

With collected data in place, the goal of bridge asset management is to develop an understanding of what set of performance measures can serve good asset management, and to establish a format for clearly communicating bridge performance information to management. The various types of performance measures can be categorized into the following categories: a) Safety, including load rating, load carrying capacity, reliability index, condition rating, sufficiency rating, appraisal rating, and health index; b)

Serviceability, including condition rating, excessive stressing, cracking, deformation, and vibration; c) Fatigue; and d) Functionality, including condition rating, sufficiency rating, bridge width, and vertical/horizontal clearances. As illustrated in Table 2.3, states and federal agencies sometimes use different performance indices to identify critical information for bridge asset management.

Table 2.3 Bridge asset management and performance index

Name	Condition rating	Performance index
FHWA	9 to 0 (excellent, very good, …failed)	• Appraisal ratings • Sufficiency rating • SD/FO classification*
AASHTO (CoRe)	1 to 3, 1 to 4, or 1 to 5 (good, fair...)	• Appraisal ratings • Sufficiency rating • SD/FO classification • Health Index (CalTrans)
AASHTO (2013)	1 to 4 (good, fair..)	• Appraisal ratings • Sufficiency rating • SD/FO classification
California (2008)	1 to 3, 1 to 4, or 1 to 5	• SD/FO classification • Health Index (CalTrans)
Florida (2014)	1 to 4	• SD/FO classification • Structural condition rating
Texas (2001)	1 to 3, 1 to 4, or 1 to 5	• SD/FO classification • Structural condition rating
Ohio (2014)	1 to 4 (summary 9-0)	• Appraisal ratings
Minnesota (2013)	1 to 3, 1 to 4, or 1 to 5	• Structural condition rating
South Dakota (2008)	1 to 3, 1 to 4, or 1 to 5	• SD/FO classification
North Dakota (2013)	1 to 4 (summary is 9-0)	• SD/FO classification

*: SD/FO- Structural Deficient and Functional Obsolete

2.3.2 Bridge Management Software (BrM)

A typical analytical method for analyzing bridge data is AASHTOWare™ Bridge Management software (BrM), formerly Pontis (AASHTO 1997), which was first developed under the National Cooperative Highway Research Program (NCHRP) as part of a project sponsored by the FHWA in the early 1990's and transferred to AASHTO. The BrM accommodates the new element definitions and also has the capability to handle subsets and agency-developed elements. It utilizes element-level inspection data to predict the future condition of the elements in the network assuming homogeneous Markov chains (Markovian deterioration models) and optimizes long-term expenditures for the preservation and the improvement of the highway bridge network. The BrM is widely used as the primary bridge management software by transportation agencies across the United States.

2.4 Survey of Bridge Owners, infrastructural inspectors, and related field engineers

To further quantify the current state of research and practices in bridge element inspection and other similar counterpart monitoring practices, Dr. Lin and his group conducted a 10-question survey of bridge/pipeline/tunnel owners and other stakeholders. The team collected 24 surveys from different agencies, including Department of Transportation (DOT) engineers, monitoring and assessment companies, fabricators and designers, other related large-scale structural engineers, and academics It was anticipated that the critical information gathered from this survey would lead to a deeper understanding of the potential factors that may affect the quality and consistency of data collection, such as element types, frequency of inspection, inspection methods, qualification of inspectors, inspector training, and methods used for bridge asset management.

The result of Q. 1 is shown in Figure 2.5. Clearly, there is a great deal of variations amongst the different survey respondents, but ultrasonic sensors were the preferred tool for monitoring structural health, with over 18 respondents (75% of total responses) choosing it. The optical sensor was the second leading system, with over 54% of users selecting it.

1) What are the preferable structural health monitoring tools you would like to use for large-scale structural inspection (such as bridges, pipelines, tunnels)?

- [ ] Ultrasonic
- [ ] Magnetic
- [ ] Optical sensor
- [ ] Long-distance guided wave
- [ ] Smart pig (pipeline applications)
- [ ] Ground penetration radar
- [ ] Destructive sampling and tests
- [ ] Other (please specify)

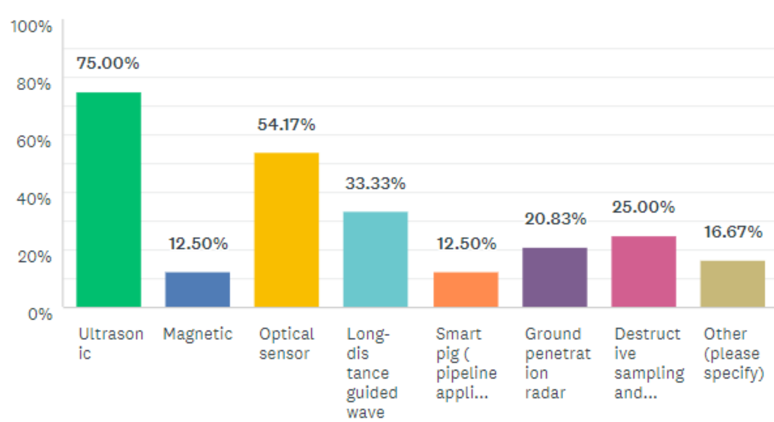

Figure 2.5 Distribution of respondents to Q #1

The results of Q. 2 are shown in Figure 2.6. Over 50% of respondents indicated that they expect a long-lasting life with the monitoring systems they choose for assessing structures.

2) What is the expected service life when you choose or design a health monitoring tools/systems for bridges, pipelines, tunnels?

- 1-5 years
- 5-10 years
- more than 10 years
- Other (please specify)

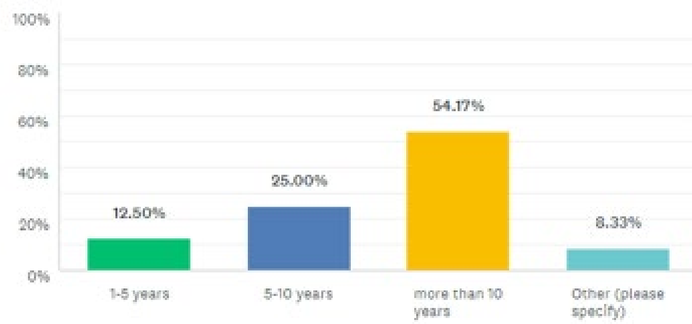

Figure 2.6 Distribution of respondents to Q #2

The results from Q.3 are shown in Figure 2.7. Although 37% of total respondents accepted the current monitoring systems, a relatively significant number (21%) showed their dissatisfaction with the current market. This demonstrates that there is a potential to improve the current practices and technologies.

3) Could the current structural health monitoring tools meet your expected service life requirement?

- Very satisfied
- Satisfied
- Neither satisfied nor dissatisfied
- Other (please specify)
- Dissatisfied
- Very dissatisfied

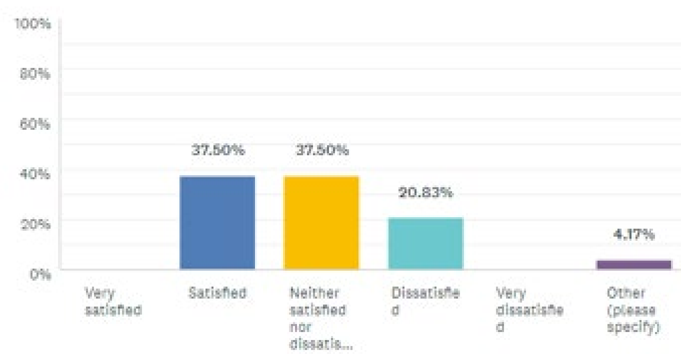

Figure 2.7 Distribution of respondents to Q #3

The results for Q. 4 are shown in Figure 2.8. Clearly, respondents agree that the four factors (durability, ease in operation, ease in data process and low cost) are important for the monitoring tools and applications. The durability of the monitoring system is the most essential, which confirms the findings in Q. #2.

4) What are the important properties when you select new structural health monitoring tools?

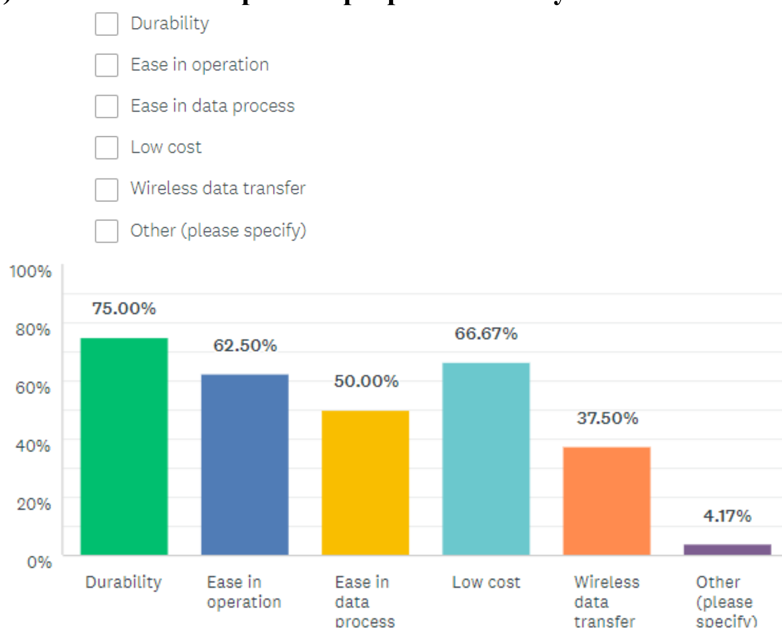

Figure 2.8 Distribution of respondents to Q #4

The results of Q. 5 are shown in Figure 2.9. Most respondents consider "ease of operation" a top priority, but not the most important, when they choose a new structural health monitoring tool, with only slightly more than 30% of respondents identifying it as the most important priority.

5) How do you rate the following properties when you choose a new structural health monitoring tools used in large-scale structures, such as bridges, pipelines, tunnels?
- Ease of operation

- ◯ The most important priority
- ◯ A top priority, but not the most important
- ◯ Not very important
- ◯ Not important at all

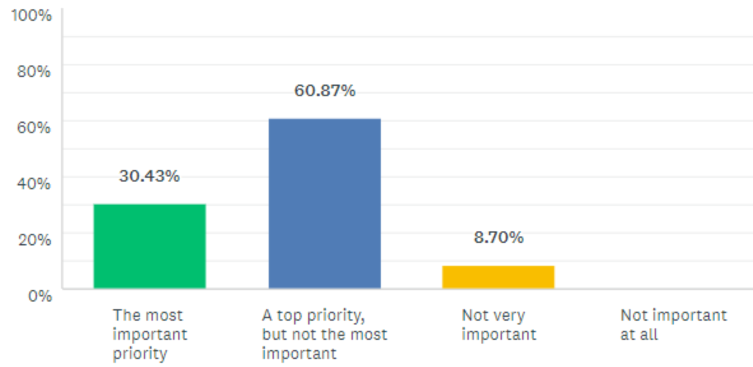

Figure 2.9 Distribution of respondents to Q #5

The results of Q. 6 are shown in Figure 2.10. Over half of respondents selected the feature of "long distance" as the second most important property in choosing a new structural health monitoring.

6) How do you rate the following properties when you choose a new structural health monitoring tools used in large-scale structures, such as bridges, pipelines, tunnels?
- Long distance

- ◯
- ◯ A top priority, but not the most important
- ◯ Not very important
- ◯ Not important at all

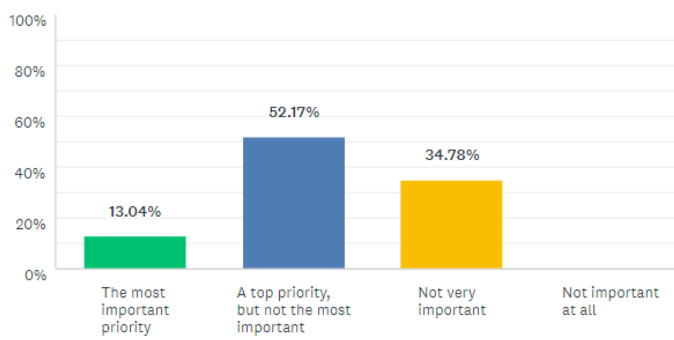

Figure 2.10 Distribution of respondents to Q #6

The results of Q. 7 are shown in Figure 2.11. The outcome indicated that most respondents selected the feature of "durability" as the top priority when choosing a new structural health monitoring tool.

7) **How do you rate the following properties when you choose a new structural health monitoring tool used in large-scale structures, such as bridges, pipelines, tunnels?**

- Durability

- The most important priority
- A top priority, but not the most important
- Not very important
- Not important at all

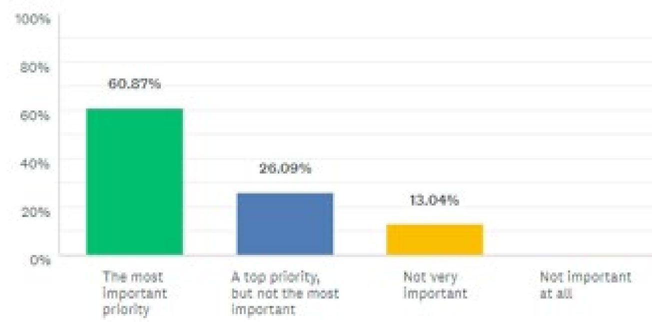

Figure 2.11 Distribution of respondents to Q #7

The results of Q. 8 are shown in Figure 2.12. Although cost is important, most respondents do not think cost should be the top priority when choosing new structural health monitoring tools/systems.

8) **How do you rate the following properties when you choose a new structural health monitoring tool used in large-scale structures, such as bridges, pipelines, tunnels?**

- Low cost

- The most important priority
- A top priority, but not the most important
- Not very important
- Not important at all

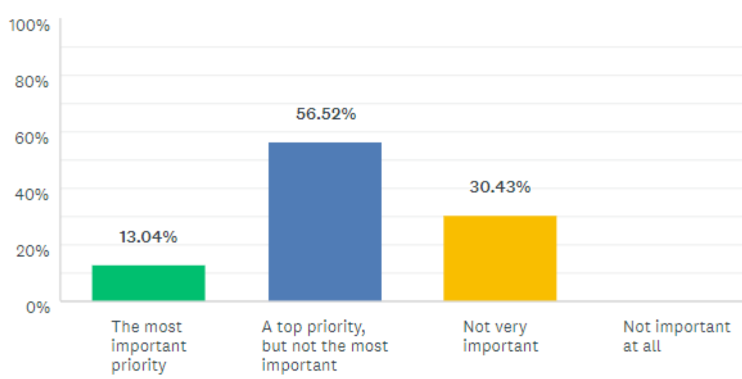

Figre 2.12 Distribution of respondents to Q #8

The results of Q. 9 are shown in Figure 2.13. There is no uniform standard for the inspection interval for most civil structures. Most respondents suggested using a 2-year period as the interval for structural health monitoring, although some selected 5 years or longer.

9) What's the inspection interval that applied in structures or you would like to suggest?

- ◯ 1 year
- ◯ 2 years
- ◯ 5 years
- ◯ 10 years
- ◯ Other (please specify)

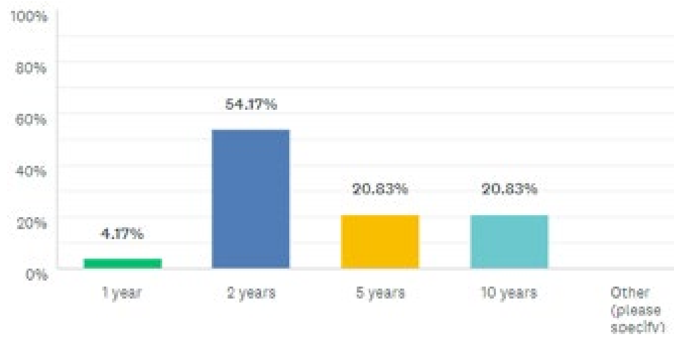

Figure 2.13 Distribution of respondents to Q #9

10) Once corrosion or corrosion-induced damage was detected, what kind of retrofitting method did you use for maintenance and does this change the inspection interval? Please specify:

There was a wide range of responses for these questions; below are a sample selected to demonstrate the variety of comments:

"*Depending on the degree of damage of the corrosion the structural member the member should be repaired or replaced with some form of retrofitting method. If the damage is bad enough then it should be replaced. If it is a reoccurring problem the inspection interval should be shortened for that specific member.* "

"Depends on extent of damage. but inspection interval will be reduced to even a year. Wireless sensor network-based monitoring"

"Would increase inspection frequency until repairs are completed."

"High performance coating can be applied after appropriate surface preparation. Another efficient option is through metalizing with active metals such as zinc, aluminum, and their alloys to produce long-lasting protective coating."

"Replace or coating again. I will change the inspection interval to short time"

"Both changing monitoring methods and revising inspection interval could work"

2.5 Summary

This section provides a brief state-of-art practice of element-level bridge inspection nationwide and worldwide. Clearly, there is no uniform standard for the inspection in bridge community, and a high level of variances exist in the current inspection practice, which pose a great challenge in data collection and data interpretation for decision making.

3. RELIABILITY-BASED HOLISTIC FRAMEWORK: FROM VISUAL INSPECTION TO IN-DEPTH INSPECTION

3.1 Reliability-based Holistic Framework for Element-Level Inspection

Bridge inspection data is an essential step in the bridge asset management operation and the bridge management system. Element-level inspection is categorized as follows: (1) routine inspection, every two years (as shown in Table 2.1); (2) underwater inspection, every five years; (3) in-depth inspection, frequency determined by program manager; and (4) initial/special/damage inspection.

The major methods for element-level inspection (e.g., routine inspection) are based on a visual inspection to examine bridges, record their condition states (rating bridges using the new National Bridge Elements (NBEs), Bridge Management Elements (BMEs), and Agency Defined Elements (NBE-ADEs and BME-ADEs), and documenting their conditions with notes, photos, and sketches.

It would seem that an improvement in the consistency of data collection could be systemically achieved through a reliability-based holistic framework, as shown in Figure 3.1.

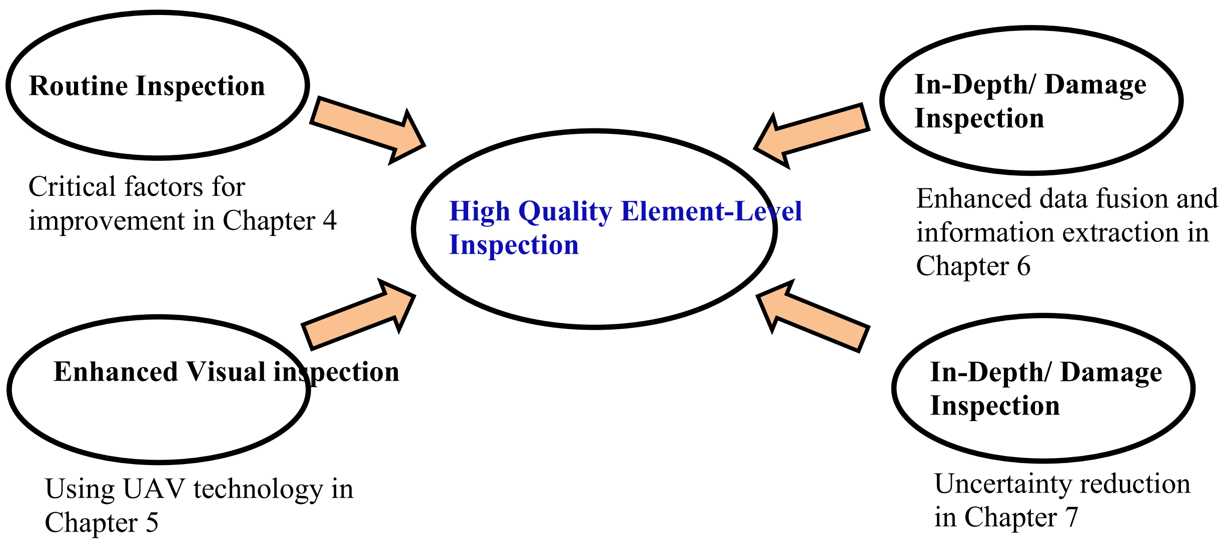

Figure 3.1 Reliability-based holistic framework for element-level inspection

This framework will focus on the following items:

a) Developing a better understanding of the critical factors affecting visual inspections in routine inspections (Chapter 4);
b) Enhancing the visual inspection in routine inspection (Chapter 5);
c) The use of data fusion and information processing in in-depth/special/damage inspection (Chapter 6);
d) The unveiling and reduction of structural uncertainty in in-depth/special/damage inspection by extracting structural information and probabilistically determining conditions with structural uncertainty (Chapter 7).

3.2 Critical Factors Affecting Visual Inspection in Routine Inspection and Improvement

The reliability-based high-quality data, at a minimum, should be as follows:

1) Objective and Repeatable - original data collection should be objective and repeatable in such a way that quality data can be stored and updated over time
2) Comprehensive and Informative - high quality data should be comprehensive and informative in such a way that it can provide enough information to support management decision-making
3) Reliable and Timely - high quality data should be reliable and timely in such a way that it can eliminate deviation and uncertainty, and provide timely management decision making
4) Accurate and Consistent - high quality data should be accurate and consistent in such way that it can help to establish accuracy levels for element conditions and applicable defect quantities to support bridge management system deterioration forecasting and evaluation.

The critical factors affecting data collection and quality of data fusion associated with conditional assessment and rating will be discussed in Chapter 4.

3.3 Enhancement of Reliable Field Data Collection for Visual Inspection in Routine Inspection

Visual inspection has been identified as one of the primary methods used in routine evaluations of bridges when the evaluation is done within a two-year period. Considering the limitation of visual inspection for large-scale bridges under different weather and environmental conditions, more advanced techniques have been utilized to provide complementary data. In recent years, the use of unmanned aerial vehicles (UAV) has emerged as a possible tool for bridge inspection that allows for the collection of reliable data in real time. This could minimize subjective judgements as well as allow for inspections of inaccessible locations. The practice of supplementing current visual inspections with the additional information and opportunities proved by UAVs will be explored in Chapter 5.

3.4 Enhancement of Data Fusion and the Information Process in In-depth/Special/Damage Inspection

Effective data collection and information fusion is critical steps for element-level inspections and conditional assessments. To effectively capture the abnormally dynamic characteristics of long-span bridges while avoiding catastrophic failures, various strategies using sensors have become widely accepted in structural health monitoring (SHM). There are many types of sensor technologies, but using wireless sensor networks to detect potential damages and facilitate SHM, as well as include the favorable features of wireless data transmission, high reliability, and ease of operation, can overcome the limitations of the traditional power-wire based sensor systems (Ge et al. 2016; Herrasti et al. 2016; Huang et al. 2015; Pan et al. 2016; Watters et al. 2002; Worden et al. 2007). Particularly, the integration of the wireless sensor networks with unmanned aerial systems (UAS) technology has demonstrated great potential for the SHM of large-scale, civil infrastructures (Ge et al. 2016; Pan et al. 2016, 2017, 2018a, 2018b, 2018c).

Use of these advanced sensor technologies enable engineers to capture large amounts of data, which in turn has led to the need to develop an effective means for analyzing and utilizing the data. Much research has been conducted on a physics-based approach to data analysis for structural condition diagnostics and damage detection (Salawu 1997; Doebling et al. 1998; Chinchalkar 2001; Yang et al. 2004; Lee 2009; Wang and Chen 2013; Lin et al. 2014; Pavlopoulou et al. 2016). These methods use captured sensor data to calibrate/interpret physics-based vibratory characteristics of structural systems including natural frequency, mode, and curvature (Salawu 1997; Chinchalkar 2001; Lee 2009; Fahim et al. 2013). Although these physics-based analytical models and simulation techniques are now well-established, rapidly and accurately interpreting large amount of data, along with pattern recognition still lag behind (Zou et al. 2000; Magalhães et al. 2012; Kopsaftopoulos and Fassois 2013; Masciotta et al. 2014; Comanducci et al. 2016). This is a particularly big challenge when the cable-stayed bridges are under complex operational or environmental interferences because the physics-based techniques may be incapable of recognizing and detecting abnormalities.

Alternatively, another type of data analysis employs a data-driven approaches. One example of this is the machine learning techniques that have focused attention on mining data for large-scale, civil infrastructure applications (Hou et al. 2000; Farrar and Worden 2013; Ko and Ni 2005; Rashedi and Hegazy 2015; Gerist and Maheri 2016; Jang 2016; Gui et al. 2017; Pan et al. 2017, 2018a). The data-driven approaches tend to extract sensitive features from large data sets, which are then used for structural diagnosis and damage detection, regardless of the complexity of the physical systems. This technique is so robust that it can extract the necessary key information from the complex and heterogeneous sensor data, which may not be appropriate for physics-based approach.

Proper selection of feature extraction methods is the key to ensuring the effectiveness of the data process in machine learning. The signal for the time-frequency feature extraction is within a short time domain. Although many time-frequency methods are available, these methods all have similar limitation in the short-time domain. Thus, it may be very time-consuming and unrealistic to run the analysis over an extended period of time. For a longer time frame, sampling using certain time intervals could overcome this drawback, and thus machine learning could fully capture statistical features under certain time intervals. Within the time interval, the time-frequency analysis could be conducted. As a result, statistical properties of a longer time signal could be captured, which could effectively avoid the use of averaging or using subjective criteria. This type of framework allows for more flexibility in choosing the criteria for the selection of the feature extraction methods. For instance, the wavelet transform has less sensitivity to noise, while the Hilbert-Huang transform and Teager-Huang transform are more sensitivity to damage. Thus, fusion of these methods for the structural diagnosis of large-scale, cable-stayed bridges could enrich the categories of feature extractions in a data-driven data process, which in turn, opens a new door for the development of data-driven approaches that may have widespread applications for large-scale, civil engineering structures.

Some pioneering studies have been undertaken in utilizing the data-driven technique for structural diagnosis and damage detection in structures, including using Bayesian networks (Masri et al. 2000), artificial neural networks (Zang and Imregun 2001) and support vector machines (SVM) (Oh and Sohn 2009; Farrar and Worden 2013; Gui et al. 2017). Note that the accuracy of these data-driven methods for structural diagnosis is associated with the proper selection of feature data. From a systematical standpoint, few attempts have been made to apply data-driven structural diagnosis and damage detection to cable-stayed bridges in terms of the applicability of feature extraction techniques and data training. As a result, findings from these previous studies may not fully account for the data processes under various scenarios in a cable-stayed bridge. Another positive aspect of employing the data-driven approach to bridge inspection is that it may also expand the functionality of the physics-based conventional methods that are defined in time-frequency series (e.g., Wavelet or short-time Fourier transforms) to be more robust and adaptive tools for feature extraction (Bin et al. 2012). In addition, other time-frequency techniques, including the Hilbert-Huang transform (Yang et al. 2004; Hsu et al. 2013) and the Teager-Huang transform (Li et al. 2010), have been proposed for the data collection process in aerospace and mechanical engineering (Kim and Melhem 2004).

Chapter 6 aims to develop a framework to assist in data fusion and the information gathering process for sensory data commonly used in the current, detailed, in-depth/special/damage inspection to improve element-level inspection, rapid condition assessment, and bridge management for large-scale bridges.

3.5 Unveiling of and Reduction of Structural Uncertainty in In-depth/Special/Damage Inspection

Structural systems are often exposed to harsh environments, and these environmental factors in turn may degrade the system over time. The structural system's health state and condition are key for structural safety control and decision-making management. Although great efforts have been made in this field to improve the processes and the tools used to assess these systems, the high level of variability due to noise and other interferences, as well as the uncertainties associated with data collection, structural performance, and in-service operational environments, pose great challenges in collecting and analyzing the proper information to assist in decision making. In recent years, the machine learning techniques have gained increased attention due to their merits for capturing information from a statistical representation of events; thus, enabling more appropriate decision making.

Chapter 7 explores the deep learning, Bayesian belief network system (DBBN) with the purpose of identifying the necessary classifiers for extracting structural information and probabilistically determining structural conditions. Different from conventional, shallow learning systems that rely heavily on the quality of hand-crafted features, deep learning is an end-to-end method that encodes information and interprets vast amount of data with minimal or no features. A case study was conducted to address the methods for structure under viabilities and uncertainties due to operation, damage and noise interferences.

3.6 Summary

In the following chapters, detailed work, from visual inspection and improvement, to in-depth inspection using data fusion of sensory data and uncertainty classification and reduction, will be systematically investigated and discussed.

4. CRITICAL FACTORS AFFECTING VISUAL INSPECTION IN ROUTINE INSPECTION AND IMPROVEMENT

4.1 Background

As summarized in Chapter 3, quality bridge inspection data should offer the following characteristics: a) objective and repeatable, b) comprehensive and informative, c) reliable and timely, and d) accurate and consistent. This chapter aims to systematically investigate the critical factors that affect the quality and consistency of bridge element inspection within the context of state and national bridge program requirements. These factors include element descriptions, quantity calculations, condition state definitions, inspection protocols, inspector qualifications, and the reporting process for bridge element condition data to the Federal Highway Administration. Thus, this chapter is to elucidate the critical factors affecting the quality of data collection and the condition ratings associated with the new element-level inspection.

4.2 Critical Factors Affecting the Quality of Data Collection

4.2.1 Objective and Repeatable Data Collection

It is clear that three critical factors may lead to subjective data results, which make it difficult to collect data that is repeatable: a) manual language; b) inspector qualification; and c) inspection operation and technologies, which are addressed below.

(a) Manual language. The 2013 AASHTO element-level inspection manual language for data collection includes subjective element descriptions, condition state definitions, and defect descriptions for element-level bridge inspection. The current language used for performance desecription is mainly qualitative and may not ensure identification of the exact performance. Currently, documentation in a field report still relies on a description written by the inspector(s), which can be subjective, although photos or sketchs may help supplement the written reports. In addition to the subjectiveness of each individuals perceptions that are reported, the bride inspection methods themselves are vague, thus making them vulnerable to eliciting very subjective descriptions depending on the qualifications and training of the inspectors. To offset this vagueness, Japan implemented using layouts of the actual bridge components during inspections to provide more visual and accurate descriptions (Oshiro et al. 2012) as shown in Figure 4.1. As such, using a physical layout of the acutal structure being inspected should generate more data that has better quality and more objective comments. In particular, more information, for example, information of age effects (new, existing, or repaired), should be recorded to assist identify the probability of failure and risk of failure with a frame of reliability.

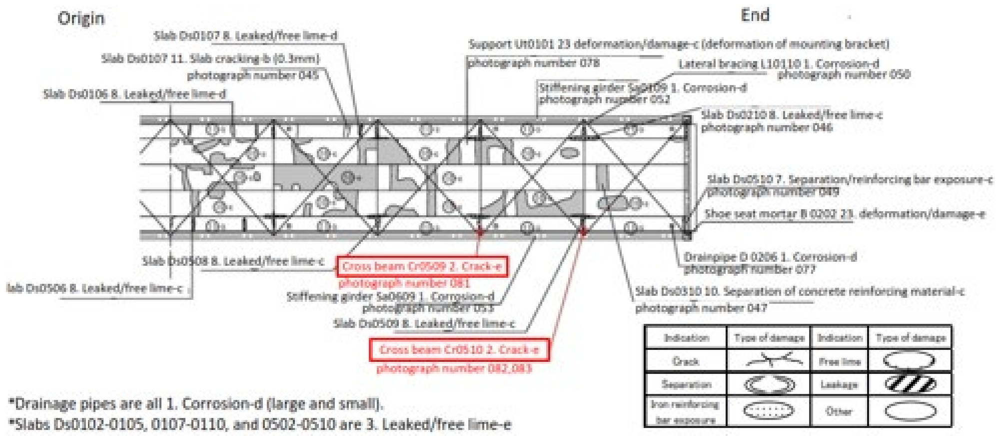

Figure 4.1 Documentation of defects on actual bridge drawing (after Oshiro et al. 2012)

(b) Inspector qualification. Information related to the bridge inspection operation is another factor that may lead to subjective data. Specifically, the number of inspectors used during the field inspection, inspector qualifications (experience, training, and reassessment), and operations often vary during the different inspection activities, thus greatly impacting the quality and consistency of data collection. Atkins (2009) reported on results from a survey that showed that the number of inspectors used in an inspection ranged from 1 to over 25. This impacts the reliability of the data from inspector to inspector since much of the data is considered subjective rather than objective. In addition to the personal lense of an inspector, inspector requirements also differ amongst the different bridge consulting companies and bridge agencies. Most inspectors need a minimum of 6 months of experience, but over 10 percent of inspectors reported having no experience at all. Most training had 3−5 days in classroom, and onsite training ranged from 2 to 12 months. The extreme variation in training completed by the inspectors can affect objective data collection. More importantly, the requirements needed for inspectors to remain up-to-date with new materials, forms of deterioration/attack, and inspection/testing techniques indicated that frequent re-training/reassessing was needed. The challenge in moving to consistency within the industry is that the NBIS requires bridge inspectors to take refresher training, but it does not provide any specific requirements for the inspectors to meet. Instead they leave it up to the states to establish the guidelines. This study showed that over 45 percent of inspectors did not undertake any periodic re-assessment (Atkins 2009). All of these variations in training, minimum experience, and ongoing training requirements may lead to data that has high subjectivity and low reliability; however, no information is available for assessing the impact of training on data quality. Therefore, the inspection qualification (IQ) factor is quantified based on their experience (e.g., training time) in a manner that establishes its effect on the quality of data collection.

(c) Inspection operation and technologies. The final area of critical factors that may lead to subjective data involves inspection methods, tools/technologies used, and inspection procedures. As shown in Table 2.3, direct visual inspection is traditionally accepted for manually identifying structural defects and classifying them into the appropriate condition states. Use of the eye and simple tools can easily lead to subjective results, which makes it difficult for the data to be repeatable, thus making it difficult to validate inspection results. Other difficulties with conventional inspection operations are the use of qualitative instead of quantitative language and high variability in the results obtained when applying the manual requirements to field inspections even with experienced operators.

Recent enhancements in technology are available that should reduce operator variability and lead to better, objective data collection. The application of efficient, non-destructive methods using high-quality, digital images, and infrared, thermography technologies for assessing the health and safety of bridges during routine bridge inspections is important for bridge owners around the world. In addition, new, enhanced, non-destructive technologies are being used in bridge inspection, which should help eliminate the high variability attributed to traditional visual inspections.

4.2.2 Comprehensive and Informative Data Collection

The condition rating a bridge inspector assigns to an element or elements should be comprehensive and informative in such a way that it allows for the determination of the performance of the individual element or the overall bridge. Three critical factors may lead to noncomprehensive results: a) element types and defect types; b) inspector qualification; and c) documentation and reporting. In addition to these critical factors, other factors, such as budget limits or resource constraints, may hinder bridge owners in developing a systematic scheme for generating comprehensive data.

(a) Element types and defect types. The CoRe elements are the most frequently elements used for bridge inspections; however, the AASHTO 2013 elements are also used in a great deal of bridge inspections, and the two systems use highly different element descriptions. Thus, the different element descriptions may cause the number of elements identified and inspected to be inconsistent, which in turn leads to variation in the data collected. In addition, due to subjective defect types and defect descriptions, the defect types may be incorrectly identified in a small number of cases. Due to the inconsistencies between these elements, the variation of condition rating for extent and severity reporting can reach up to 50% (Atkins 2009). Incomprehensive data reporting may overlook some structural deficiency that may lead to relatively more widespread failure. Along with these deficiencies, limited consideration was given in current state manuals or the AASHTO 2013 manual for how to account for interacting defects.

(b) Inspector qualification. It is vital that qualified inspectors identify all structural defects and rate the condition states, thereby reporting comprehsensive and informative data. To address this point, one example that was used in the literuare (Atkins 2009) is presented below.

Case Study: De la Concorde overpass collapse, Laval, Canada. As shown in Figure 4.2, the De la Concorde overpass, a 40-m span reinforced concrete cast-in-place bridge, collapsed in 2006, which resulted in six people injured and five fatalities. The bridge was supposed to have a 70-year lifespan, but it only lasted for slightly more than half of that time - 36 years. Although a majority of the blame was placed on the design, construction, and repair, the investigation revealed that the inspection conducted by engineer Christian Mercier in 2004 was incomplete, and that appropriate inspection practices and competent staff could have provided sufficient information to pre-warn of the collapse (Atkins 2009). This highlights the point stated earlier that noncomprehsenvie data reporting may overlook some structural deficiencies that can lead to relatively more widespread failure.

Figure 4.2 Overpass collapse (after Atkins 2009)

(c) Documentation and reporting. Comprehensive and informative data collection rely on accurate documentation and reporting. Unified document formats and requirements can improve data collection. For example, all quantities in condition levels of CS 3 and CS 4 must be recorded in a format of detailed comments, photos, and sketches for future use (the next inspector to quantify, rate structural degradation over time).

4.2.3 Reliable and Timely Data Collection

An emphasis is placed on following the critical factors that affect reliable and timely data collection: a) uncertainty; and b) inspection operations and technologies.

(a) Uncertainty. Though the AASHTO 2013 manual provides a comprehensive set of elements, defect descriptions, and condition ratings, there is nothing provided that can account for uncertainty in the data collection. For example, there is no information on how the condition rating of an element changes between inspections (improving and degrading) if there are many combined effects, such as environmental factors and different inspector qualifications. Information in condition rating of a element cannot account for uncertainty, and thus cannot identify the probability of failure and risk of failure with a frame of reliability.

(b) Inspection operations and technologies. Reliabilty of traditional visual inspection methods is essential in impactimg the quality data. In a previous study by Moore et al. (2001) on 49 bridges, it was found that eyesight, accessibility, and location affected the reliability of visual inspection, which in turn affect the quality of data collection. Sensitivity analysis will be carried out based on the database in the literature (Moore et al., 2001) to quantify the effects in data collection.

4.2.4 Accurate and Consistent Data Collection

The accuracy and consistency of data collection is investigated by doing the following: a) establishing accuracy levels for element conditions and b) establishing applicable defect descriptions and quantities.

(a) Establishing accuracy levels for element conditions. The AASHTO 2013 manual for data collection provides criteria for element condition ratings and defect descriptions, but these are without reliability-based calibration. The lack of reliability-based calibration is one of the factors that can affect the quality and consistence of data collection, causing high variability. In addition to this, the identification of the structural importance of bridge elements is necessary as well as the different actions that should be undertaken. Some elements require more attention than the others in terms of material vulnerability and/or structural significance (Tee et al. 1988; Melhem and Aturaliya 1996; Abu Dabous and Alkass 2010; Rashidi and Gibson 2012). For example, reinforced concrete over time is more likely to sustain damage than steel. A main girder in girder bridges will require more urgent attention than the bridge drainage outlets. However, the determination of element conditions did not account for these effects. Therefore, reliability-based correlations between levels of element conditions and critical factors (including inspector quality, structural importance factor, defect type/location factor, material vulnerability factor, and environmental factor) are necessary.

(b) Applicable defect descriptions and quantities. Existing manuals introduce material distress for condition rating, while overlook the assessment of bridge element conditions. The current methods cannot account for performance, probability of failure, and risk of failure, and thus cannot guarantee the desirable performance in some cases. New guidelines should be developed to address these concerns.

4.3 Reliability Indices for Identified Critical Factors

The critical factors, including inspector qualification factor (IQ), structural importance factor (SI), material vulnerability factor (MV), defect description and location factor (DDL), age factor (AF), and environmental factor (EF), are categorized and quantified in terms of condition rating with the corresponding performance measures as commentary. To maintain a consistent format as stated in the current manuals, condition ratings range from 1 to 4. Similar to the definition of weight factor at Eqn. (2), the weight factors for each condition are given: CS_1=1, CS_2=0.75, CS_3=0.5 and CS_4=0, which remains the same, unless otherwise noted.

4.3.1 Inspector Qualification Factor (IQ)

As illustrated in Figure 4.3, there are large variations in inspector qualifications, experience, training, and reassessment, as well as the number of inspectors involved in inspections (Atkins 2009). During the consistency study, besides the specific requirements for inspector qualification, an inspector qualification factor, IQ, will be proposed to account for the effects of the number of inspectors used during field inspection, inspector experience, training, and reassessment.

The inspector qualification factor, illustrated in Table 4.1, will be defined based on the number of inspectors, inspector experience, training, and refresh assessment. The condition rating will be quantified in accordance with performance. The biggest challenge for this task is determining how to quantify the subjective description, as shown in Table 4.1, as a quantitative index.

Table 4.1 Inspector qualification factor, IQ

Rating	Inspector qualification factor, IQ	Performance measure
Well qualified	1 (CS_1=1)	• Annual Refresh/reassessment • Capable to identify all deficiency and documentation • Over one years' experience • More than two inspectors during inspection • Enhanced non-destructive technologies
Fair qualified	2 (CS_2=0.75)	• Capability to identify element types, defects and documentation • Over one years' experience and over 6 months training • Two inspectors during inspection
Poor qualified	3 (CS_2=0.5)	• Training less than 6 months • Less than one-year background of inspection • One inspector
Failed	4 (CS_2=0)	• No on-site training experiences • No background of inspection

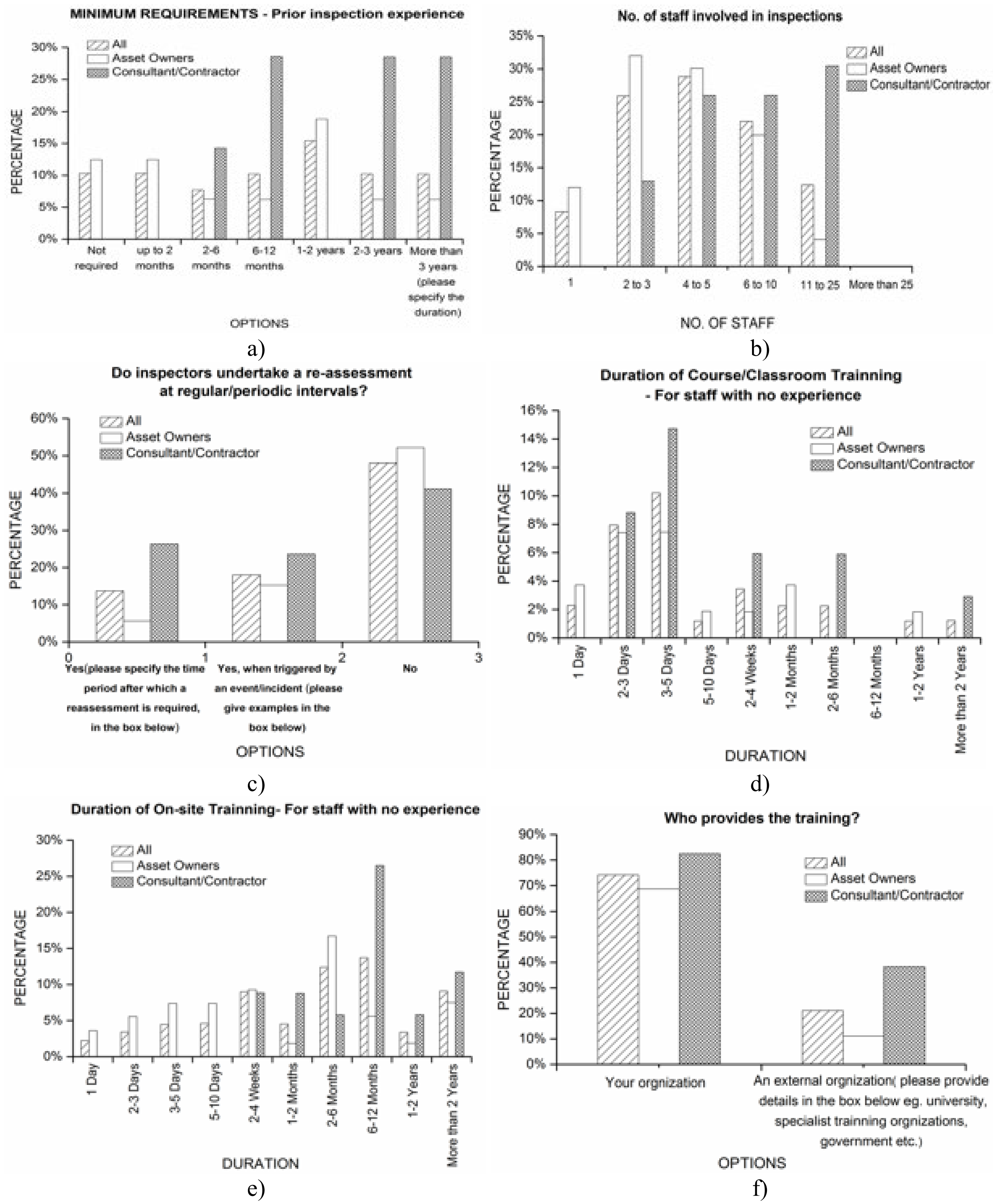

Figure 4.3 Variation of inspector qualification (Re-plot after Atkins 2009)

4.3.2 Structural Importance Factor (SI)

Some elements require more attention than the others in terms of structural importance. Bridge elements may be quantified from their performance measures that can be categorized as follows: a) safety; b) serviceability, including excessive stresses, cracking, deformation, vibration; c) fatigue; and d) functionality. To account for the different treatments for different structural elements, a structural importance factor, SI, was defined in this study.

Several studies (Tee et al. 1988; Melhem and Aturaliya 1996; Samsal and Ramanjaneyulu 2008; Abu Dabous and Alkass 2010; Rashidi and Gibson 2012) have been conducted to assess the importance of bridge elements. Tee et al. (1988) reported their findings based on a survey study of 46 bridge inspectors and bridge experts in an effort to quantify the structural importance factor through a comparison of elements at different condition ratings. Abu Dabous and Alkass (2010) reported using the structural importance factor by taking the element level and the safety of the overall structural using Analytical Hierarchy Process (AHP) could better estimate the value of that parameter. The database was built from structured field interviews with bridge engineers/inspectors. Table 4.2 is the SI proposed based on the data from Rashidi and Gibson (2012).

Table 4.2 Structural importance factor, SI (Reshidi and Gibson 2012)

Element	Structural importance factor, SI	Performance measure
Barrier, curb, joints,	1 (CS_1=1)	• Ancillary structures whose failure may not weaken components.
Bearings, deck, wingwall	2 (CS_2=0.75)	• Serviceability: second structural system whose failure may weaken other adjacent elements but still maintain functionality, mostly excessive stresses, cracking, deformation
Abutment, stiffener, load-carrying wearing	3 (CS_2=0.5)	• Serviceability and functionality: major structural components whose failure may cause local failure and lose functionality
Column, girder fractural critical components	4 (CS_2=0)	• Serviceability and functionality: major structural components whose failure may cause adjacent failure • Safety: failure may threaten public safety

4.3.3 Material Vulnerability Factor (MV)

Another key factor that affects structural integrity is material. This factor is defined as the material vulnerability (MV) factor. A few studies have been carried out to address the impacts of different materials on condition ratings (Austroads (2004); Valenzuela et al. (2010); and Rashidi and Gibson (2012)). Rashidi and Gibson (2012) defined the material vulnerability factor with a 4-level system ranging from CS 1 for steel to CS 4 for prestressed concrete, where the higher value denotes the material with higher vulnerability. It should be noted that the materials studied in previous studies were mainly steel, reinforced concrete, and prestressed concrete. Table 4.3 shows the ratings for material vulnerability. As newer bridge types (with new materials) become more common, additions to these inspection ratings will be needed to improve the uniformity and consistency of inspections. The new materials should be quantified for accurate condition rating to accommodate this need. These materials include fiber reinforced concrete, high performance concrete, and fiber reinforced polymer composite.

Table 4.3 Material Vulnerability factor, MV

Material	Material Vulnerability factor, MV	Performance measure
Composite, high performance concrete	1 (CS_1=1)	• Ductile, superior corrosion resistance, high durability
Steel, precast concrete, fiber reinforced concrete	2 (CS_2=0.75)	• Ductile, corrosion resistance, high durability
Reinforced concrete, wood	3 (CS_2=0.5)	• Relative low ductile and low durability
Prestressed concrete	4 (CS_2=0)	• Low reliability, catastrophic failure

4.3.4 Age Factor (AF) and Environmental Factor (EF)

To account for the impacts of age and environment on the element condition rating, it was necessary to define the age factor (AF) and environmental factor (EF). Frangopol et al. (1999) defined the bridge reliability index vs. age and its concept which was used in this study. Four condition rating were defined over time in terms of a reliability index, as shown in Table 4.4 and Figure 4.4.

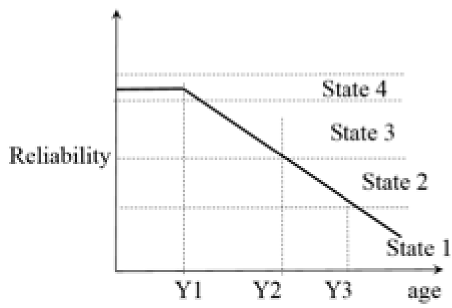

Figure 4.4 Bridge reliability index vs. age for a bridge (revised after Frangopol et al., 1999)

Table 4.4 Age factor, AF

Age	Age factor, AF	performance measure
New constructed	1 (CS_1=1)	• Within Y1
New, rehabilitation	2 (CS_2=0.75)	• Age ranging from Y1 to Y2,
Old, repaired	3 (CS_3=0.5)	• Age ranging from Y2 to Y3
Very old	4 (CS_2=0)	• Age over Y3

In regard to environmental factors, the major concerns are chemical attacks, deicing salt, freeze and thaw cycles, chloride ingress, sulphate attack, acid attacks, and alkali-aggregate reactions (Rashidi and Lemass 2011; Rashidi and Gibson 2012). CalTrans took into consideration the impacts of the environment on the element condition rating. The challenge with these performance measures is that they are highly dependent on a subjective description. The environment factor (EF) uses CS 1 to 4 to represent the aggressiveness of the operating practices or local environment of each element, as shown in Table 4.5.

Table 4.5 Environmental factor, EF

Level	Environmental factor, EF	performance measure
Benign	1 (CS_1=1)	• No environmental effects
Low	2 (CS_2=0.75)	• Little environmental effects
Moderate	3 (CS_3=0.5)	• Medium environmental effects
Severe	4 (CS_2=0)	• Severe F/T or chloride ingress

4.4 Element Condition Rating

Without factors considered, the element condition rating is defined by (Rashidi and Gibson, 2012)

$$\mathrm{ECR} = \sum_{j=1}^{4}(q_j \times CS_j) / \sum_{j=1}^{4}(q_j)\,, \tag{4-1}$$

where, CS_j = the condition state j, CS_1=1, CS_2=0.75, CS_3=0.5 and CS_4=0.

With reliability indices for critical factors in place, the unified element condition rating for at certain time i, is proposed by

$$\mathrm{UECR}(i) = \mathrm{ECR} \times \mathrm{CR}(i) \times 100\,, \tag{4-2}$$

where, CR denotes the product of critical factors to the inspection:

$$\mathrm{CR}(i) = \mathrm{IQ*SI*MV*DDLI*AF*EF}\,, \tag{4-3}$$

As shown in Eqn. (4-2), the unified element condition rating is categorized on a 0-100 ranking system (from 100% in the best state to 0% in the worst state) as the performance index for an element. By weighting factors, the element condition rating can account for the effects of various critical factors over time. The element condition rating that is shown in Eqn. (4-2) also makes it possible to assess the overall condition of a bridge in this aggregate form for bridge management system use, as stated by Rashidi and Gibson (2012).

4.5 Summary

In this chapter, major factors, including structural importance, material vulnerability factor, aging effect factor, and others, have been discussed, as well as their effects on the structures conditional state and rating. Rashidi and Gibson (2012) and other researchers have attempted to propose different condition ratings by integrating these critical factors into the element-level inspection, which should provide more reliable data for the bridge conditional assessment. Additional data sets could further quantify their weight in the determination in future work.

With advances in technology and sensors, implementation of these advances, including UAV, wireless sensor networks, or other sensors, could dramatically enhance the quality of data collection and data fusion which will be discussed in chapters 5 and 6.

5. ENHANCEMENT OF RELIABLE FIELD DATA COLLECTION FOR VISUAL INSPECTION IN ROUTINE INSPECTION

5.1 Background

To enable UAV for bridge inspection, Dr. Na Gong, Dr. Zhibin Lin, and Dr. Jinhui Wang developed the NDSU UAV System Lab in 2016. The NDSU UAV System Lab has the potential to be used in research to assist in civil structural health monitoring, including bridges, pipelines and other large-scale systems. In Figure 5.1, the PIs demonstrated the feasibility of using UAV assisted strategy for data collection for large-scale bridge systems. Since beginning the project, the UAV lab has been further strengthened by the purchase of two of the newest UAV models, the PHANTOM 4 with the high quality imagery collection, and MATRIC 100 for payload development. In addition, the use of two thermal infrared cameras, models DJI 4K UHD and DJ1 Zenmuse XT Radiometric, have great potential for large-scale bridge and pipeline monitoring. Along with the addition of equipment, Co-PIs Dr. Na Gong and Dr. Jinhui Wang successfully completed training and are now certificated UAV pilots. As illustrated in Figure 5.1, the PIs have attempted to demonstrate the feasibility of using UAV assisted strategy for the data collection for large-scale bridge systems.

Figure 5.1 UAV flight trial for demonstration in the NDSU UAV System Lab

5.2 Field Inspection Exercise Using Mixed Visual Inspection and UAV Flight

To effectively implement the proposed concept to improve data collection in the field, a field inspection exercise was conducted at North Dakota. The field inspection exercise started at the NP bridge which spans the Red River in Fargo, ND.

5.2.1 NP Bridge over the Red River, North Dakota

5.2.1.1 Basic Information

The bridge in Figure 5.2 is located on NP Avenue in Fargo, ND over the Red River. The information about the bridge was collected from City-data.com:

- Location: **NP AVE.-FARGO**
- Year Built: **1937**
- Year Reconstructed: **1987**

- Lanes on structure: **4**
- Lanes under structure: **2**
- Approaching Roadway Width: **14.6m (47.9ft)**
- Skew: **3 degrees**
- Material/Design: **Steel**
- Design/Construction: **Stringer/Multi-beam**
- Number Of Spans In Main Unit: **13**
- Length of Maximum Span: **32.6m (107.0ft)**
- Curb or Sidewalk Widths: Left: **0.0m**, Right: **1.6m (5.2ft)**
- Curb-To-Curb Width: **14.6m (47.9ft)**
- Out-to-Out Width: **16.8m (55.1ft)**
- Deck Structure Type: **Concrete Cast-in-Place**
- Wearing Surface/Protective System: Wearing Surface: **Monolithic Concrete**

Figure 5.2 Overview of the girder-type bridge at NP avenue, Fargo, ND

5.2.1.2 Visual Inspection

(a) Elements associated with superstructures. Field visits were held in April as a class demonstration for undergraduates at NDSU. Mixed visual inspection and UAV technology were used to collect data for the bridge inspection. Figure 5.3 shows the condition underneath the bridge deck and of the girders. The deck was identified as in a good condition state; however, hairy transverse cracks (efflorescence/buildup white but not heavy) were observed in the deck. These buildups white typically aligned with the reinforcement that was parallel to the cracks. These cracks could lead to penetration by water, chlorides, or moisture to the deck and the reinforcement. Note that the data collected below were based on the observations of the researchers and the participating students, not of certified bridge inspectors, and thus information could be subjective based on the limited field experience of the collectors.

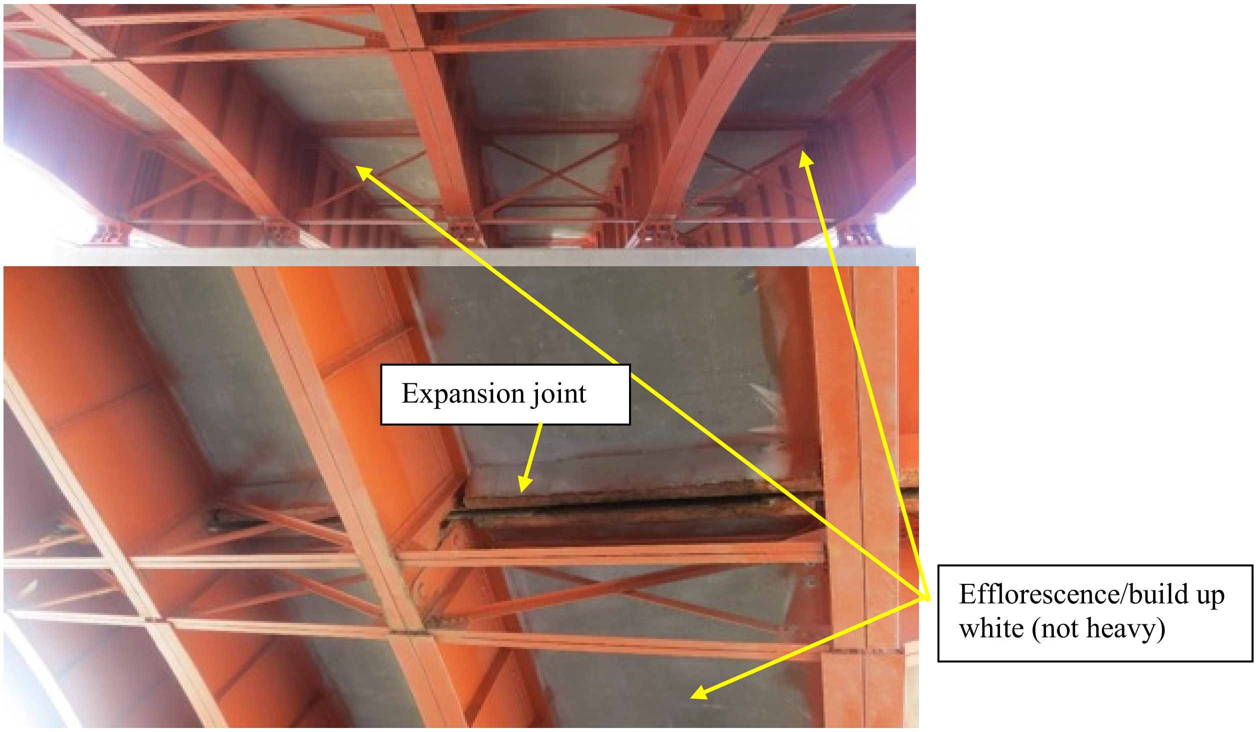

Figure 5.3 Overview of the bridge deck and girder

As clearly illustrated in Figure 5.4, the bridge girders had been given a new protective coating, and thus they were maintained in fairly good shape.

Figure 5.4 Overview of the bridge girder

There was, however, an issue related to leaking runoff behind the steel railing. This runoff had caused erosion on the steel and concrete decking, as shown in Figure 5.5.

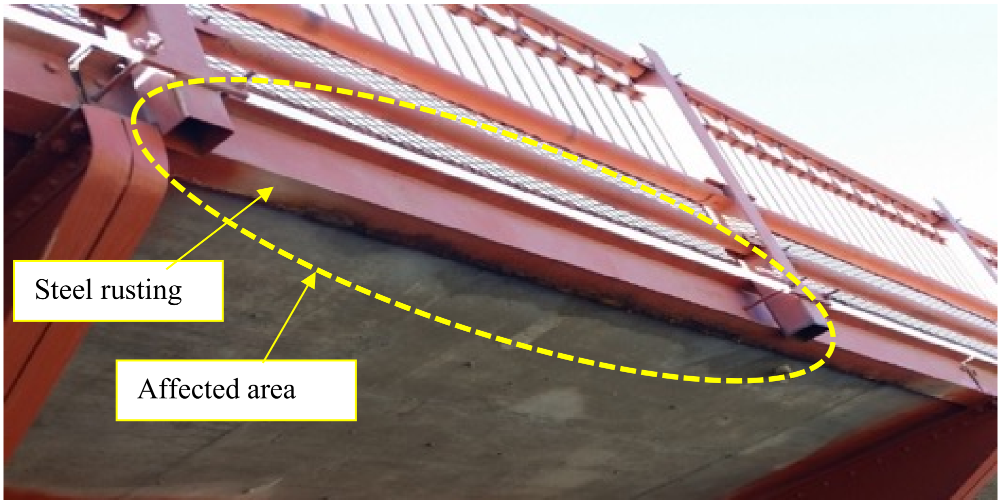

Figure 5.5 Overview of underneath the bridge shoulder

As shown in Figure 5.6, there was a pin-connected joint that had shifted slightly away from the pier bent support. This strategy could effectively avoid the runoff directly on top of pier, while maintaining the rotation necessary to release thermal or other expansion as well as to accommodate shrinkage.

Figure 5.6 Overview of expansion joint and pin connection near the west side of the bridge abutment

However, as illustrated in Figure 5.7, the expansion joint was in critical condition and had deteriorated severely from water runoff. The runoff had leaked onto the supporting girder and cross frame members as well, and despite the protective coating on the girders, the girders and cross-frame members also exhibited a certain level of corrosion.

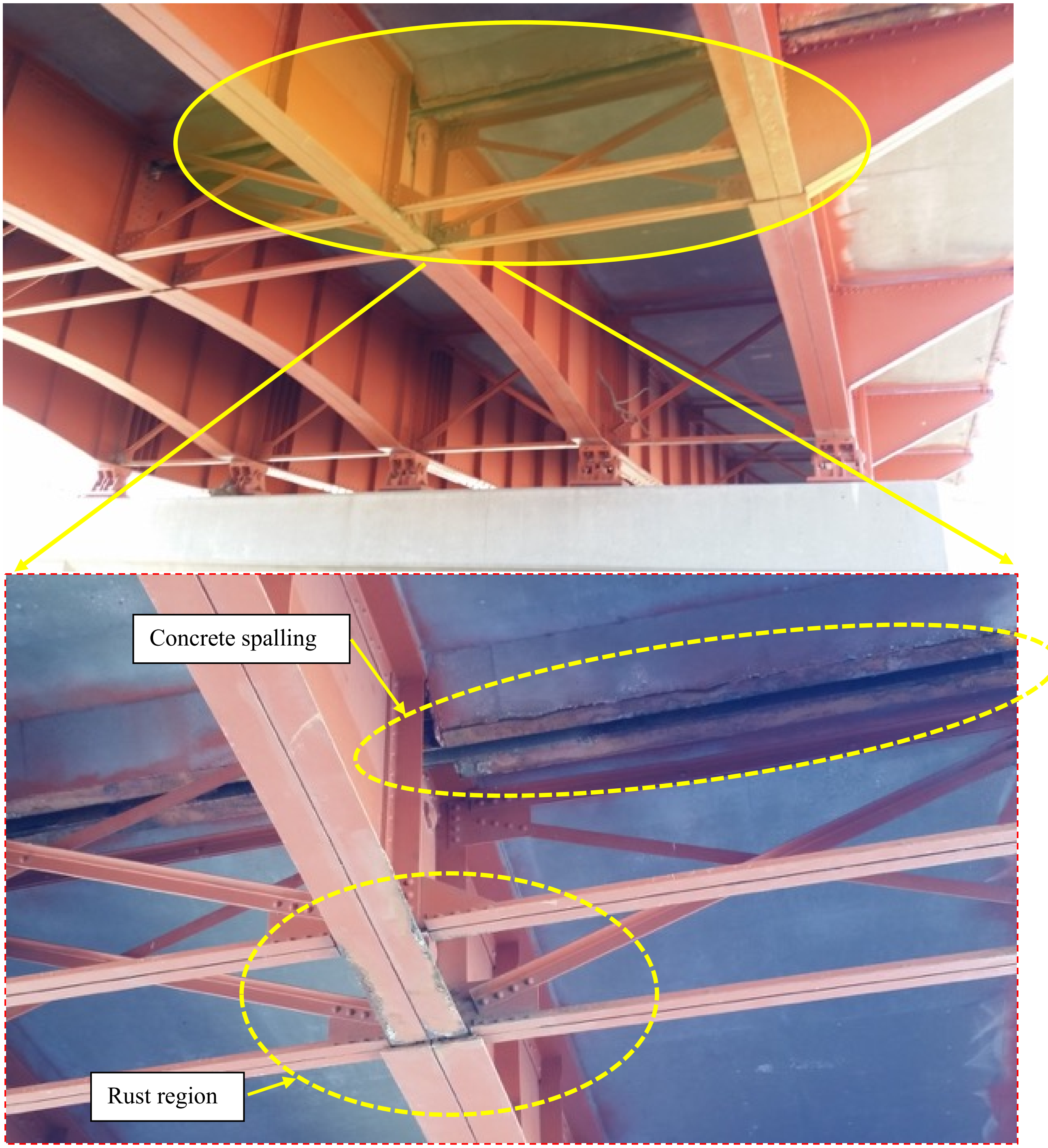

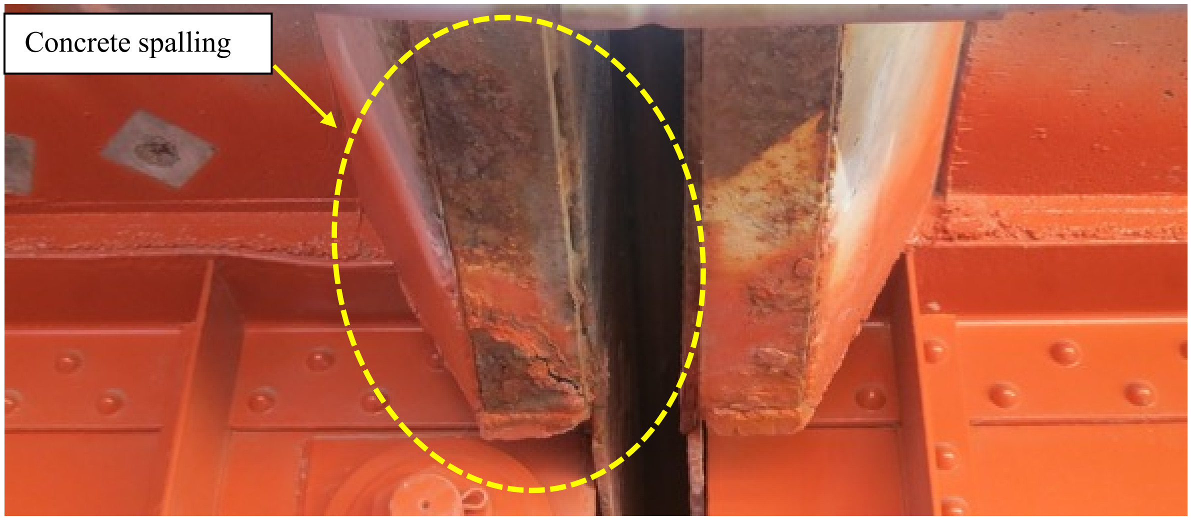

Figure 5.7 Deterioration of expansion joint near the west side of the bridge abutment

Corresponding to the expansion joint at the deck surface, shown in Figure 5.8, certain deterioration of the expansion joint was observed, which led to an uneven bridge surface that could be affected by a vehicle bumping over it, thereby potentially leading to further damage.

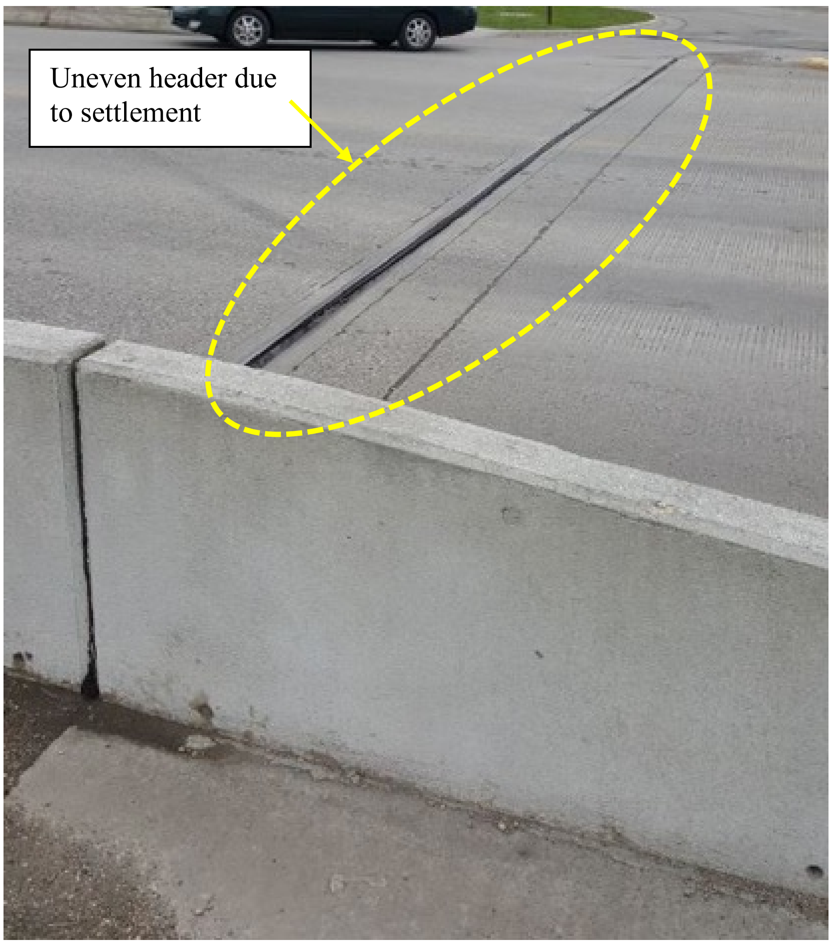

Figure 5.8 Deterioration of expansion joint near the west side of the bridge abutment

(b) Elements associated with substructures. Reinforced concrete bridge pier walls were observed in this bridge to be in good condition state, as shown in Figure 5.9.

Figure 5.9 Pier walls used as the support of girders

There was no concrete spalling or reinforcement corrosion on the surface of the pier walls, however, a light level of bridge scour (about less than one foot) was observed on the major piers near the east side of the bank at the front of the flow direction, as shown in Figs. 5.10 and 5.11.

The bridge abutment and bearing at east side of the bridge were illustrated in Figure 5.11. Clearly, there were some cracks smeared on the abutment. The metal bearing exhibited certain rusting, which may affect the effectiveness of the rotation.

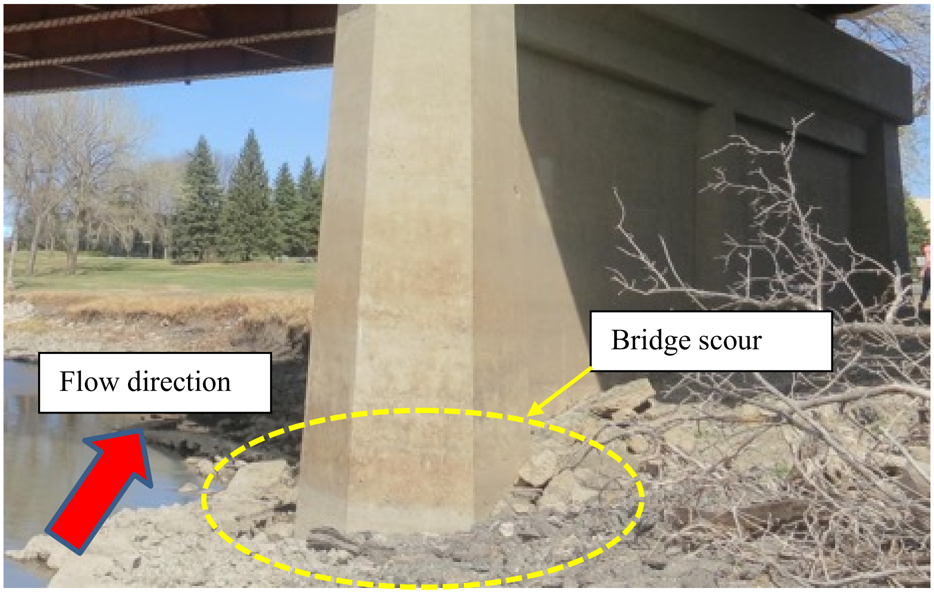

Figure 5.10 Bridge scour at east side of the pier walls

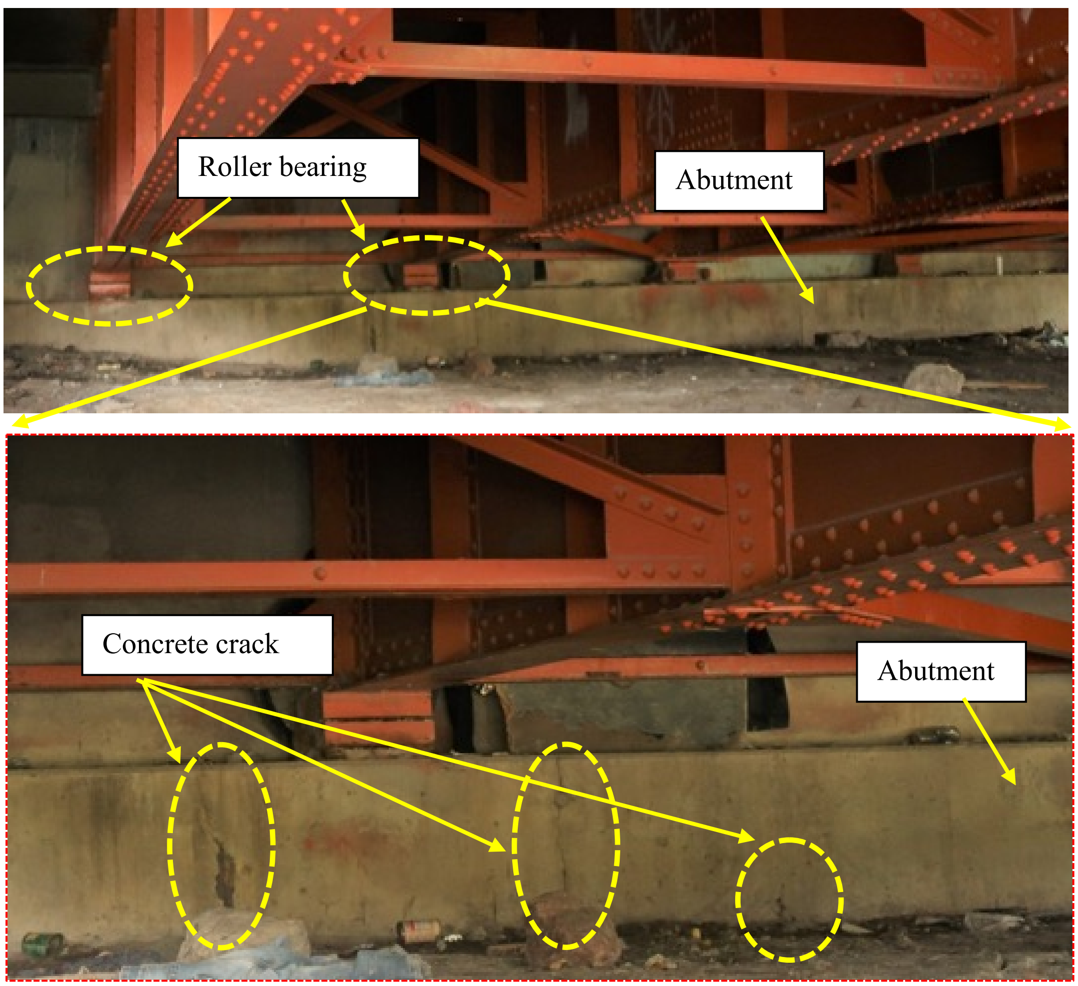

Figure 5.11 Bridge abutment and bearings

Figure 5.12 displayed the wingwall with apparent deterioration, e.g., concrete spalling, rebar corrosion, and associated cracks. These damage-induced defects could be the result of the direct contact of the wingwall with the corrosive soil.

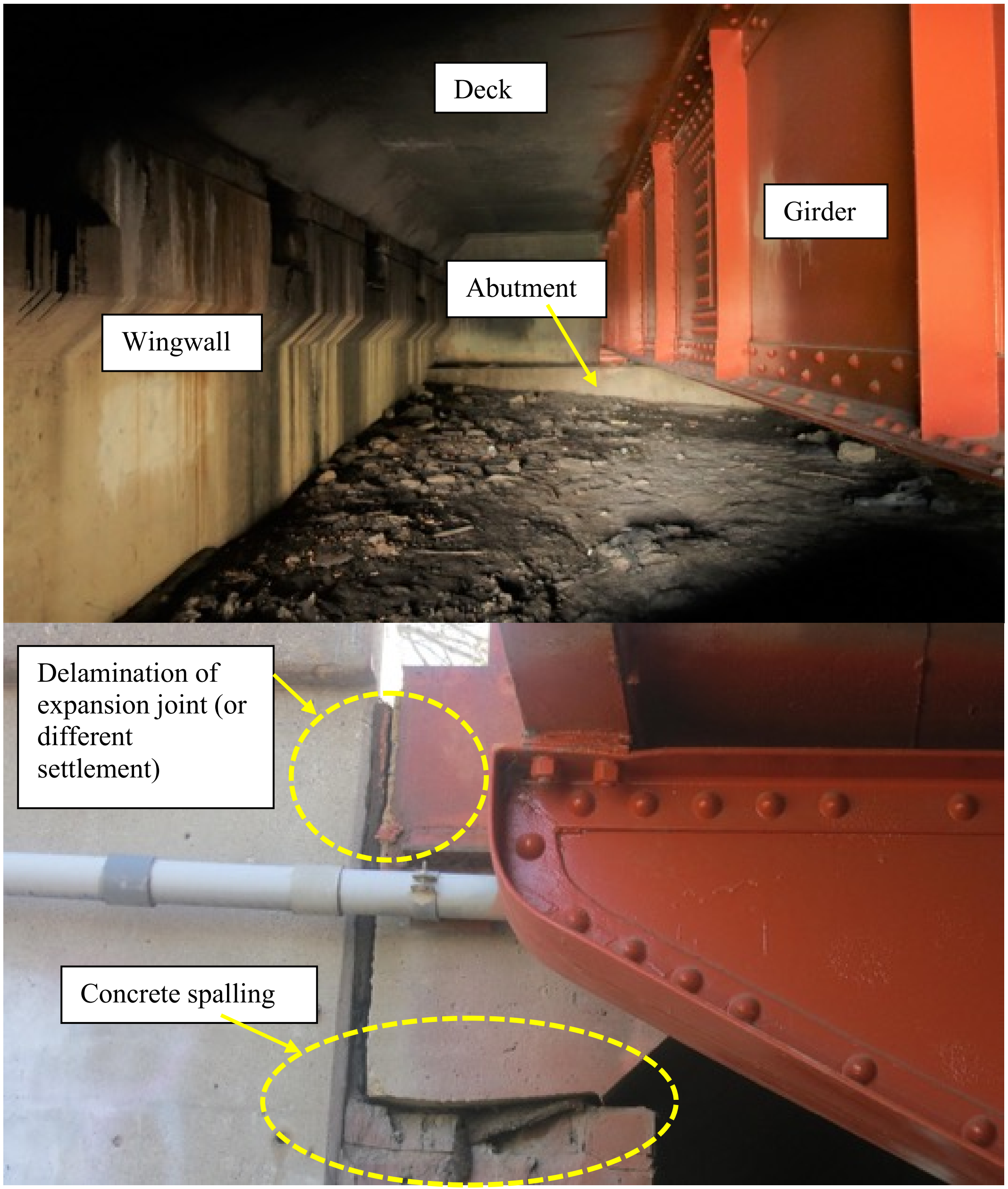

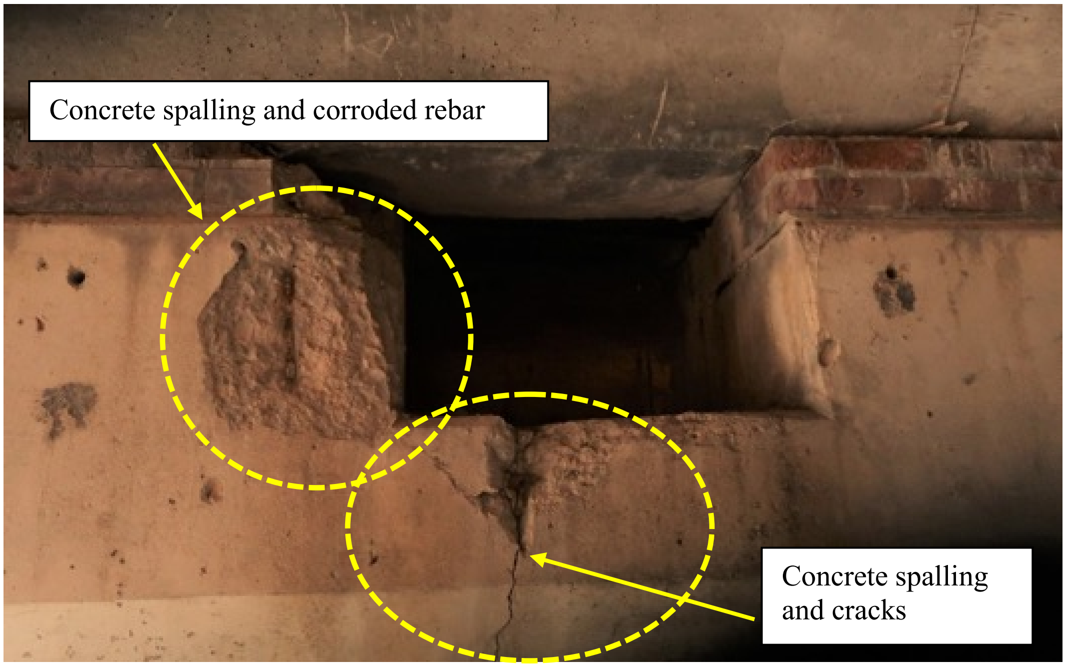

Figure 5.12 Deteriorted bridge wingwall at east side of the bridge

(c) Elements condition state. The bridge was inspected and rated by its condition state, as shown in Table 5.1, where the elements were first identified by their I.D. number and then estimated by their quantities with different quantities associated with different condition states. Clearly, there was a high level of variance and uncertainty associated with manual, visual inspection, even in accordance with the new bridge element-level inspection manual (2013). The I.D. of defects associated with the parent's elements were identified as well, and shown in Table 5.1, which could better assist bridge engineers and managers when planning their retrofit strategies.Table 5.1 clearly demonstrated that the defects related to expansion joints were the major root causes for deck deterioration, girder rusting, and cross-frame beam corrosion. In addition, the reinforced concrete abutment exhibited certain cracks and concrete spalls, as confirmed in Figure 5.14. Moreover, due to direct exposure to soil, the wingwall exhibited concrete spall, rebar corrosion, and cracks.

Table 5.1 Summary of element condition states

Element	Element description	Total Qty	Units	Condition State Quantity			
				CS 1	CS 2	CS 3	CS 4
12	RC Deck	5885	Sq. ft.		5774.8	110.2	
1130	Cracking	110.2	Sq. ft.			110.2	
1080	Delamination/Spall	5885	ft.		5774.8		
330	Railing	107	ft.			107	
1120	Rust Staining	107	ft.			107	
107	Steel Open Girder	107	ft.	105	2		
1120	Rust Staining	2	ft.		2		
515	Steel Protective Coating	4458.3	Sq. ft.	4375.0		83.3	
1120	Rust Staining		Sq. ft.			83.3	
313	Fixed Bearing	5	Each		5		
1000	Corrosion (rusting)		Sq. ft.		5		
314	Pivot Bearing	5	ea.	5			
300	Strip Seal Expansion Joint	55.1	ft.			55.1	
2330	Seal Damage		ft.			10	
1020	Connection		ft.			10	
2360	Adjacent Deck		ft.			10	
2370	Metal Deterioration		ft.			25.1	
215	RC Abutment	55.1	ft.	51.1	4		
1130	Cracking		ft.		2		
1080	Delamination/Spall		ft.		2		
210	RC Pier Wall	55.1	ft.	53.1	2		
6000	Scour		ft.		2		
220	Pier Footing		ea.				
321	Approach Slab	26244.41	Sq. ft.	26148.61	95.8		
1130	Cracking		Sq. ft.		95.8		
8400	Wingwall		ea.				
8903	Wingwall Deterioration		ea.				

5.2.2 UAV Used for Improvement of Visual Inspection

In the spring of 2019, there was major flooding in Fargo-Moorhead region, as shown in Figure 5.13. The NP bridge was not accessible at most locations by traditional means, so the UAV was used to monitor the bridge and collect image-based data for further analysis. Some images, as illustrated in Figure 5.14 and 5.15, were shown to demonstrate the different perspectives for visual inspection of the bridges. Clearly, the UAV technology had no limitations for approaching the areas of interest on the bridge and provided real-time data. Figure 5.15 revealed that with the enhancement of the UAV, nearly any bridge element could be inspected in great detail (Figure 5.15b), yet the bridge could also be observed on the system-level scale (Figure 5.15c).

Figure 5.13 Most locations of the bridges on the Red River were in the water during 2019 flooding

Figure 5.14 A series of images from UAV for NP Ave bridge visual inspection

(a) Inspection of the inaccessible location during flooding

(b) Inspection of specific location in detail

(c) Inspection of moderately large areas in system level

Figure 5.15 Benefit of UAV-assisted visual inspection

5.3 Summary

Although further data analysis for UAV images/videos could be achieved by providing bridge vibration, associated bridge stiffness, damping ratio, and loading rating, this study was conducted primarily to demonstrate the new advances in bridge and system inspections using UAV for enhanced visual inspection, where traditionally, manual, visual inspection could be limited. Particularly, with the integration of mounted sensors, we could provide full-spectrum reliable data sets for bridge inspection and ratings.

6. ENHANCEMENT OF DATA FUSION AND INFORMATION PROCESS IN IN-DEPTH/SPECIAL/DAMAGE INSPECTION

6.1 Background

Effective data collection and fusion are critical steps in the in-depth/special/damage inspection process for element-level inspections and conditional assessments. This chapter aims to develop a framework to assist with the data fusion and information process for sensory data. Sensory data is commonly used in the detailed inspection methods to improve element-level inspections, rapid condition assessments, and bridge management of large-scale bridges. Three representative feature extraction methods, including the wavelet transform, the Hilbert-Huang transform, and the Teager-Huang transform, were selected for the data fusion and information process. A numerical simulation was used to verify the concept and demonstrate the effectiveness and sensitivity of the data-driven damage detection for cable-stayed bridges. Moreover, a further parametric study was conducted to address the impacts of damage level, damage location, sensor location, and moving loading on the data classification.

6.2 Data Fusion and Data Process Techniques

6.2.1 Overview

Dynamic characteristics of bridges exhibit non-stationary and nonlinear behavior (Bornn et al. 2010). Time-, frequency, and time-frequency analysis, including the wavelet transform, short-time Fourier transform, and Wigner-Ville distribution (Feng et al. 2013), are effective ways to track the change of a system and its nonlinear behavior (Li et al. 2010). These methods have some drawbacks in terms of data analysis, such as high computational time and less adaptive features. The emerging techniques, the Hilbert-Huang transform (HHT) and Teager-Huang transform (THT), have also demonstrated great potential for data-driven time-frequency analysis (Li et al. 2010; Yang et al. 2004; Hsu et al. 2013). The HHT and THT display a sparse feature and are not limited by the Heisenberg uncertainty principle, as compared to their conventional counterparts which are, but these two methods do have noise sensitivity limitations. A literature review showed that few attempts have been made to address the impacts of the various feature extraction methods on structural condition assessment and damage detection, particularly for large-scale, cable-stayed bridges. Thus, we selected three representative feature extraction and data process methods that used supervised machine learning, including the wavelet transform, the Hilbert-Huang transform, and the Teager-Huang transform, as discussed below.

6.2.2 Data Fusion using Wavelet Transform

Wavelet transform is an effective tool for the excellent local zooming property, great for time-frequency decomposition to analyze nonstationary signals. In this study, the multi-resolution wavelet analysis was used to decompose the signal in time and frequency domain, while the continuous wavelet transforms of a continuous signal, $x(t)$, is defined by:

$$Wx(a,b) = x \otimes \psi_{b,a}(t) = \frac{1}{\sqrt{a}}\int_{-\infty}^{+\infty} x(t)\psi^*(\frac{t-b}{a})dt \tag{6-1}$$

where ψ and ψ^* are the basic function and its complex conjugate; a and b are the scale and translation factors, respectively. Eqn. (1) is to decompose $x(t)$ into basic function $\Psi((t-b)/a)$, named the mother wavelet. The scale factor a is equal to 2. The frequency spectrum of the wavelet is stretched by a factor of 2, and all frequency components shift up by a factor of 2. The discrete wavelet transform can be treated as a band-pass filter:

$$\mathrm{Wx}(\mathrm{j},\mathrm{k}) = \int_{-\infty}^{+\infty} \mathrm{x}(\mathrm{t}) 2^{\frac{\mathrm{j}}{2}} \psi^{*}(2^{\mathrm{j}}\mathrm{t}-\mathrm{k})\mathrm{dt} \tag{6-2}$$

Wavelet packet analysis behaves as a further generalized wavelet transform. It has different time-frequency windows to decompose signals, which are inconvenient in the wavelet decomposition. A wavelet packet function can be written as:

$$\psi_{j,k}^{\mathrm{i}}(t) = 2^{\frac{j}{2}} \psi^{i}\left(2^{j}t-k\right) \quad i = 1, 2, \ \ldots, \tag{6-3}$$

where i, j, and k are the modulation, the scale, and the translation parameter, respectively. The ψ^{i} is obtained by using recursive relationship:

$$\psi^{2i}(t) = \sqrt{2} \sum_{k=-\infty}^{\infty} h(k) \psi^{i}(2t-k) \tag{6-4a}$$

$$\psi^{2i+1}(t) = \sqrt{2} \sum_{k=-\infty}^{\infty} g(k) \psi^{i}(2t-k) \tag{6-4b}$$

where $h(k)$ and $g(k)$ are the quadrature mirror filters. It is determined by the mother wavelet (ψ^{1}) and the scaling function. The mother wavelet has some significant properties, including invariability and orthogonality. Wavelet packets have an adjustable time and frequency resolution with a different time and frequency resolution at every level. The top level has good resolution in the time domain and the bottom level has good resolution in the frequency domain. The frequency recursive relationships are shown in Figure 6.1 for a full third level wavelet packet decomposition, called the Mallat-tree decomposition.

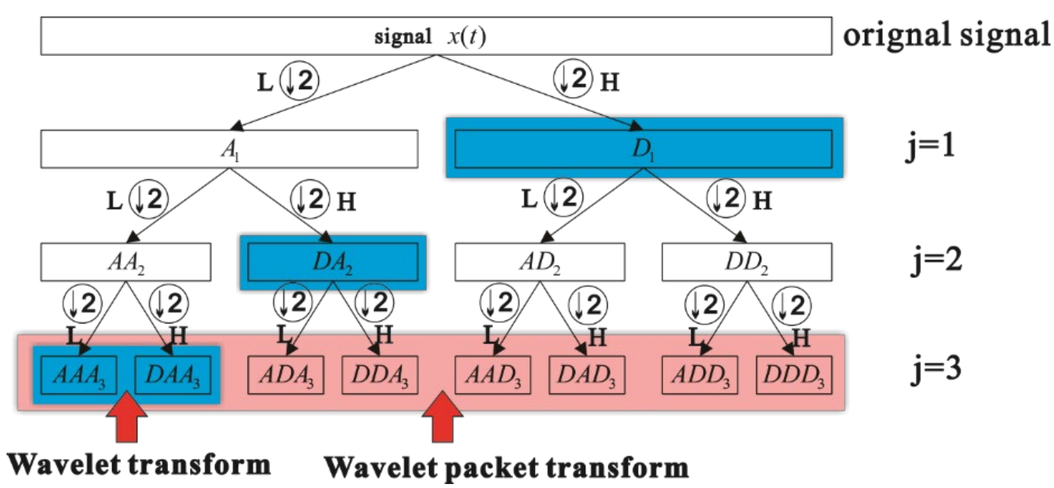

Figure 6.1 3rd level wavelet transform and wavelet packet transform

As illustrated in Figure 6.1, the blue box and the pink box indicate the wavelet transform and wavelet packet transform of the signal, where *H* means high-pass filtering, and *L* means low-pass filtering. *A* and *D* denote the approximation coefficients and detail coefficients, respectively. The recursive relationships between the j^{th} and the $(j+1)^{\text{th}}$ level are by the form:

$$x_{j}^{i}(t) = x_{j+1}^{2i-1}(t) + x_{j+1}^{2i}(t) \tag{6-5a}$$
$$x_{j+1}^{2i-1}(t) = (x_{j}^{i}(t) * h) \ \downarrow 2 \tag{6-5b}$$
$$x_{j+1}^{2i}(t) = (x_{j}^{i}(t) * g) \ \downarrow 2 \tag{6-5c}$$

By using the inverse Fourier transform, Eqn. (6-2) is converted into the time domain as

$$Wx(a,t) = \mathcal{F}^{-1}\{Wx(a,f)\} \tag{6-5d}$$

where $\mathcal{F}^{-1}\{\cdot\}$ denotes the inverse Fourier transform. The variation of the scale factor, a, could yield different resolutions in different domains. A relatively small-scale factor could provide a high resolution in the time domain, while another one could have a better resolution in the frequency domain with the increase of the scale factor. As a result, the continuous wavelet transform is more capable of generating adjustable time and frequency resolutions at any scale than the other two methods. Note that the continuous wavelet transform will be later abbreviated as the wavelet transform for simplicity, unless otherwise noted.

6.2.3 Data Fusion using Hilbert-Huang Transform (HHT)

Hilbert-Huang transformation is a novel technique of signal decomposition that has many interesting properties. The HHT consists of empirical mode decomposition and Hilbert spectral analysis (Huang and Wu 2008). In this section, we will discuss the generation of intrinsic mode function (IMF) using the empirical mode decomposition (EMD) and the HHT time-frequency description of time series for the obtained IMFs.

The EMD is effective to decompose signals into IMFs, and more importantly, since this method does not project data into a predefined function space (harmonic, wavelet), it is a useful tool to decompose nonlinear and non-stationary signals (Mandic et al. 2013). In the EMD, it is assumed that every signal includes different intrinsic mode oscillation. By using the data from the time dominant field, the intrinsic oscillatory modes can be identified progressively. The intrinsic model is characterized by the time lapse between the successive extremes.

The IMF must satisfy the following conditions: (1) The number of zero-crossing and the number of extrema must be equal or differ by one, and (2) The local maxima and minima envelope should have zero means. The process of EMD to decompose the simple imbedded oscillatory mode from any signal $x(t)$ can be illustrated as follows (Huang et al. 1998):

Step 1: Calculate all the local extrema, and then use two cubic splines to envelope all the local maxima and minima.

Step 2: The mean of the upper and lower envelopes is defined as m_1, and if the decomposition is ideal, the first component h_1 is an IMF yield:

$$h_1 = x(t) - m_1 \tag{6-6}$$

Step 3: If the h_1 is not an IMF, then repeat Step 1 and 2 until $h_{1\mathrm{k}}$ becomes an IMF,

$$h_{1k} = h_{1(k-1)} - m_{1k} \tag{6-7}$$

Step 4: Subtract the first IMF from the original signal as：

$$r_1 = x(t) - h_{1k} \tag{6-8}$$

Step 5: Treat r_1 as the original data, and repeat steps 1 to 4 *n* times to get n-IMFs decomposed signal from $x(t)$.

$$\begin{aligned} r_2 &= r_1 - h_{1k} \\ &\vdots \\ r_n &= r_{n-1} - h_{(n-1)k} \end{aligned} \tag{6-9}$$

The acceptance criteria is based on the r_n, for which no more IMFs can be extracted. So, the whole decomposition results can be defined as:

$$\mathrm{x(t)} = \sum_{j=1}^{n} h_{jk} + r_n \tag{6-10}$$

The EMD acts essentially as a dyadic filter bank resembling those involved in wavelet decompositions (Flandrin et al. 2004). The frequency bands range from high to low as the increase of the IMFs. The residue r_n represents the central tendency of signal $x(t)$ (Yu et al. 2005). By using this algorithm, the beginning $h_{1\mathrm{k}}(t)$ will contain the highest frequency. With the obtained IMF $h_{\mathrm{ik}}(t)$ through Steps 1 to 5 above, the Hilbert transform is used to describe the IMFs:

$$H[h_{\mathrm{ik}}(t)] = \frac{1}{\pi}\int_{-\infty}^{+\infty} \frac{h_{ik}(\tau)}{t-\tau} d\tau \tag{6-11}$$

With this definition $h_{\mathrm{ik}}(t)$ and $H[h_{\mathrm{ik}}(t)]$ in Eqn. (11), the complex data is

$$\mathrm{z_i}(t) = h_{ik} + jH[h_{ik}(t)] = a_i(t)e^{j\Phi_{\mathrm{i}}(t)} \tag{6-12}$$

in which

$$a_i(t) = \sqrt{h_{ik}^2(t) + H^2[h_{ik}(t)]} \tag{6-13a}$$

$$\Phi_i(t) = arctan\frac{H[h_{ik}(t)]}{h_{ik}(t)} \tag{6-13b}$$

From Eqn. (12), we can have the instantaneous frequency as

$$w_i(t) = \frac{d\Phi_i(t)}{dt} \tag{6-14}$$

After using the Hilbert transform to each IMF, the signal $x(t)$ can be defined as follows:

$$x(t) = Re\sum_{i=1}^{n} a_i(t)e^{j\int \omega_i(t)dt} \tag{6-15}$$

where Re stands for ‘real part’, $\omega_j(t) = 2\pi f_j(t)$ and $j = \sqrt{-1}$. The Hilbert-Huang time-frequency spectrum $H(\omega, \mathrm{t})$ can be expressed as follows:

$$H(\omega, \mathrm{t}) = Re\sum_{i=1}^{n} a_i(t)e^{j\int \omega_i(t)dt} \tag{6-16}$$

6.2.4 Data Fusion using Teager-Huang transform (THT)

TH transform was introduced by Cexus and Boudraa in 2006 (Cexus and Boudraa 2006), and it has been used in the fields of aerospace and mechanical engineering (Cexus et al. 2010; Junsheng et al. 2007; Li et al. 2009). This method combines the EMD and Teager energy operator. The EMD is not a time-frequency representation like the wavelet transform, but instead the EMD decomposes the signal $x(t)$ into a multicomponent AM-FM signal in a band-pass filter way (Flandrin et al. 2004). The whole process of the THT is illustrated in Figure 6.2. Each intrinsic mode function (IMFs) includes a reduced number of oscillatory modes. The IMFs are demodulated into instantaneous frequency (IF) and instantaneous amplitude (IA) signals. The Teager-Kaiser energy operator (TKEO) was selected as an energy demodulation method to simultaneously track these IF and IA components. The TKEO relies on no prior choice on the number of AM-FM components of the analyzed signal. Furthermore, it is built on an adaptive basis and thus is not constrained by the uncertainty principle (Bouchikhi et al. 2014). Additionally, the TKEO has high time resolution and ease in operation, while maintaining the meaningful quantity frequency and amplitude of each IMFs. Using the TKEO will generate the intrinsic frequency series, which is used to identify the embedded oscillation property in the data. The total information will be accurately captured by collecting all the spectra from each IMF and easily visualized using a two-dimensional plot.

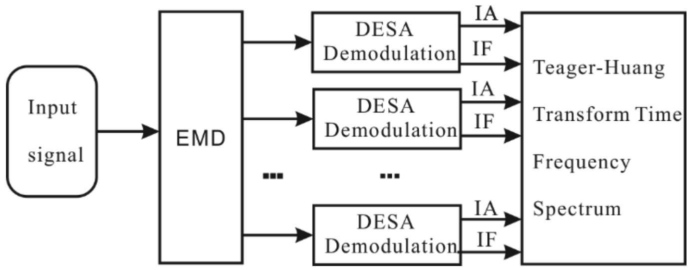

Figure 6.2 Flowchart of the THT (Li et al. 2009)

The signal $x(t)$ can be express as the following form using the THT:

$$x(t) = Re \sum_{i=1}^{n} a_i(t) e^{j\int \omega_i(t)dt} + r_n(t) \qquad (6\text{-}17)$$

This equation can be written as a tree-dimensional figure $(t, f_i(t), a_i(t))$. The Teager-Kaiser spectrum (TKS), can be defined as follows:

$$TK(t,f) = \begin{cases} a_1(t)\ f_1(t)\ and\ t\ for\ IMF1 \\ a_2(t)\ f_2(t)\ and\ t\ for\ IMF2 \\ \vdots \\ a_n(t)\ f_n(t)\ and\ t\ for\ IMFn \end{cases} \qquad (6\text{-}18)$$

Teager-Kaiser spectrum can be rewritten as

$$TK(t,f) = \sum_{j=1}^{n} a_j(t)\delta(f - f_j(t)) \qquad (6\text{-}19)$$

The advantage of TKS analysis is it circumvents the limitation of Bedrosian's theorem (Bouchikhi et al. 2014). The time-frequency spectrum of TKS is a sparse matrix. The dimension of the TKEO for each IMFs is N_f if the dimension of signal $x(t)$ is *T*. The layer of IMF is relatively smaller than *T* and Eqn. (6-19) shows that the time-frequency distribution just has *K* 1D trajectories to be non-zero. Thus, the number of points is KT dimensions, which are concentrated in some trajectories and are smaller than other time-frequency spectrums, such as the wavelet transform.

The signal is the dynamic response of a bridge, and it is inevitable that it will be contaminated by noise interference. Figure 6.3 shows the dynamic vibration of the original cable-stayed bridge without any damage. It shows that the IMFs has some local turbulence, the frequency will have a high variation, and the amplitude will have some abnormal points. There are two abnormal points in the amplitude in Figure 6.3. The mean value of each layer IMFs has been calculated as μ, while the standard deviation, σ, and $\mu + 3\sigma$ are selected as the upper limitation.

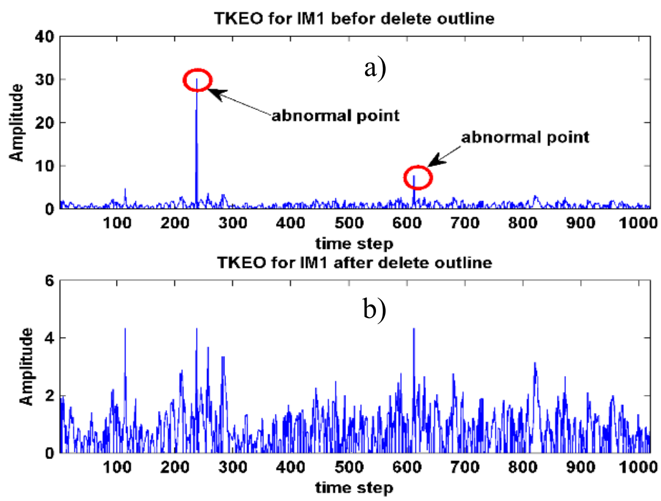

Figure 6.3 Truncation of data in instantaneous frequency: a) original data and b) truncated data

6.2.5 Information Fusion and Process using Support Vector Machine

Support vector machine (SVM) is one of the effective techniques used in data classification. In this method, a hyperplane is used to separate the two different classes of samples based on the SVM training algorithm (training data) and by maximizing the ''margin,'' which is the distance from the hyperplane to the closest data points in either class. By defining the Kernel function as the inner product, the data can be mapped into a higher dimensional feature space; thus, the SVM can be applied for nonlinear classification problems. For this purpose, various Kernel functions can be used such as linear, polynomial, or Gaussian radial basis function.

Since it is not always possible to separate the acquired data, it is reasonable to ignore the outlier data points and use a soft margin SVM that includes slack variable ξ_i and the error penalty c. Thus, the margin is defined as:

$$\text{Margin}=\frac{2}{\|w\|^2}, \tag{6-20}$$

Therefore, the optimization problem is defined as:

$$\min \left(\frac{1}{2}\|w\|^2 + c\sum_{i=1}^{N}\xi_i\right), \tag{6-21a}$$

$$\text{Subject to } \; y_i(\langle w, x_i\rangle + b) \geq 1 - \xi_i, \quad \xi_i \geq 0 \tag{6-21b}$$

where w and b are the vector and scalar that define the position of the hyperplane, ξ_i is a measure of how much an observation fails to satisfy the target margin. Therefore, the nonlinear decision function can be defined using Lagrange multipliers algorithm and by solving the dual optimization problem as:

$$f(x) = sign(\sum_{i=1}^{N} \alpha_i y_i K(x, x_i) + b) \tag{6-22}$$

6.3 Case Study of a Cable-Stayed Bridge

6.3.1 Overview

Manavgat cable-stayed bridge, located in Turkey, was selected for numerical analysis. The layout and the cross-sections of the structural members of the bridge are shown in Figure 6.4. The bridge is 202 m long with equal spans of 101 m, and a total of 28 steel cables connect the 13.7 m wide deck to the λ-shape steel tower. The tower is approximately 42 m high with a hollow hexagonal cross section, and it is placed on a concrete footing. The deck has a composite cross-section, which consists of 25 cm of concrete, 10 cm of pavement, and two continuous steel girders that are laterally restrained by I-beams at approximately every three meters.

The distance of the nearest cable to the center of the pylon is 19.6 m, and the distance between the cables is 12 m. The last cables are connected to the deck in 9.4 m away from the abutments. Cables A1 to A7 include 14, 16, 19, 19, 22, 19, and 24 strands, respectively. Each strand has a cross section area of 150 mm^2, elastic modulus of 197 GPa, and ultimate strength of 1860 MPa. The elastic modulus for the concrete and steel materials have been defined as 34 GPa and 200 GPa, respectively.

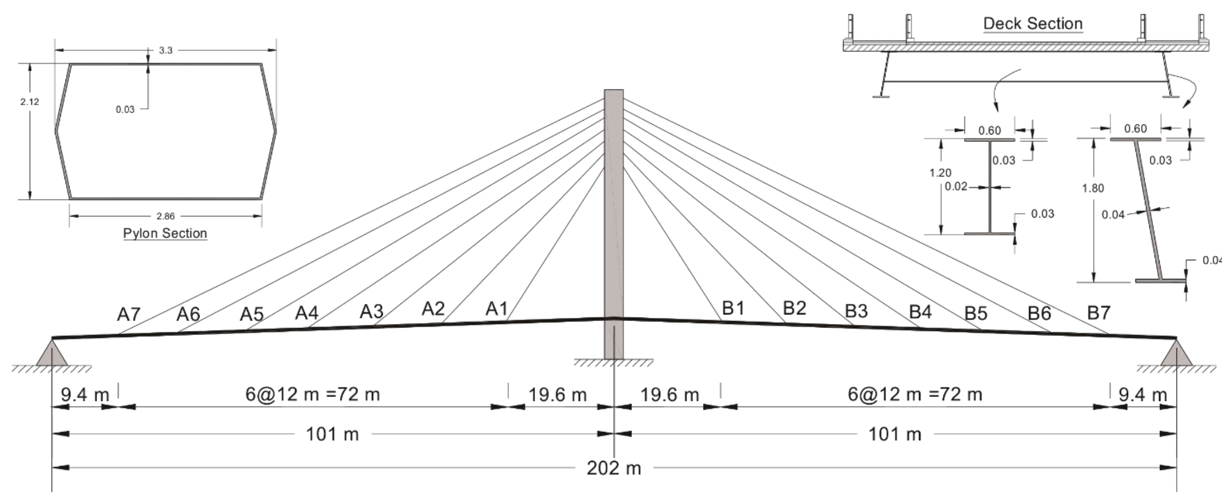

Figure 6.4 Manavgat cable-stayed bridge layout and the cross-section of the structural members

6.3.2 Data Acquisition from Sensory Data by Simulation

Nonlinear time-history analyses were carried out using the commercially available SAP2000® software (2014). The following assumptions were made to idealize the finite element modeling: (a) the deck was continuous; (b) the cables carried only axial forces; and (c) the soil-structure interaction and the effects of nonstructural components were negligible. To calibrate the model, the modal analyses revealed that the first six periods of the bridge predicted by this study, ranging from 0.309s to 0.825s, matched well with those in the literature (Atmaca et al. 2015; Atmaca et al. 2014). The representative mode shapes are shown in Figure 6.5.

Since the damping ratio is considerably high, and the natural frequencies of the bridge are very close to each other, instead of impact load, a chirp excitation with time-dependent amplitude and frequency (sweeping frequency) was applied to the deck at the midpoint of the left span. The acceleration of all 28 joints (end of cables) was captured using accelerometer sensors. The excitation had a sweeping signal from 0 to 5 Hz. The sampling rate of this model was 100 Hz.

A total of 15 test cases were defined to verify the effectiveness and accuracy of the proposed approaches, as listed in Table 6.1. The dynamic responses at the location of A4 in Figure 6.4 were selected to demonstrate the proposed concept, unless stated elsewhere. State #1 was used as the baseline condition without any damages, while States #2-4 were designed to simulate the bridge under fully loaded with vehicles at both astatic load and the AASHTO HL-93 moving design truck for the consideration of the operational influence. States #5-15 were designed for various damage scenarios. Among them, States #3-9 were designed to simulate the defects using reduction of cable stiffness, under five different damage levels in stay cables (from 10% to 50% of cable area at location of A4). States #10-13 were used to determine the effects of damage locations on data classification, where States #11 represents the location of a quarter span and States #10 is at location of three-quarter span. The last two cases were designed to account for the combined effects of a moving loading, as well as the reduction of cable area, in which two speeds of the design truck are 10 m/s and 20 m/s, respectively, in accordance with the operational conditions at State #3 and #4.

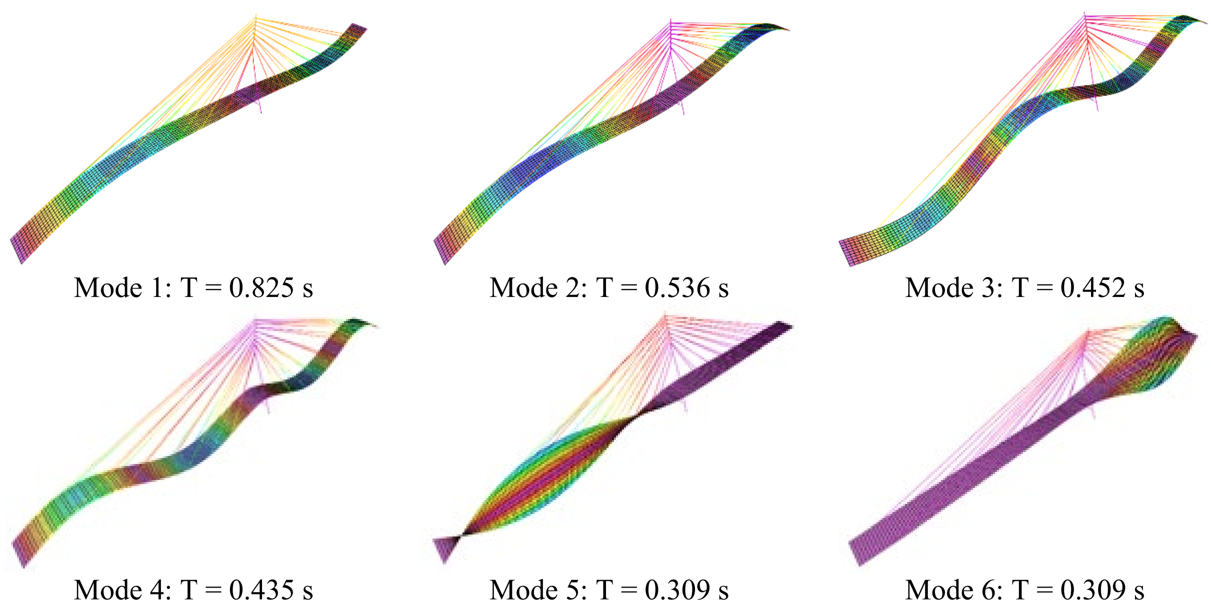

Figure 6.5 Mode shapes and periods of the cable-stayed bridge

Table 6.1 Test cases used in the data analysis

Label	Condition	Description
Undamaged states (# 1 to 4)		
State#1	Undamaged	Baseline condition
State#2	Undamaged	Added 8% additional mass uniformly on the bridge deck (static)
State#3	Undamaged	AASHTO HL-93 Design truck moving through the span (dynamic, v=10 m/s)
State#4	Undamaged	AASHTO HL-93 Design truck moving through the span (dynamic, v=20 m/s)
Damaged states (# 5 to 15)		
State#5	Damaged	10% reduction of cable area at the A4 (one side)
State#6	Damaged	20% reduction of cable area at the A4 (one side)
State#7	Damaged	30% reduction of cable area at the A4 (one side)
State#8	Damaged	40% reduction of cable area at the A4 (one side)
State#9	Damaged	50% reduction of cable area at the A4 (one side)
State#10	Damaged	20% reduction of cable area at the A2 (one side)
State#11	Damaged	20% reduction of cable area at the A6 (one side)
State#12	Damaged	40% reduction of cable area at the A2 (one side)
State#13	Damaged	40% reduction of cable area at the A6 (one side)
State#14	Damaged	40% reduction of cable area at the A4 (one side) + moving load (10 m/s)
State#15	Damaged	40% reduction of cable area at the A4 (one side) + moving load (20 m/s)

6.3.3 Uncertainty in Data Acquisition

Noise is a challenge for damage detection (Simonovski and Bolte 2003; Pakrashi et al. 2007); therefore, in this study, noise was added to the response of the bridge signals. Different noise levels were selected as the representative sensor data for the support vector machine (SVM) learning to check the sensitivity of the damage feature. The training data for SVM was simulated by adding different noises based on the signal to noise ratio (SNR) that represents the ratio of the signal strength to the background noise strength (Simonovski and Bolte 2003; Pakrashi et al. 2007). The SNR is usually described in dB scale as:

$$SNR_{dB} = 10\log_{10}\left(\frac{P_{\text{signal}}}{P_{\text{noise}}}\right) \tag{6-23}$$

where P_{signal} and P_{noise} are the average power of signal and noise, respectively. Five different levels of the SNRs were used in this study: 5dB, 10dB, 20dB, 40dB, and 50dB (see Figure 6.6). In addition, for each SNR level, 100 samples were selected to train the SVM model (4 cases×5 SNRs×100 samples=20000 signals in total). The final samples were separated randomly into two equal parts as training data and testing data. To prevent overfitting of the problem, the cross-validation procedure was used to get the effective estimation of the models, and the testing data was used to evaluate the performance of the machine learning algorithm. For simplicity, each group of samples was named in accordance with the feature extraction method and the level of the SNR. For example, 20-SNR-Wavelet denotes the data predicted by the wavelet with a value of SNR of 20dB, while 50-SNR-THT represents the data predicted by the THT method with a SNF of 50dB.

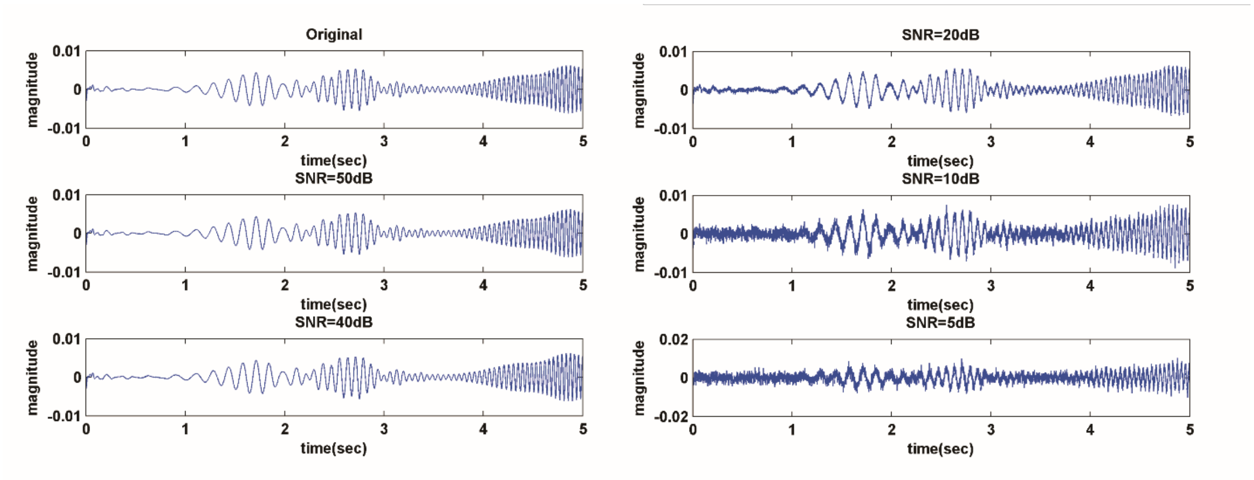

Figure 6.6 Framework of data-driven data mining process for SHM and damage detection

6.4 Data Analysis and Discussion

6.4.1 Features and Sensitivity

The sampling frequency of this model is 100Hz. A sweeping signal from 0 to 5 Hz is excited at the midpoint of the left span. The time-frequency representation of wavelet transform, Hilbert-Huang transform, and Teager-Huang transform under the sweeping signal are plotted in Figs. 6.7 (a)-(c). Clearly, for a regular signal, the THT, due to the high time resolution, has the highest concentration and has the fewest boundary effects as compared to other two methods. Although the Hilbert-Huang transform has similar sparse characteristics as that of the THT, the HHT still displays certain boundary effects under regular signals, as shown in Figure 6.7 (b). Apparently the wavelet has the highest boundary effects with a wide band. Further comparison of the time-frequency distribution predicted by the HHT and THT demonstrates that the THT is more sensitive to the change of the signal.

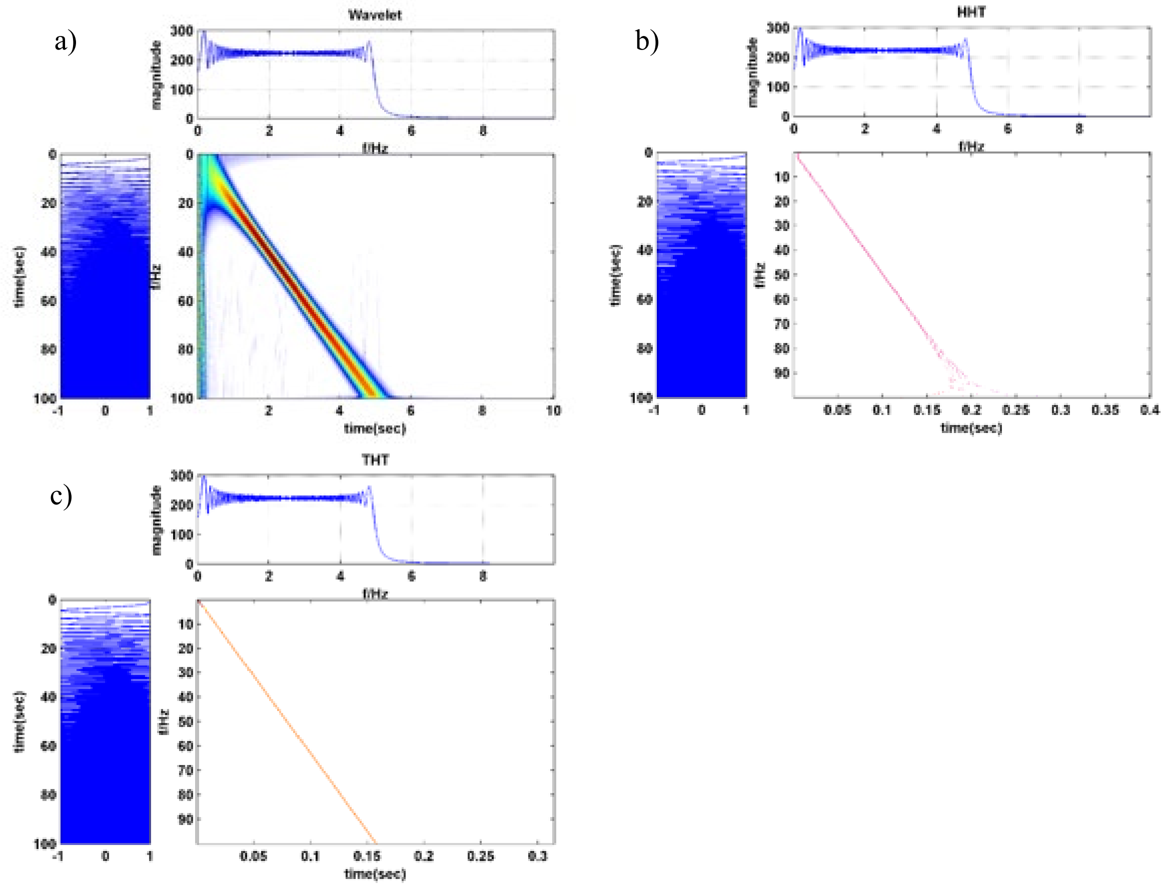

Figure 6.7 Input sweeping excitation forces under three different methods: (a)-(c)

The time-frequency plane is capable of providing more key information than that of the time-domain or frequency domain field. It is also more effective to track some sensitive features from this plane. The two-dimensional box is used to separate the damage sensitive features, as shown in Figure 6.8.

A feature selection process, the time-frequency box, was used to choose the best sensitive feature (Lin and Qu 2000). The concept of the feature selection process is based on counting the maximum number of the outline samples that exceed the 5% and 95% of the feature value at the baseline condition. This feature is also relevant to the main frequency and main time domain point, as reported in the literature (Lin and Qu 2000). The mean value of each box contained time-frequency representation point is used to eliminate the influence of noise in the signal as:

$$Feature_i = \frac{\sum_{i=1}^{N} TFR_i}{N} \qquad (6\text{-}24)$$

where the N is representing the number of time-frequency representation point. TFR_i is the time representation point in the time-frequency Figures 6.8 (a)-(c). The wavelet function is used in the wavelet transform. Different boxes through the whole time-frequency domain are used to select the damage features, as shown in Figure 6.8 (a). The box information represents all of the dynamic information of the response of the signal, and thus there will be eleven boxes covering all of the main frequency field. For the HHT and THT features in Figures 6.8 (b) and 6.8 (c), the selected box has some differences from the wavelet, and a total of thirteen parallelogram boxes have been selected. The average time-frequency representation point is greater than zero in the box and thus has been chosen as the damage feature as:

$$Feature_i = \frac{\sum_{i=1}^{N}(TFR_i > 0)}{N} \tag{6-25}$$

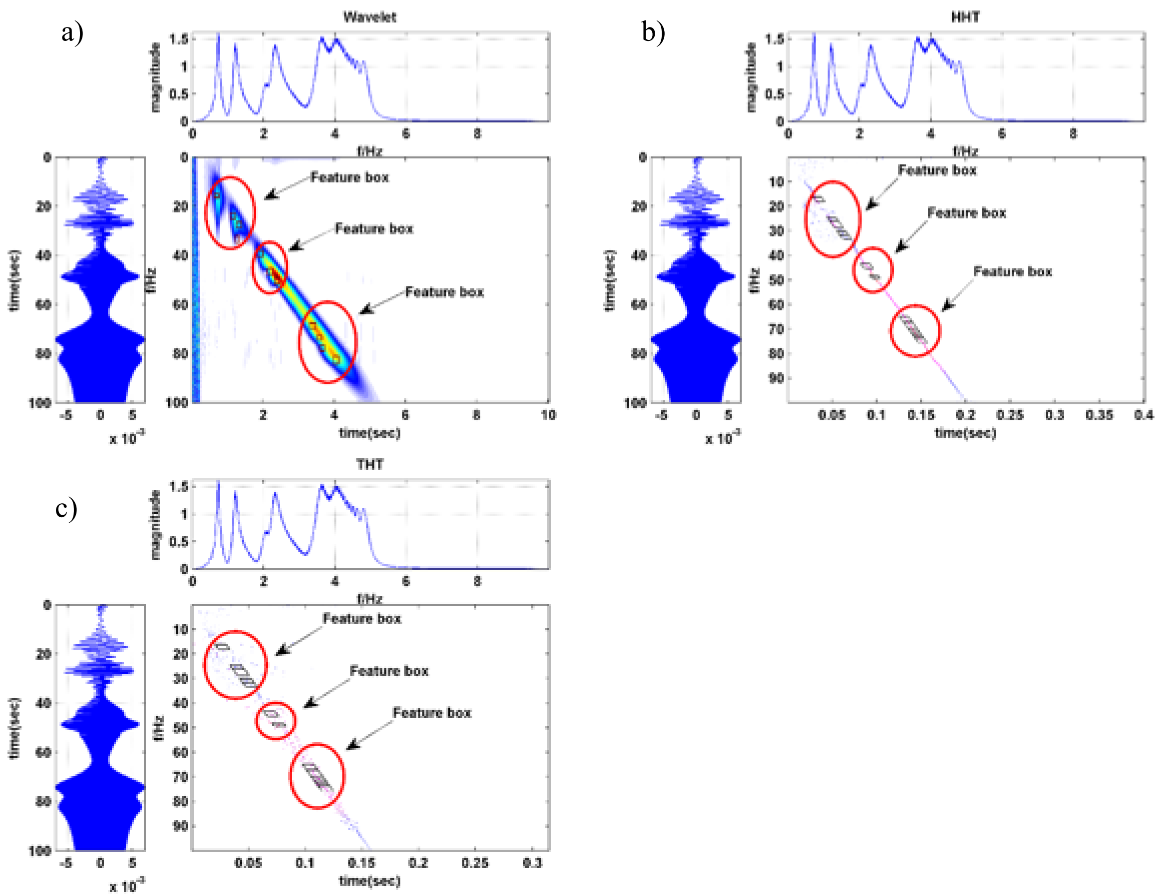

Figure 6.8 Feature extraction from time-frequency distribution planes: (a)-(c)

6.4.2 Effectiveness of Various Data Fusion Methods

To demonstrate the cost-effectiveness of each feature extraction in computation, the consumed time is determined under the identical situation using MATLAB software. Clearly, the wavelet has a computation time of 6.996 s, way longer than those of the HHT or THT by 0.775 s or 0.7201 s, respectively. As discussed previously in Section 2, the HHT and THT algorithms have great potential for data-driven time-frequency analysis, particularly in terms of a sparse feature and no limitation by Heisenberg uncertainty principle, and thus they perform approximately ten times faster than the wavelet algorithm. Note that such a comparison is only for the demonstration of time consumption by their nature under current identical computation capacity, and other resources could compensate for their computation capacity.

To better understand the performance of the machine learning techniques, the selection of effective and sensitive damage features is essential. A perfect damage sensitive feature is theoretically sensitive and robust to all kind of damages even under high variations and other interference. The data identification was demonstrated using a 3D scatter plot as shown in Figure 6.9, where red circles and blue stars denote individual specimens under damage and undamaged states, respectively. Note that the main feature of each feature extraction method should be constant when estimated based on the data obtained from the numerical model. However, the influence of the different ratio of noise and the presence of operational conditions as well as damage could make the data separate. As clearly illustrated in Figures 6.9 (a) through 6.9(i), all nine plots exhibit the significant difference in data trends that to allow for the clear identification of undamaged or damaged cases. The feature is expected to have different cluster accordingly. For example, for the case of 20-SNR-Wavelet shown in Figure 6.9, there exist four clusters, and each cluster is totally separated. Clearly when the SNR is under a certain level, three different feature extraction methods would help maintain a high sensitivity to the presence of damage. The cluster appeared for the wavelet method, as the SNR increased from 5 to 20 dB. In contrast, the clusters of the HHT and THT started as the SNR varies from 20 to 50 dB. That is, the wavelet has a lower divergent than the HHT and THT when the SNR is equal to the level of 20 dB.

The feature vectors were split in the test and training matrices. The training matrix was composed of different features from 50 out of 100 simulated signals, which had different noise levels of the SNR. Thus, for each SNR scenario, the training matrix with a dimension of $[Feature\ number] \times [Cases \times 50]$ was used for the SVM to discover the underlying distribution and dependency of all the damaged and undamaged states. During the testing process, the SVM was expected to detect the defects (reduction of cable stiffness herein) from the original conditions when the features are under Cases 5-13, even in the presence of operation effects.

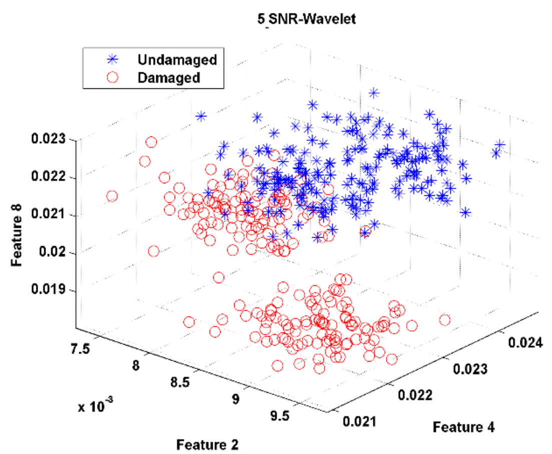

(a)

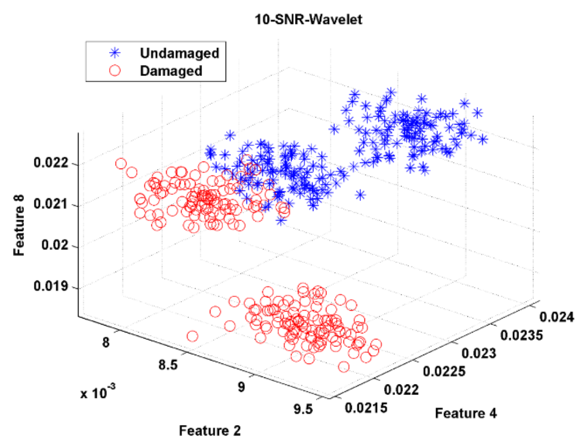

(b)

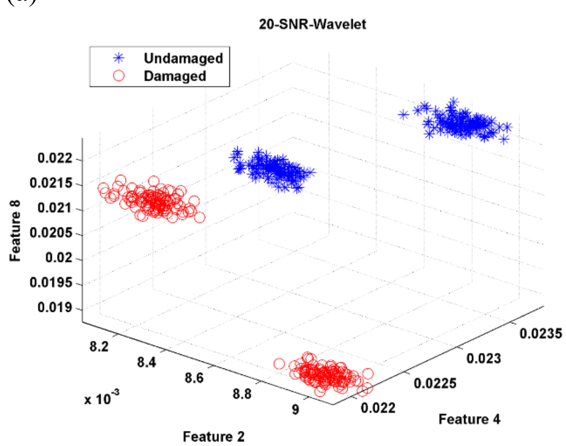

(c)

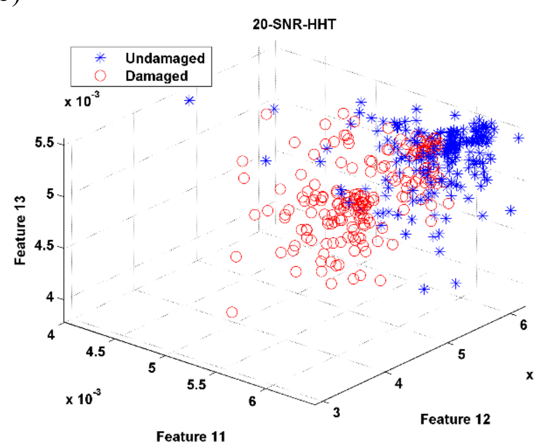

(d)

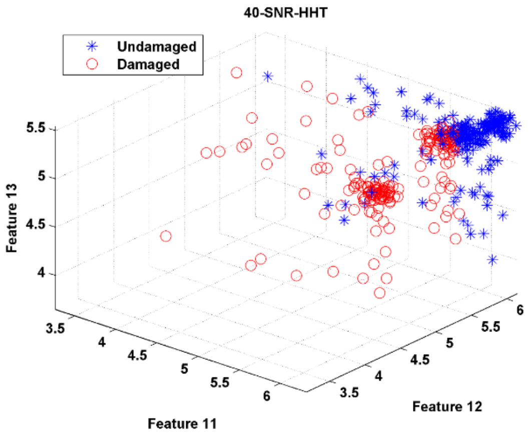

(e)

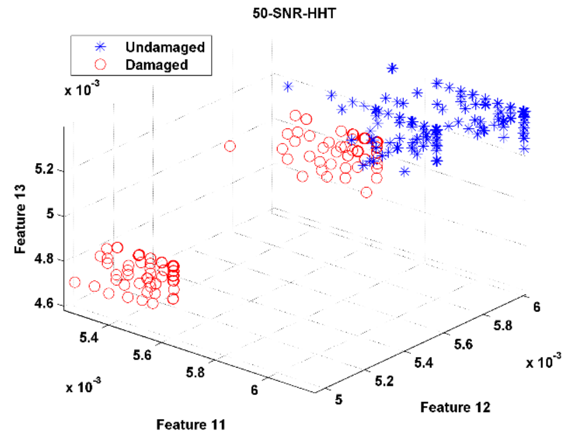

(f)

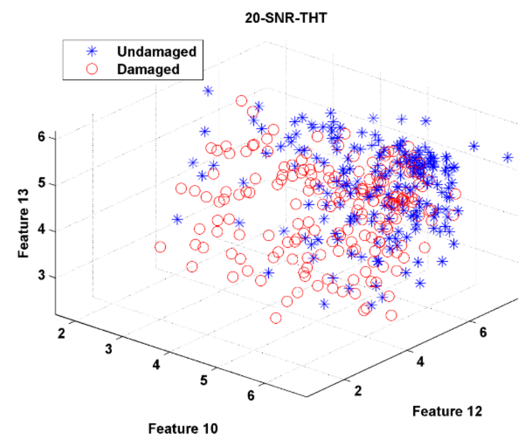

(g)

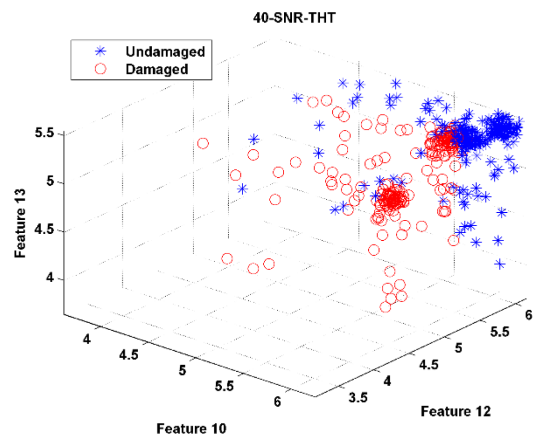

(h)

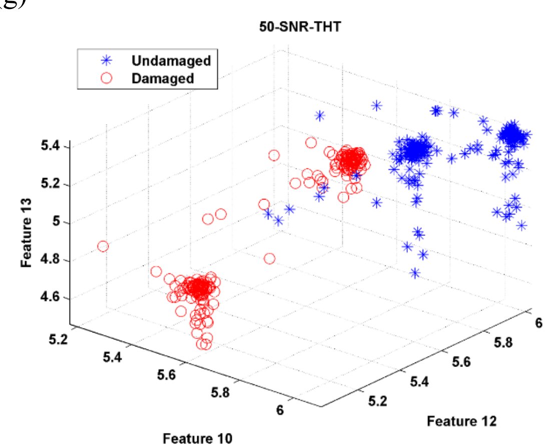

(i)

Figure 6.9 Scatter plots of three main features: (a)-(i)

To further verify the accuracy of the data-driven SVM method herein, the receiver operating characteristic (ROC) curve and the area under the curve (AUC) were used (Gui et al. 2017). Both methods also help to determine how accurate the proposed damage identification is for distinguishing between undamaged and damaged cases. The ROC curves of testing groups were plotted for all eleven cases, as shown in Figures 6.10 (a)-(c). Qualitatively, the wavelet-feature based curves go through the left-upper corner, suggesting that it has the best accuracy in damage classification when the SNR is larger than 20 dB, as shown in Figure 6.10 (a). The ROC curves demonstrated that the wavelet has better accuracy for distinguishing the damaged cases from undamaged data than those of the HHT and THT when the noise of signal is assigned as 20 dB. Figure 6.10 (c) shows that all of the damage features have greater accuracy when the SNR reaches up to 40 dB or larger. The plots also demonstrate that the wavelet feature extraction is less impacted by noise, and, moreover, performs better than THT with an SNR of 40 dB, even when the SNR in the wavelet method is equal to 10 dB.

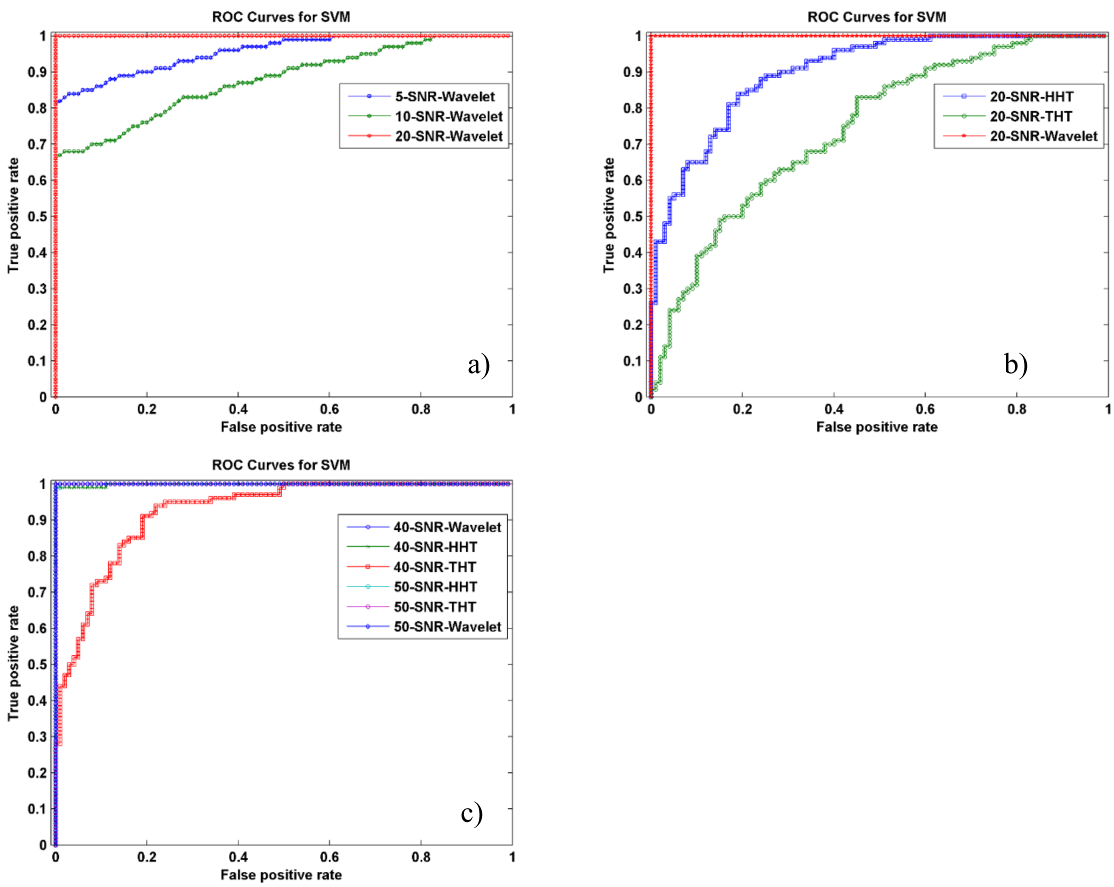

Figure 6.10 ROC curves for various SNR signals using different feature extraction method

Using the levels of the AUC as acceptance criteria has been widely accepted in clinical studies (Fan et al. 2006). The AUC values for each case are listed in Table 6.2, where the value of the AUC equal to one denotes a one hundred percent precise prediction and the predicted results will be unacceptable when the ROC curve has an $\mathrm{AUC} \leq 0.75$. As clearly illustrated in Figure 6.10 (c), the data predicted by the THT with a value of SNR of 20 dB will not be acceptable since it has a low value of $\mathrm{AUC} = 0.7344$, which is smaller than the threshold of 0.75. It is highlighted in red in Table 6.2.

Table 6.2 AUC values of different methods and various levels of the SNR

Signal to Noise Ratio (SNR/dB)	Algorithm		
	Wavelet	HHT	THT
5	0.9688	/	/
10	0.9792	/	/
20	0.9900	0.8912	0.7344
40	1.0000	0.9889	0.9134
50	1.0000	0.9899	0.99

6.4.3 Various Uncertainties for Data Fusion

From an engineering standpoint, engineers may be concerned about the effectiveness of the damage identification, at what levels the damages/defects are at, and the sensitivity of the techniques with regards to where the sensor should be placed. Therefore, a more parametric study was conducted herein and the discussions below are characterized by the major factors of interest, including the effects of damage level, damage location, sensor location, and moving load.

6.4.3.1 Effects of Damage Level on Data Fusion

As initially designed in Table 6.1, the introduction of stiffness degradation in stay cables was done by reducing the cross-sectional area of a cable from 10% to 50% to simulate various damage levels. The damage index (DI) is defined as the values from the feature vectors as follows:

$$DI_i = \sum_{i=1}^{N} \alpha_i * Label_i * Kernel(Fea_i, Feature_i) + b) \qquad (6\text{-}26)$$

where $Label_i$, α_i, b, $Feature_i$ are derived and selected as the support vector points from the training process.. Fea_i is the feature from the input data while $Feature_i$ is the resulting feature, as predicted by Eqn. (6-25). This index helps to assess the performance of the classifiers of the SVM with enhanced feature extraction methods. Figures 6.11 (a)- 6.11 (f) plot the DIs of different damage scenarios along with a threshold based on the 95% cut off of the baseline condition.

As shown in Figures 6.11 (a)-8(f), a threshold at 95% of the undamaged state in red dashed line is used for discrimination of the damage and undamaged states. Each slot represents a state as labeled in Figures 6.11 (a)- 6.11 (f) and defined in Table 1, while damaged states are plotted in red dots and undamaged ones in blue dots. Clearly, all the scenarios show a great classification performance, regardless of the different feature extraction methods. Specifically, the results in the THT and HHT methods exhibit clear discrimination between each damaged state and have apparently separable relationship between damaged and undamaged states, even under operational and environmental variability. As discussed early, the data classification could be a challenge with the increase of noise level, and as illustrated in Figure 6.11 (b), data points show much higher scatter due to the higher level of noise. Note that since the machine learning herein is a binary algorithm, the physical insights of each data cannot fully account for the levels of the damage. A further study is required in advanced machine learning to build up a stronger correlation of data with the physical characteristics of a structure system.

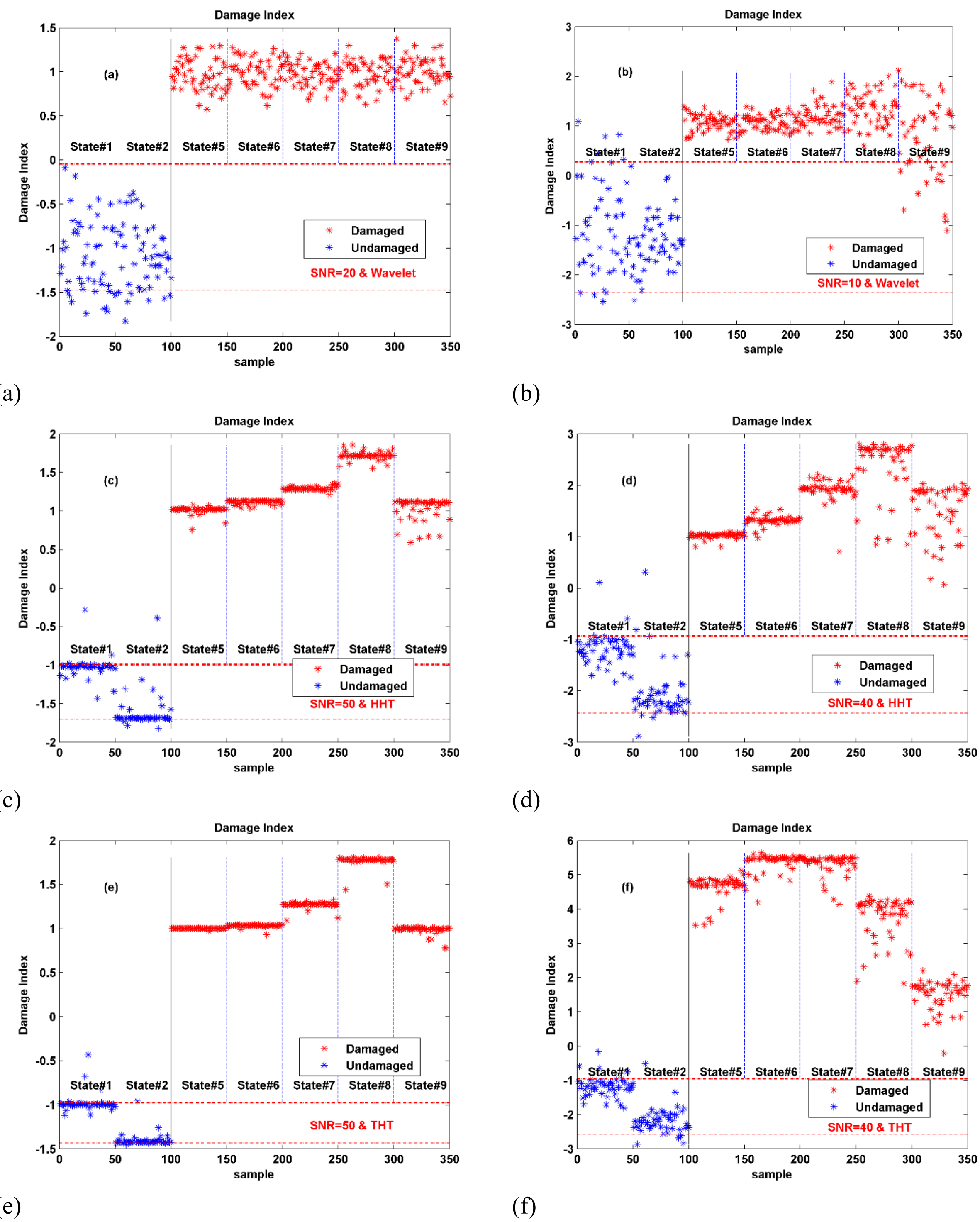

Figure 6.11 DIs from feature vectors under different damage levels: (a)-(f)

The performance of data-driven classification and the effects of damage levels on their effectiveness could be assessed by defining Type I and Type II errors (Figueiredo et al. 2011). Type I is defined as the false-positive classification while the Type II is defined as a false-negative one. From a system level, engineers could use the Type I more than the Type II. Table 3 summarizes the number of Type I and Type II errors for each algorithm. In an overall analysis, different feature extraction methods and SNR show a trade-off between Type I and Type II errors, with the THT-based algorithms having better performance for detecting damage (0.29% and 0.0%), and the HHT-based algorithms have a better performance for avoiding Type II error (0.0% and 0.0%).

6.4.3.2 Effects of Damage Location on Data Fusion

To demonstrate the damage distribution over span, six States #6, 8, and 10-13 were designed and organized to address the effects of damage locations under two different damage levels on data classification. The first set, States #6, 10 and 11, represents three damage locations at a quarter-span, mid-span, and three-quarter span, respectively, while the second set, States #8, 12 and 13, had a higher damage level of 40% cable stiffness reduction at the identical locations of the first set.

The result of the DIs of these scenarios are plotted in Figures 6.12 (a)-(f). Theoretically, the damaged location can lead to a change in frequency response. As a result, data exhibits a slightly higher variation due to different locations, particularly when exposed to different damage levels. A comparison of the three different damage locations revealed that the data at the quarter span exhibited a sparser scatter distribution than other two cases. In general, the selected chirp excitation includes a wide frequency band, hence being capable of capturing the response of different states easily by using the support vector machine learning.

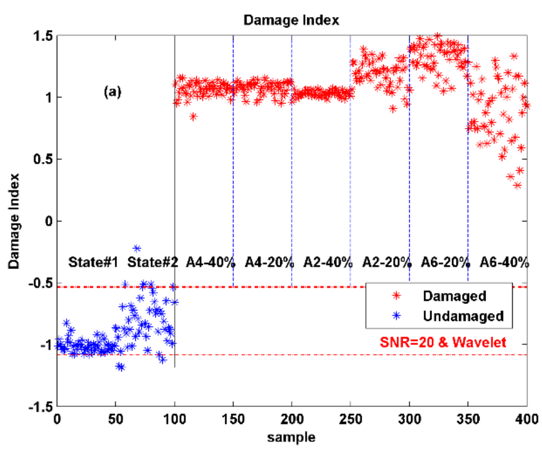

(a)

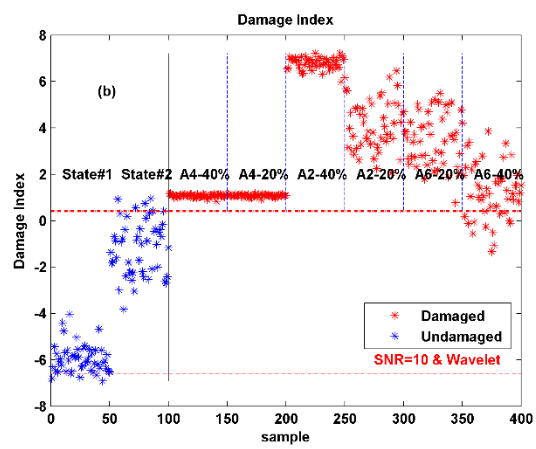

(b)

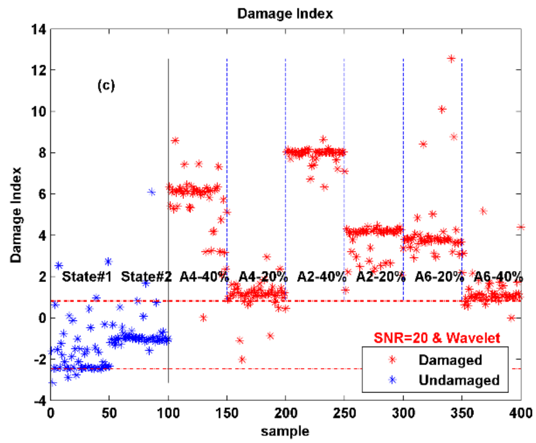

(c)

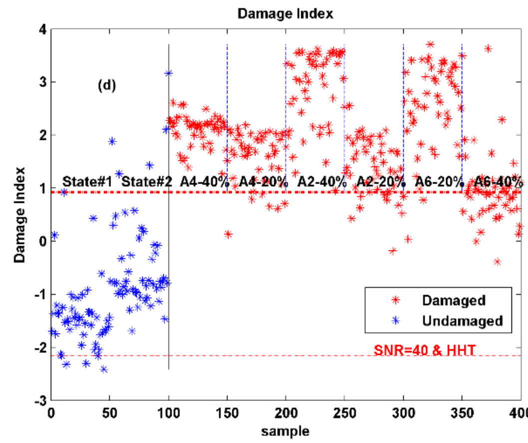

(d)

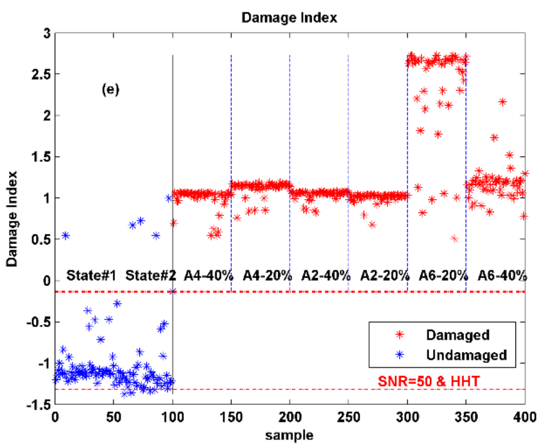

(e)

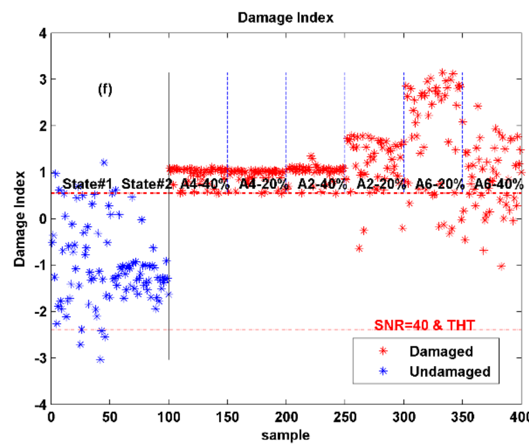

(f)

Figure 6.12 DIs from feature vectors under different damage locations: (a)-(f)

6.4.3.3 Effects of Sensor Location on Data Fusion

Another critical concern for the bridge engineering community is the sensor distribution. Logically, the closer the sensors are placed to the actual spots with damages/defects, the more sensitive the data should be for data identification. For a large-scale, cable-stayed bridge, it is impossible to spatially distribute a large amount of sensor nodes to each location. As a result, the reduction in the density of the sensor nodes could lead to missed readings of some of the damage-sensitive locations. Thus, the large-scale structure requires that the data captured from other locations will still be capable of ensuring an effective data classification.

To demonstrate the effectiveness of the proposed data-driven methods and address the effects of the different sensor locations, three different locations were selected from quarter span, mid span and three-quarter span, respectively, when subjected to the damage condition as discussed in States #5-9. Figures 6.13 (a)-(c) plot the DIs of the results from the three different sensor locations. Clearly, all of the cases exhibit separable relation for the damage cases from the undamaged ones, regardless of the different locations, thereby suggesting that the data classifiers could still maintain a higher prediction even at a location away from the damage spot. The reason behind this phenomenon is mainly because of the feature selection process. In this study, a feature selection method was used before the machine learning data process, while the trained features for all the cases were the highest separable data. Consider that the actual data in the field could be easily contaminated by complex operational conditions, where some dynamic information may disappear due to other localized interferences.

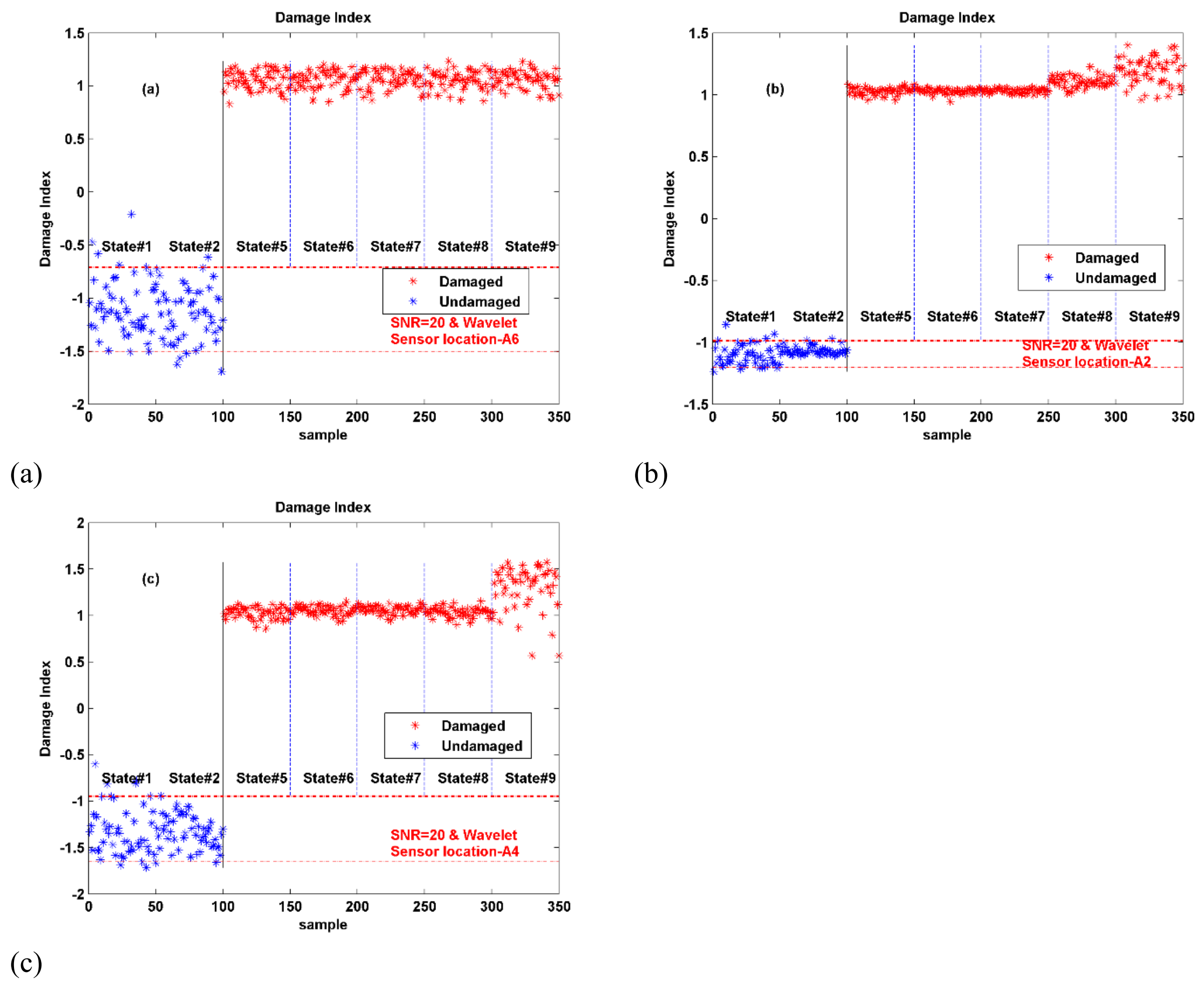

Figure 6.13 DIs from feature vectors under different sensor locations: (a)-(f)

6.4.3.4 Effects of Moving Vehicle Load on Data Fusion

Moving vehicles have been identified as excitation in the system identification and damage detection for bridges (Zhang et al. 2012; Zhu and Law 2015). The load of a moving vehicle may excite structural vibrations with large amplitudes and high signal-to-noise ratios (Zhang et al. 2012; Zhu and Law 2015). To discuss the effects of the moving vehicle on the data identification, States #14-15 were designed using the AASHTO HL-93 design truck with two speeds as compared to the baselines at States #3 and #4. For simplicity, only the results using machine learning with the wavelet transform are presented here. It can be envisioned that the major trends of the effectiveness by other two methods will be identical to the early observation in the previous sections.

Bridge responses, including dynamic displacement, velocity, and acceleration at the mid span of the first span, are plotted in Figure 6.14. Clearly, dynamic characteristics of the cable-stayed bridge under two speeds have no high variation. In addition, from the point-of-view of the dynamic response caused by moving vehicle, there is no clear separable relation between damaged and undamaged cases, as reported in the literature (Zhang et al. 2017). It is partially because the reduction of single cable stiffness may not be sensitive to the dynamic response of the whole, large-scale bridge.

Interestingly, the DIs of the results using the support vector machine learning, illustrated in Figures 6.15(a) and 6.15(b), revealed that the classifiers still have a high ability to ensure the identification of damaged and undamaged cases, even under the noise level of 20 dB.

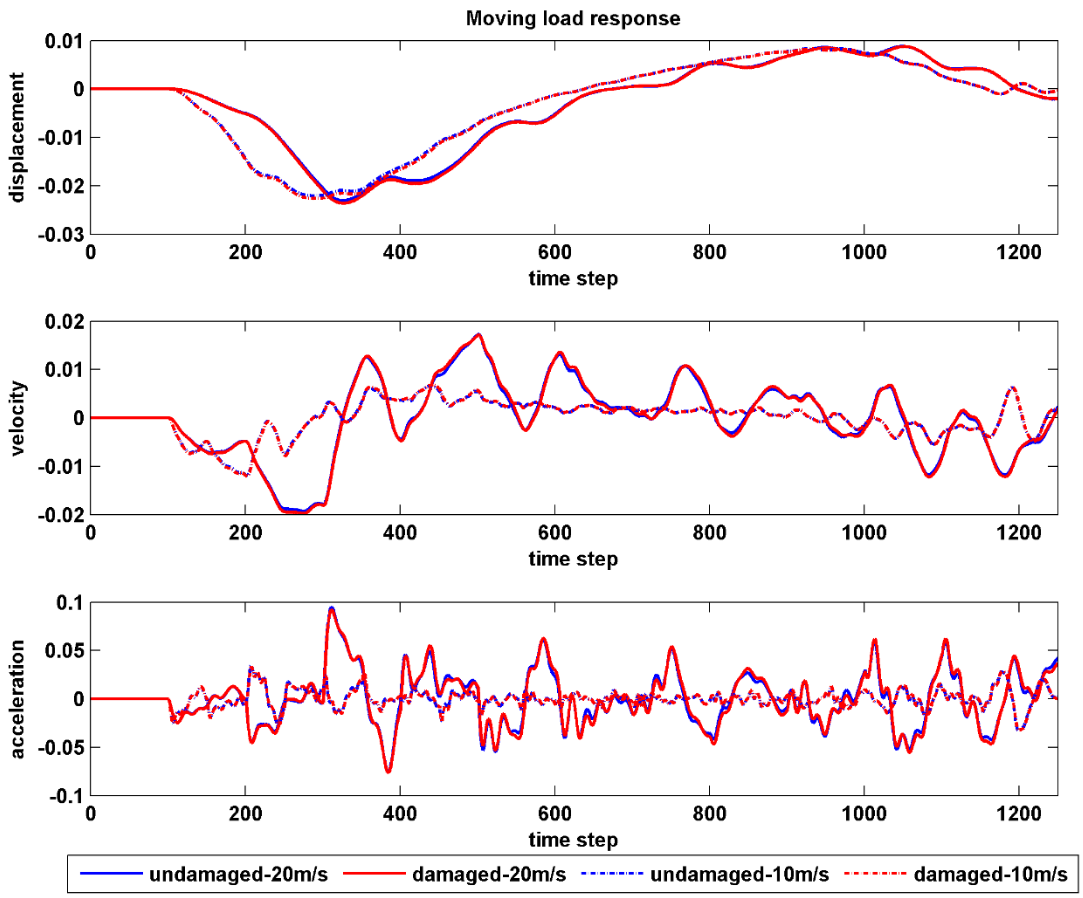

Figure 6.14 DIs from feature vectors under different sensor locations: (a)-(f)

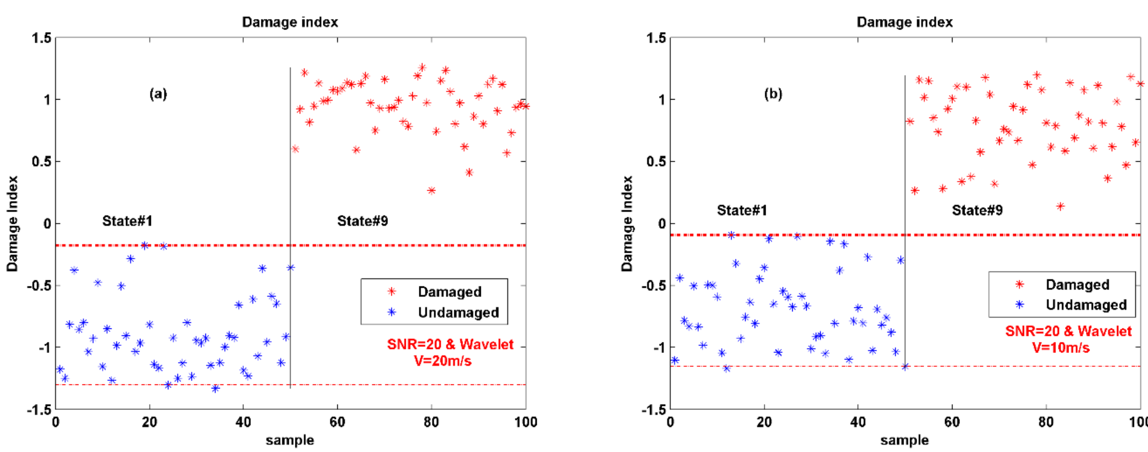

(a) (b)

Figure 6.15 DIs for the cases of the wavelet transform under moving loads: (a)-(b)

6.5 Summary

This chapter aimed to present a time-frequency based data fusion and information process for sensory data that are often collected in detailed inspection. Three representative, feature extraction techniques were selected to enhance the features extraction for sensor data, while the kernel function based SVM was used to facilitate pattern recognition and improve the identification of damaged and undamaged cases. The time-frequency analysis revealed that different data-driven algorithms demonstrated advantages in different aspects. The strategies developed were finally illustrated through a case study. The ROC curves and AUC values were used as tools to quantify the accuracy of the optimization based SVMs. A further parametric study was conducted to address some major concerns for practical applications in cable-stayed bridges. In summary, conclusions can be drawn as follows:

a) The data-driven damage detection techniques exhibit high accuracy for distinguishing between undamaged and damaged cases, even when there are certain noise interferences, as well as operational conditions.
b) The time-frequency analysis is effective for damage detection in that the time-frequency analysis is more sensitive to damage, when its dynamics change from different state. In addition, the change of the dynamic characteristic of the bridges has an influence on the time-frequency plane, which provides more key information than just the time or frequency domains. Accordingly, using data-driven machine learning can lead to a high classification accuracy in time series.
c) Results have demonstrated the importance of the selection of damage features techniques for damage detection. Clearly, the wavelet transform has significantly higher accuracy in noise interference than that of the HTH and THT. The THT is the best algorithm for the data analysis of regular signals, but for irregular signals, it has a poor performance, as it has higher sensitivity to local fluctuation. Furthermore, the ROC curves and value of the AUC confirm that the wavelet transform behaves as a filter in the lower frequency part, and thus leads to more reliable data identification as compared to other two techniques.
d) The computation time is key for the data process, and this study shows that the THT and HHT are almost ten times faster than the wavelet transform, which will be extremely important for processing the massive amounts of data captured from large-scale, cable-stayed bridges in practice.
e) An extensive parametric study reveals that the data-driven classification could effectively address the major factors of interest, including effects of damage level, damage location, sensor location, and moving load. The results in the THT and HHT methods exhibit clear discrimination between each damaged state, even under operational and environmental variability. The damage indexes of the results under moving vehicle revealed that the classifiers still perform at a high level and ensure the identification of damaged and undamaged cases, even under the noise level of 20 dB.

7. UNVEILING AND REDUCTION OF STRUCTURAL UNCERTAINTY IN IN-DEPTH/SPECIAL/DAMAGE INSPECTION

7.1 Background

In this chapter, the deep Bayesian belief network (DBBN) learning was used to extract structural information and probabilistically determine structural conditions. Different from conventional shallow learning that highly relies on the quality of the hand-crafted features, the deep learning is an end-to-end method to encode the information and interpret vast amount of data with minimal or no features. A case study was conducted to address the methods for structure under viabilities and uncertainties due to operation, damage and noise interferences.

7.2 Structural Uncertainty

7.2.1 Nonlinear System for Bridges

Bridges are dynamic complex systems that are designed to withstand different types of loads, but they are usually vulnerable to damage and degradation over time (Lin et al. 2012; Lin et al. 2013; Lin et al. 2014). The structural health monitoring (SHM) is often framed using various sensors to collect performance data for health assessment and decision-making (Sohn et al. 2001; Worden et al. 2007; Farrar and Worden 2007; Kaveh et al. 2015). For a linear or linearized dynamic system, the linear dynamic response could be derived from the continuous stochastic state-space model by a linear form,

$$\dot{\boldsymbol{q}}(t) = \boldsymbol{A}\boldsymbol{q}(t) + \boldsymbol{B}u(t), \tag{7-1}$$

where, $\boldsymbol{A}$ and $\boldsymbol{B}$ are related to mass and stiffness matrix of the system. As such, system identification or other physics-based methods could be used to inversely determine structural health state. However, such data interpretation will be not straightforward, as the structural systems are inherently nonlinear under various uncertainties, while the general state space in Eqn. (7-1) should be revised as:

$$\dot{\boldsymbol{q}}(t) = f(\boldsymbol{q}(t), t) + g(t)u(t), \tag{7-2}$$

where $f(\cdot)$ and $g(\cdot)$ represent nonlinear functions. Clearly, nonlinearities post great challenges to find any close-form analytical solutions or difficulty even in numerical simulation due to the high level of variability in noise and other interferences, and high uncertainties associated with unclear excitation, boundary, and operational conditions.

The machine learning techniques (Ko and Ni 2005; Rashedi and Hegazy 2015; Gerist and Maheri 2016; Jang 2016; Gui et al. 2017; Pan et al. 2017) in recent years have been gaining increasing attentions due to their merits as data analytics to overcome conventional physics-based methods by extracting statistical information from data with less prior physics inputs. This is particularly important for those complex structures under high uncertainties of interest. The machine learning in general can be categorized as shallow learning, deep learning, and reinforcement learning.

The shallow learning techniques include random forest, decision trees, kernel-based support vector machine (SVM) (Oh and Sohn 2009; Farrar and Worden 2013; Gui et al. 2017; Pan et al., 2017), and Navie Bayes. The shallow learning is widely used as effective tools for structural engineering, particularly in data classification for damage detection (Farrar and Worden 2013; Gui et al., 2017; Pan et al., 2016 and 2017) or optimization analysis (Bennett and Demiriz, 199; Shawe-Taylor and Sun, 2011). From the point-of-view of learning architecture, the shallow learning, such as the SVM or conventional artificial neural network, uses one or zero hidden layers for a shallow linear pattern separation, while the deep learning algorithms are framed by a deep architecture using multiple hidden layers to extract more complex nonlinear representation (Deng and Yu 2014). The shallow learning relies heavily on the quality of the hand-crafted features, suitable for well-constrained cases (Deng and Yu 2014; Pan et al. 2016a; Zhao et al. 2015). The deep learning, however, is an end-to-end method to interpret vast amounts of raw data with little or no predetermined feature extraction and to decode the high-order information. As such, the deep learning is more flexible for handling complex representations from big datasets collected from real-world applications. The deep learning algorithms currently include deep neural networks (Vesely et al. 2013), deep belief network (Hinton et al. 2006 and 2012) and Convolutional neural networks (Zeiler 2014), each of which differs in its applicability.

From the probabilistic standpoint, the Bayesian network models are effective graphic models for representing a set of random variables and discriminating their conditional dependencies (Masri et al. 2000). The Bayesian-based deep learning developed as probabilistic generative learning for diverse applications in civil engineering, including traffic control and damage detection (Hinton et al. 2006; Hinton et al. 2012; Zhao et al. 2015). There are few documents about these methods in structural conditional assessment and structural diagnostics, particularly about how to effectively design the learning architecture with risk-based applications to engineering structures under uncertainties.

This chapter aims to use the deep Bayesian belief network (DBBN) learning as probabilistic learning for determining structural conditions, thus enabling timely decision making for civil engineering structures under uncertainties. Learning architecture and layers as key information were further discussed. A case study was selected and modified to demonstrate the effectiveness of the methods for civil engineering structure under viabilities and uncertainties due to operation, damage, and noise interferences.

7.2.2 Data-Driven Structural Conditional Assessment

Effective damage detection of structures and the correlation of damage with structural conditions are difficult. This is because civil, mechanical, and aerospace engineering structures under in-serve stages are inherently nonlinear with high uncertainty. The sensory data associated with structural response are usually collected by assessing the structural state in the SHM. As illustrated in Figures 7.1(a) and 7.1(b), the shallow and deep learning algorithms (Zhao et al. 2015), as branches of the machine learning, have effective classifiers able to handle and analyze the sensory data. Clearly, prior to data training and testing, shallow learning requires feature extraction (hand-crafted features) and/or feature selection in the learning process, as shown in Figure 7.1(a). The schematics of deep learning, presented in Figure 7.1(b), show that the deep learning architecture is constructed by stacking multiple layers for raw data mining. More formally, deep learning contains implicit feature extraction and/or automatic feature selection through the layers. Note that the training of such deep learning architecture still demands considerable and wise design (Deng and Yu 2014). Some comprehensive reviews have been reported (Hinton et al. 2006; Zhao et al. 2015), and the interested readers are referred to the review paper by Zhao et al. (2015), where there is a great demonstration of the difference between shallow learning and deep learning. The review below is mainly focused on the typical shallow learning, SVM, and the deep belief network.

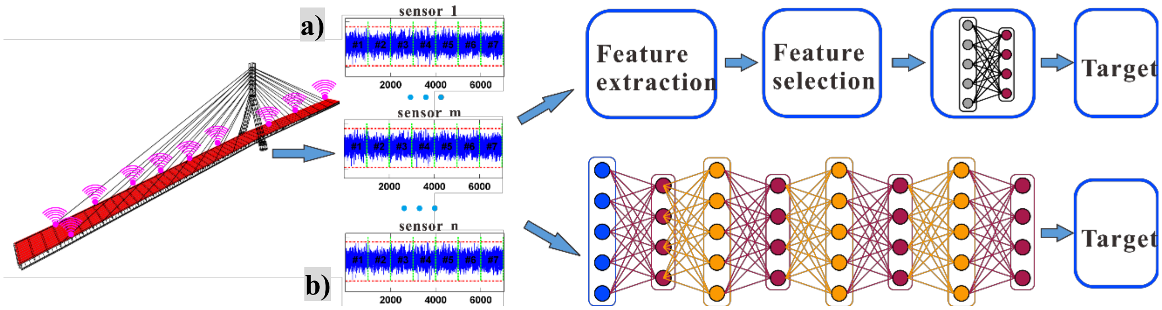

Figure 7.1 Schematics of (a) shallow and (b) deep learning (modified from Zhao et al. 2015)

7.2.2.1 Support Vector Machine (SVM) with a Shallow Architecture

Many of the data classification algorithms are shallow architecture. Among them, the SVM is the most successful method used for damage detection and fault diagnosis in civil, mechanical, and aerospace engineering (Ko and Ni 2005; Farrar and Worden 2013; Rashedi and Hegazy 2015; Gerist and Maheri 2016; Jang 2016; Gui et al. 2017; Pan et al. 2017). The SVM is one of the linear classifiers in a wide variety of damage detection applications, and it attempts to discriminate the datasets by mapping them in a new, high-dimensional kernel space with a maximal margin on a decision function by the form:

$$f(x) = sign(\sum_{i=1}^{N} \alpha_i y_i K(x, x_i) + b) \qquad (7\text{-}3)$$

where the $K(x, x_{\mathrm{i}})$ is the kernel function, and the three commonly used types are listed below (Santos et al. 2016):

a) the Gaussian radial basis function (RBF):

$$K(x, x_{\mathrm{i}}) = \exp(-\gamma \|x_i - x\ \|^2), \quad \gamma > 0 \qquad (7\text{-}4a)$$

b) the polynomial function:

$$K(x, x_i) = (\langle x, x_i \rangle + 1)^p \qquad (7\text{-}4b)$$

c) the sigmoid function:

$$K(x, x_i) = \tanh(\langle x, x_i \rangle + 1) \qquad (7\text{-}4c)$$

In general, these three kernel functions, shown in equations (7-4a) to (7-4c), tend to construct a higher dimensional feature space and allow data projection for this hyperplane(s) to achieve being linearly separable (Hofmann 2006). These different kernel functions have their own applicability, including computation costs and parameter tuning. As a result, the toughest challenges in the SVM (or other kernel-based shallow learning) lie in the selection of kernel functions and the determination or tuning of the kernel parameters (Santos et al. 2016). The model performance could depend on the datasets and lie in the complexity of the targeted structures. For example, a wide variability of kernel parameters (e.g., sigma and epsilon) in the RBF could significantly alter the performance (Gui et al., 2017), while the polynomial kernel may require multiple computation efforts in a trial-and-error manner.

7.2.2.2 Deep Learning, and Deep Bayesian Belief Network

Deep learning, as a branch of machine learning, stems originally from the artificial neural networks with one shallow, hidden layer architecture (Zhao et al. 2015). The deep learnings are constructed by stacking multiple layers in hierarchical architectures (Mohamed et al. 2012), as illustrated in Figure 1(b). The deep architectures (Hinton et al. 2006; Hinton et al. 2012; Zhao et al. 2015) exhibit their merits over their counterparts (e.g., shallow learning), as they attempt to find statistical representations based on end-to-end decoding without applying any preprocessing (predetermined features) nor applying any post-processing (feature extraction and/or feature selection). Deep learning has been successfully adopted in diverse fields, including image processing, speech recognition, audio recognition, and bioinformatics. On the other hand, the Bayesian belief network (BBN) is used to determine the state probabilities of each variable from the predetermined conditions or prior probabilities. The belief in node *A* is given by propagating the influence of the evidence at *E* through the network, and the mixing weight used in integrating the results for each value of *A*. The conditional probability can be described by using Bayes' rule (Krieg 2001; Chaturvedi et al. 2016):

$$P(a|e) = P(e|a)P(\mathrm{a}) \qquad \text{(5a)}$$

and the learning architecture of stochastic binary variables between layers ***v*** and ***h*** through the energy-based method using Boltzmann machine (Hinton et al. 2006; Hinton et al. 2012):

$$E(\boldsymbol{v},\boldsymbol{h}) = -\sum a_i v_i - \sum b_j h_j - \sum h'_j W v_i - \sum v'_i U v_i - \sum h'_j V h_j \qquad \text{(5b)}$$

where *a* and *b* are the biases of the stochastic variables ***v*** and ***h***, respectively; *W*, *U*, *V* are the weights of each connection; and the joint states of *v'* and *v (or h'* and *h*) denote the adjacent connection of the variables within a layer. As illustrated in Figure 7.2, the deep Bayesian belief network (Zhao et al. 2015; Chaturvedi et al. 2016) is a multiple layer, neural network. This model is effective in performing top-down as well as bottom-up generative weights, which enables back propagation for fine-tuning for optimized discrimination/regression.

To sum up, when considering an engineering structure with high uncertainties due to various operational and environmental factors, noise, and other interferences, the SVM algorithms may not be enough to extract proper information. The SVM is a binary algorithm which cannot directly provide the probabilistically conditional classifications that engineers mostly pay attention to, though there are some attempts at using the multi-class SVM. In addition, noisy datasets could post significant challenges in the quality of the data classification in both training and testing. Moreover, similar to other shallow learning algorithms as schematically demonstrated in Figure 1(a), the SVM requires the construction of hand-crafted features, even though these hand-crafted features may not guarantee their quality for better data classification in all cases. Different from the shallow learning, the merits of the DBBN include flexible modeling using the neural network, multiple non-linear hidden layers, and pre-training using lower layers as input (Hinton et al. 2012). Thus, in this study, we selected the DBBN for data classification and merits for probabilistically conditional assessment. For a comparison, the SVM with the Gaussian kernel in Eqn. (4a) was used as the kernel function to demonstrate differences to deep-based learning.

7.3 Deep Bayesian Belief Network for Probabilistically Conditional Assessment

The DBBN are constructed using multiple, restricted Boltzmann machines (RBMs) (Hinton et al. 2006; Hinton et al. 2012; Zhao et al., 2015). As schematically illustrated in Figure 7.2, the architecture of the DBBN consists of undirected multiple levels of the RBMs, where the hierarchical architecture should allow for the automation of feature extraction from lower to upper layers, and the final layer could be constructed using a different activation function for either classification or logistic regression of interest.

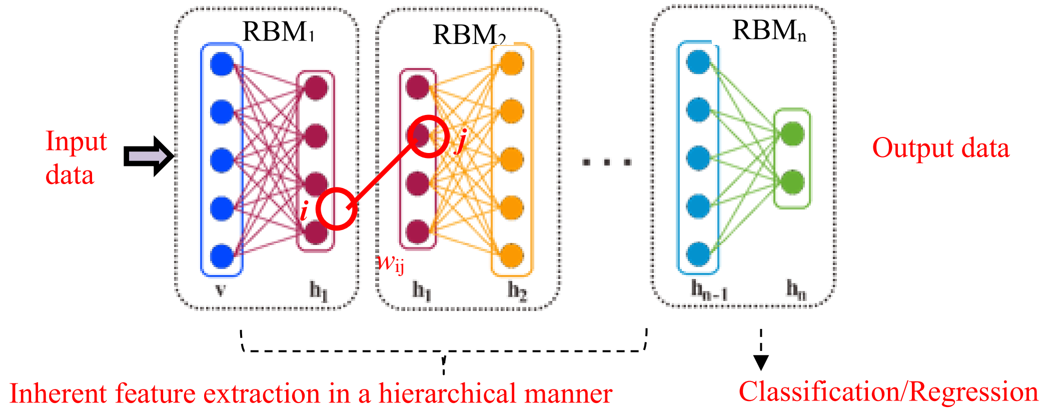

Figure 7.2 Architecture of the DBBN

7.3.1 Concept of the RBM and Its Architectures

To avoid the complexity and difficulty in determining parameters in Boltzmann machine, as shown in Eqn. (5b), the RBM was developed by an undirected graphical machine without visible-visible or hidden-hidden connections (Mohamed et al. 2012). Take one unit of the RBM (e.g., RBM_1 in Figure 7.2) as an example, the visible variable, v_i, and the hidden variable, h_j, are connected and assigned by a weight, w_{ij}. The probability of the joint states to the visible and hidden vector is defined by the energy-based function (Hinton et al. 2006; Hinton et al. 2012)

$$p(\boldsymbol{v},\boldsymbol{h}) = \frac{e^{-E(\boldsymbol{v},\boldsymbol{h})}}{\sum_{i=1}^{V}\sum_{j=1}^{H} e^{-E(\boldsymbol{v},\boldsymbol{h})}} \tag{7-6}$$

where $\sum$ is the summation over all visible and hidden variables and the $E()$ is the energy-based function, as typically defined in Eqns. (7-7a)-(7-7c). Considering that the structural data of interest could be binary data, such as black or white color in image recognition, or be more complex sensory information, three different data types (either in visible or hidden layer) were defined as follows (Hinton et al. 2010):

a) Binary data unit at both visible and hidden layers

There were no visible-visible or hidden-hidden connections (adjacent connection within a layer). Thus, the learning architecture over the joint states of the visible and hidden units, v and h ($\boldsymbol{v},\boldsymbol{h} \in \{0,1\}$), can be reduced from Eqn. (7-5b) to the form:

$$E(\boldsymbol{v},\boldsymbol{h}) = -\sum_{i=1}^{V}\sum_{j=1}^{H} w_{ij}v_i h_j - \sum_{i=1}^{V} a v_i - \sum_{j=1}^{H} b_j h_j \tag{7-7a}$$

b) Gaussian data at visible layers and binary data unit at hidden layers

Considering the data in input visible units have the Gaussian distribution and stochastic binary values at the hidden units, Eqn. (7-7a) could be rewritten with the standard deviation, σ:

$$E(\boldsymbol{v},\boldsymbol{h}) = -\sum_{i=1}^{V}\sum_{j=1}^{H} \frac{v_i}{\sigma_i} w_{ij}h_j - \sum_{i=1}^{V} \frac{(v_i - a_i)^2}{2\sigma_i^2} - \sum_{j=1}^{H} b_j h_j \tag{7-7b}$$

c) *Gaussian data at both visible and hidden layers*

When both visible and hidden units satisfy the Gaussian distribution which are more common in the sensory data collected from structural systems, Eqn. (7-7a) can be further revised by:

$$E(\boldsymbol{v}, \boldsymbol{h}) = -\sum_{i=1}^{V}\sum_{j=1}^{H}\frac{v_i}{\sigma_i}w_{ij}h_j - \sum_{i=1}^{V}\frac{(v_i-a_i)^2}{2\sigma_i^2} - \sum_{j=1}^{H}\frac{\left(h_j-b_j\right)^2}{2\sigma_j^2} \qquad \text{(7-7c)}$$

where *V* and *H* denote the numbers of visible and hidden variables, respectively; w_{ij} denotes the weight between visible unit i and hidden unit j, respectively; the variables, b_i and a_j, denote the bias terms, respectively. Thus, the learning process is achieved by minimizing the energy in Eqn. (7-7) by a log-likelihood gradient (Hinton et al. 2010; Zhang and Zhao 2017):

$$\Delta w_{ij} = \frac{v_i}{\sigma_i}\frac{h_j}{\sigma_j}_{data} - \frac{v_i}{\sigma_i}\frac{h_j}{\sigma_j}_{reconstruction} \qquad \text{(7-8a)}$$

and the updating of the biases during the learning is:

$$\Delta a_i = \frac{v_i}{\sigma_i}_{data} - \frac{v_i}{\sigma_i}_{reconstruction} \qquad \text{(7-8b)}$$

$$\Delta b_i = \frac{h_j}{\sigma_j}_{data} - \frac{h_j}{\sigma_j}_{reconstruction} \qquad \text{(7-8c)}$$

The conditional distribution, $p(h|\boldsymbol{v})$ and $p(v|\boldsymbol{h})$, are derived using Gibbs sampling associated with no hidden-hidden connections and no visible-visible connections, respectively. An RBM can be achieved by obtaining the weights from learning, which can be used in the input layer for the next module in the same manner. Note that the conventional concept of the maximum likelihood learning is used as the criterion in this study, but there are other criteria, such as maximum entropy (Lin et al. 2016), which have been proposed.

7.3.2 Concept of the DBBN and Its Architectures

As illustrated in Figure 7.2, the DBBN is constructed by a stack of multiple RBMs. Let one visible unit and the *N* hidden units, and the probability to the joint states is expanded from Eqn. (7-5a).

$$p\left(\boldsymbol{v}, \boldsymbol{h^1}, \boldsymbol{h^2}, \ldots, \boldsymbol{h^N}\right) = p\left(\boldsymbol{v}\middle|\boldsymbol{h^1}\right)p\left(\boldsymbol{h^1}\middle|\boldsymbol{h^2}\right)\cdots p\left(\boldsymbol{h^{N-2}}\middle|\boldsymbol{h^{N-1}}\right)p\left(\boldsymbol{h^{N-1}}\middle|\boldsymbol{h^N}\right) \qquad \text{(7-9)}$$

where $\boldsymbol{h^i}$ denote the i^{th} hidden variables. The learning process of the DBBN, illustrated in Figure 7.2 or Eqn. (7-9), is to maintain the first $p\left(\boldsymbol{v}\middle|\boldsymbol{h^1}\right)$ at the first RBM layer, and train the learning network using the next level RBM. As such, the flowchart of the DBBN is summarized in Figure 7.3. Clearly, the DBBN is to be achieved using pre-training layer by layer in the sequence (also see Figure 7.4a) in such way that the higher-layer RBM is trained using the lower-layer learned RBM with the values of its hidden units as its input vectors (Jiang et al. 2016). The higher-layer output will then be used as the input for the next higher layers. Thus, the concept of the DBBN tends to capture statistical information from each level of the RBM (Hilton 2006). With the pre-training steps shown in Figure 7.4(a), the back-propagation (BP) technique (Wang et al. 2016), illustrated in Figure 7.4(b), was utilized as a classifier to finely tune the weights and biases until full optimization, as detailed elsewhere (Hilton 2006 and Hilton et al. 2010).

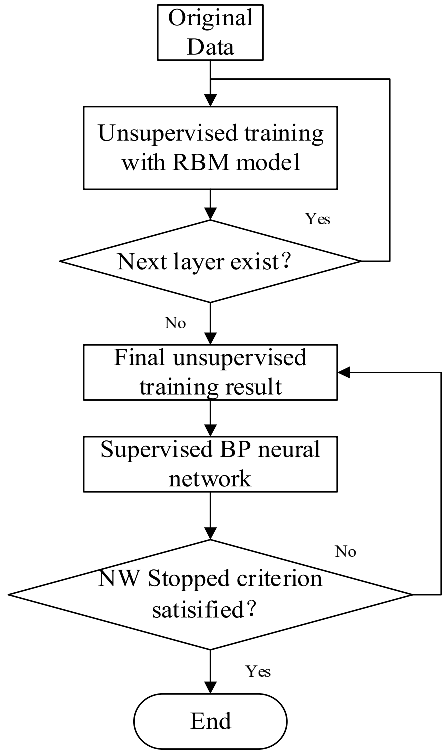

Figure 7.3 Flowchart of the training and testing in the DBBN

7.3.3 DBBN-Based Data Classification and Probabilistically Conditional Assessment

The key purpose of the components in SHM for a structural system are to detect damage and classify the severity of the damage. By choosing different deep architectures, the DBBN-based framework can accomplish these tasks, being particularly effective in assessing the complex structural conditions with high uncertainties that usually challenge the conventional, shallow learning.

a) DBBN-based data classification

Figure 7.2 illustrates the frame of the DBBN. The features automatically extracted from the stack of the multiple deep layers will be classified by the softmax function (Hilton 2010), $S(h)$, in the final layer that discriminates the data in a binary state:

$$S(\boldsymbol{h}) = \begin{cases} 0 & if\ h_j \neq 1 \\ 1 & if\ h_j = 1 \end{cases} \tag{7-10a}$$

b) DBBN-based probabilistically conditional assessment

The probabilistic framework of the DBBN is to set up its multiple, higher layers to graphically correlate the hidden structural information of the data that are collected from engineering structures under uncertainties to probabilistically assess structural health and conditions. As such, the softmax function *S*() ($\in \{0, 1\}$) is defined by the logistic sigmoid function (Hilton 2010):

$$S(\boldsymbol{h}) = \frac{1}{1+\exp(-h_j)} \tag{7-10b}$$

Some researchers (Larochelle and Bengio 2008; Lin et al. 2016) argue that the depth of the deep learning may not guarantee the statistical representation needed from higher layers [e.g., over-trained status or issues related to supervised BP learning tasks from upper layer(s)], and thus the design of the layers in the DBBN will be discussed later in the discussion section. The impacts of structural uncertainties due to the high level of variability in noise and other interferences, and high uncertainties associated with unclear boundary and operational conditions will be addressed in detail through the case study.

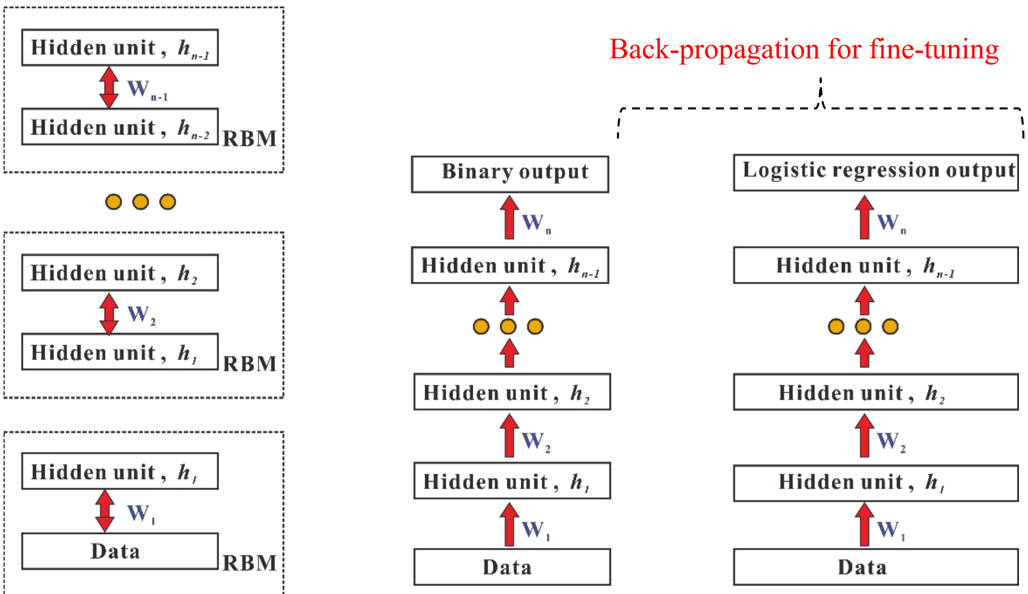

(a) Pre-training (b) fine-tuning for data classification (c) fine-tuning for probabilistically conditional assessment

Figure 7.4 Pre-training and fine-tuning of learning architecture of the DBBN

7.4 Case Study

7.4.1 Prototype Structures

A well-designed, three-story frame structure, illustrated Figure 7.5(a), was utilized as the case study for the method demonstration. Note that this was for demonstration and the ways that the uncertainty classification and reduction could be for bridges and other structures. The bolted structure had a dimension of 53.1 cm by 30.5 cm by 30.5 cm, and consisted of four columns and slab plates, as detailed in the literature (Figueiredo et al. 2009). One additional column was mounted at the top floor to form an adjustable gap with a bumper at the second floor, as seen zoomed in on, in Figure 7.5(b). During the structural vibration, the bumper and the column generated impact-induced waves to simulate the damage (e.g., crack opening and closing or loose bolt connection), while the different damage levels were achieved using different gap distances between the column and the bumper (see Figure 7.5(b)). An electro-dynamic shaker at the base excited the whole structure, while the dynamic response was recorded by four mounted accelerators, as labelled by sensors # 1 through 4 as shown in Figure 7.5(a).

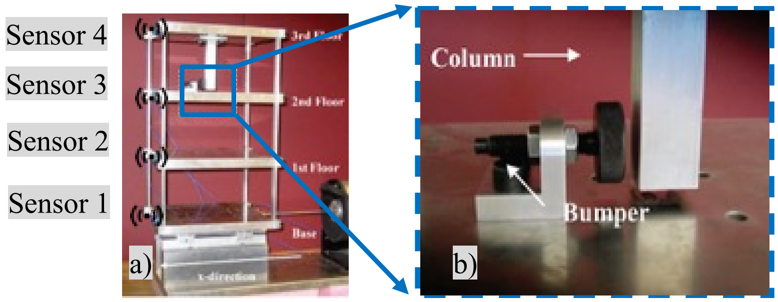

(a) Overview (b) Detailed bumper and column

Figure 7.5 Prototype structure (Pan et al. 2017; Figueiredo et al. 2009)

7.4.2 Design of Test Cases and Inclusion of Noise Interference

In the initial work by Figueiredo et al. (2009), 17 cases were designed to address data classification, in which each scenario included ten times identically repeated tests, and the four sensors recorded the response data. Based on this work, modification were made in this study to incorporate a total of 33 different scenarios, as listed in Table 7.1. As illustrated in Table 1, the scenarios were classified into five categories: a) Controlling case - the first undamaged state was the control test for the baseline; b) Variability and uncertainties associated with operational conditions - States # 2-9 were designed for mass or stiffness changes, which accounted for variability and uncertainties due to operational conditions, such as temperature impacts; c) Variability and uncertainties associated with operational conditions and noise interference - States # 10-17 were designed for mass or stiffness changes as well as different noise levels, which accounted for the interaction of operational conditions; c) Uncertainties associated with damages - States # 18-25 were designed for impact-induced damage, which accounted for uncertainties associated with damages; and d) Uncertainties associated with damages and inclusion of noise interference - States # 26-33 were designed for the inclusion of noise interference at different noise levels.

Response data from the sensors can easily be contaminated by noise (Prendergast et al. 2016; Pan et al. 2017), so noise was added to the collected signals based on the signal to noise ratio (SNR) that represented the ratio of the signal strength to the background noise strength as:

$$SNR_{dB} = 10\log_{10}\left(\frac{P_{\text{signal}}}{P_{\text{noise}}}\right) \tag{7-11}$$

where P_{signal} and P_{noise} are the average power of signal and noise by dB scale, respectively. Seven different noise levels - 5dB, 10dB, 15dB, 20dB, 30dB, 40dB, and 50dB - were selected to States # 10-17 and 26-33 so machine learning could check for the sensitivity of the uncertainty due to noise.

7.4.3 Performance of Data Classification and Structural Conditional Assessment

The 33 well-defined cases shown in Table 7.1 will be used to demonstrate the DBBN-based framework in Eqns. (7-6)-(7-9) for data classification (in Eqn. (10a)) and structural conditional assessment (in Eqn. (10b)). Note that rather than being in a binary state, the experimental sensory data in Table 7.1 will train the weights and biases using Eqn. (7-7c) with a Gaussian distribution. Data covering structural uncertainties, including operational conditions, damage noise, and other interferences defined in Table 7.1, will quantify the design of the learning architecture and layer.

Table 7.1 Test matrix of the case study (revised from Gui et al., 2017)

Case design	Label	State Condition	Description
	Undamaged states (# 1 to 17)		
Controlling	State#1	Undamaged	Baseline condition
Variability & uncertainties associated with operational conditions	State#2	Undamaged	Added mass (1.2 kg) at the base
	State#3	Undamaged	Added mass (1.2 kg) on the 1st floor
	State#4	Undamaged	States 4–9: 87.5% stiffness reduction at various positions to simulate temperature impact (more in detail by Figueiredo et al., 2009)
	State#5	Undamaged	
	State#6	Undamaged	
	State#7	Undamaged	
	State#8	Undamaged	
	State#9	Undamaged	
Variability & uncertainties associated with operational conditions + noise interference	State#10	Undamaged	Added mass (1.2 kg) at the base + noise level of 5dB~50dB
	State#11	Undamaged	Added mass (1.2 kg) on the 1st floor + noise level of 5dB~50dB
	State#12	Undamaged	States 4–9: 87.5% stiffness reduction at various positions to simulate temperature impact (more in detail by Figueiredo et al., 2009) + noise level of 5dB~50dB
	State#13	Undamaged	
	State#14	Undamaged	
	State#15	Undamaged	
	State#16	Undamaged	
	State#17	Undamaged	
	Damaged states (# 18 to 33)		
Uncertainties associated with damages	State#18	Damaged	Gap (0.20 mm)
	State#19	Damaged	Gap (0.15 mm)
	State#20	Damaged	Gap (0.13 mm)
	State#21	Damaged	Gap (0.10 mm)
	State#22	Damaged	Gap (0.05 mm)
	State#23	Damaged	Gap (0.20 mm) and mass (1.2 kg) at the base
	State#24	Damaged	Gap (0.20 mm) and mass (1.2 kg) on the 1st floor
	State#25	Damaged	Gap (0.10 mm) and mass (1.2 kg) on the 1st floor
Uncertainties associated with damages + noise interference	State#26	Damaged	Gap (0.20 mm) + noise level of 5dB~50dB
	State#27	Damaged	Gap (0.15 mm) + noise level of 5dB~50dB
	State#28	Damaged	Gap (0.13 mm) + noise level of 5dB~50dB
	State#29	Damaged	Gap (0.10 mm) + noise level of 5dB~50dB
	State#30	Damaged	Gap (0.05 mm) + noise level of 5dB~50dB
	State#31	Damaged	Gap (0.20 mm) and mass (1.2 kg) at the base + noise level of 5dB~50dB
	State#32	Damaged	Gap (0.20 mm) and mass (1.2 kg) at 1st floor + noise level of 5dB~50dB
	State#33	Damaged	Gap (0.10 mm) and mass (1.2 kg) at 1st floor + noise level of 5dB~50dB

7.5 Results and Discussion

7.5.1 Effectiveness of the DBBN for Structural Uncertainties due to Noise Interferences

Noise interferences commonly contaminate the sensory data from a structure, and thus lead to a high degree of variability for data analysis. To calibrate the influence of noise levels to the DBBN, we selected seven noise levels, with the values of the SNR from 5 to 50dB. The noise was added to the originally vibration data in States # 10-17 and 26-33, as listed in Table 7.1.

Further calibration of the effectiveness of the DBBN was carried out, and the results were plotted in Figure 7.6, where the results predicted by the SVM were also displayed for a comparison. Clearly, the noise has high adverse impacts on the effectiveness of both methods. The SVM has an error of 7.5%, which then increased to 31%, when the noise level increased from 5 to 50 dB. Although the DBBN exhibits higher effectiveness even with the noise, the classification errors with the DBBN still reach up to 18%, when the noise level increased to SNR=5dB.

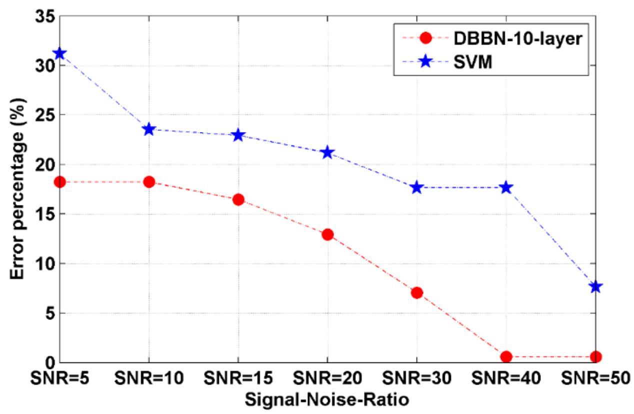

Figure 7.6 Classification errors of the DBBN and SVM under different noise levels (dB)

7.5.2 Structural Health Condition through Damage Level using the DBBN

The shallow learning is usually a binary algorithm, and the value of each data representation cannot fully account for the levels of the damage. In this section, the DBBN-based condition assessment using damage level was investigated. The damage levels were intentionally defined based on the gap in Figure 7.5(b), as listed in Table 7.2. For example, the severe impact-induced damage was associated with the small gap of 0.05 mm, and the damage level was defined as 50% of the full strength/capacity. In general, an attempt was made to demonstrate the concept. Note that such definition is certainly subjective, and actual damage severity should rely on the full analysis of the structure, using the finite element simulation to predict the remaining life or export recommendations as an indicator.

Table 7.2 Definition of damage severity level

Description	Physical and level definition				
Gap (mm) in Table 1	0.2	0.15	0.13	0.1	0.05
Damage severity	10%	20%	30%	40%	50%

A total number of 170 test samples were used for testing/predicting the accuracy of the trained model. The damage severity of the structure was predicted by the DBBN and then was compared to the real values as initial targets, as plotted in Figure 7.7, where the black solid lines are the origin data and the dashed lines are the values predicted by the DBBN. The comparison demonstrates that the DBBN is capable of predicting the structural condition by detecting damage levels with a high accuracy, about 10% errors, even with the structures that had high uncertainties due to damages that were interacted with by operational and environmental effects. This prediction was based on the four-layer architecture in the DBBN, but higher accuracy could be achieved by using ten layers.

With further inclusion of noise interferences, the impacts of the noise on the effectiveness of the DBBN were also plotted in Figure 7.7 (in dashed lines with circle markers). Although there are certain scatter points in prediction, the DBBN still exhibited high accuracy of prediction, even under the high noise level.

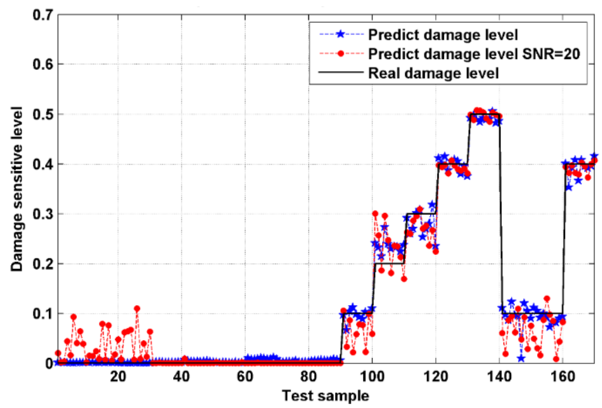

Figure 7.7 Comparison of results predicted by DBBN to the actual cases (four-layer learning)

7.6 Summary

This chapter addressed the enhanced structural condition assessment using the deep learning for better decision making in in-depth/special/damage inspection for structures with uncertainties. The DBBN was used to extract statistical representations from vast amounts of structural data to probabilistically determining structural condition and health state for decision making, with specific conclusions as shown below:

a) When compared to the conventional shallow learning SVM, the DBBN, one of the deep learning methods, is more capable of accurately capturing structural information;
b) The DBBN can achieve high accuracy in structural diagnostics, but it can be further improved by tailoring the layers and their architecture to account for the higher-order and highly non-linear statistical structural information, as experienced by a complex structure under high uncertainties and variability of interest;
c) It should be noted that the noise interference could contaminate the data representation, and in turn, increase the risk of the data mining, although the deep learning can reduce the impacts as compared to conventional shallow learning techniques.

8. CONCLUSIONS AND FUTURE WORK

8.1 Conclusions

Bridge inspection data is an essential part of the entire bridge asset management operation and the bridge management system. As such, a reliability-based holistic framework was proposed to effectively collect reliable data and perform data fusion and information fusion of sensory data used for element-level inspection and conditional assessment.

Timely information of bridge conditions obtained during the inspections will be used for determining needed maintenance and repairs, for prioritizing rehabilitations and replacements, for allocating resources, and for evaluating and improving the design for new bridges. The accuracy and consistency of the inspection, documentation, and levels of element conditions are vital because it not only impacts bridge funding appropriations, but also affects public safety.

8.1.1 Critical Factors Affecting Visual Inspection in Routine Inspection

A comprehensive literature review was conducted to better understand the current state of the research and practices in bridge element inspection. The current state of knowledge about the quality of bridge element inspection data and the consistency of bridge element inspection led to identifying the critical factors affecting the visual inspection in routine inspections, including structural importance factor, material vulnerability, aging effects, and others. The study confirmed that different condition ratings should be considered that will integrate these critical factors into the element-level inspection, which will provide more reliable data for bridge condition assessment, while more practices and datasets could further quantify their weight in the determination of future work.

8.1.2 Enhancement of Reliable Field Data Collection for Visual Inspection in Routine Inspection

Visual inspection is often dominant in routine inspection, yet it still faces challenges due to weather, environmental, and location conditions. The UAV has been identified as an emerging technology for bridge inspection that will allow for the collection of reliable, real time data, while minimizing subjective judgement, and allowing access to previously inaccessible locations, where traditional manual visual inspection could be limited.

8.1.3 Enhancement of Data Fusion and Information Process in In-Depth/Special/Damage Inspection

Effective data fusion and information process are crucial for in-depth/special/damage inspections. This study explored the new data fusion methods based on three representative feature extraction techniques used to enhance the features extraction for sensor data, while the kernel function based SVM was used to facilitate pattern recognition and improve identification. Results confirmed that these data-driven techniques exhibited high accuracy for distinguishing between undamaged and damaged cases, even when there are certain noise interferences as well as operational conditions. Moreover, the data-driven classification methods in this study could effectively address the major factors of interest, including the effects of damage level, damage location, sensor location, and moving load. The results in the THT and HHT methods exhibit clear discrimination between each damaged state, even under operational and environmental variability. The damage indexes of the results under moving vehicle effects revealed that the classifiers still have perform highly in the identification of damaged and undamaged cases, even under the noise level of 20 dB.

8.1.4 Unveiling and Reduction of Structural Uncertainty in In-depth/Special/Damage Inspection

This chapter addressed the enhanced structural condition assessment using deep learning for better decision making in in-depth/special/damage inspection for structures with uncertainties. The DBBN was used to extract statistical representations from vast amounts of structural data. This data was then used to probabilistically determine structural condition and health state for decision making. The new DBBN achieved high accuracy in structural diagnostics and can be further improved by tailoring the layers and their architecture to account for higher-order and highly non-linear statistical structural information, as experienced by a complex structure under high uncertainties and variability of interest.

8.2 Future Work

This study attempted to provide a new, reliabilty-based holistic framework to address the challenges associated with the new, element-level inspection. Despite the efforts in this study and other researchers, there are still several challenge the element-level inspection is faced with:

- Incomplete data, qualification of inspectors, and other human-made measurement errors could present great challenges for data collection and data fusion.
- The mix of different data types and formats could also pose challenges for data fusion and particularly slow down information fusion in inspection and condition rating.
- There are high levels of variances experienced in data collection including uncertainty assocated with noise interferences, leading to difficulty in information extraction for element-level inspection and conditional assessment.

REFERENCES

AASHTO Manual for Bridge Element Inspection, 1st edition, 2013.

AASHTO. Guide for Commonly Recognized (CoRe) Structural Elements, 2002.

AASHTO, Pontis Release 3.2 Users Manual, American Association of State Highway and Transportation Officials, Washington, DC, 1997.

Abu Dabous S and Alkass S "A Stochastic Method for Condition Rating of Concrete Bridges". ASCE Conf. Proc, 2010.

Abu Dabous S and Alkass S "A multi-attribute ranking method for bridge management", *Journal of Engineering, Construction and Architectural Management* Volume 17(3), pp 282-291, 2010.

ATKINS, Review of Bridge Inspection Competence and Training, Report, No. PPRO 04/045/004, 2009

Atmaca, B., Yurdakul, M., and Ates, S. (2015). "Dynamic Behavior Of Cables Of Cable-Stayed Bridge Isolated with SCFP Placed Under Pylon." Advance in Structural Engineering and Mechanics, Incheon, August, pp. 25-29.

Atmaca, B., Yurdakul, M., and Ateş, Ş. (2014). "Nonlinear dynamic analysis of base isolated cable-stayed bridge under earthquake excitations." Soil Dynamics and Earthquake Engineering, Vol. 66, pp. 314-318.

Battista, R. C., Pfeil, M. S., and Carvalho, E. M. (2008). "Fatigue life estimates for a slender orthotropic steel deck." Journal of Constructional Steel Research, Vol. 64, pp. 134-143.

Bin, G. F., Gao, J. J., Li, X. J., and Dhillon, B. S. (2012). "Early fault diagnosis of rotating machinery based on wavelet packets—Empirical mode decomposition feature extraction and neural network." Mechanical Systems and Signal Processing, Vol. 27, pp. 696-711.

Bisgin, H., Kilinc, O. U., Ugur, A., Xu, X., and Tuzcu, V. (2011). "Diagnosis of long QT syndrome via support vector machines classification." Journal of Biomedical Science and Engineering, vol. Vol.04No.04, pp. 4. DOI:10.4236/jbise.2011.44036.

Bornn, L., Farrar, C. R., and Park, G. (2010). "Damage detection in initially nonlinear systems." International Journal of Engineering Science, Vol. 48, pp. 909-920.Bennett, K., A. Demiriz, (1999). "Semi-supervised support vector machines.", Advances in Neural Information Processing Systems 11 368–374. DOI:10.1016/j.neucom.2011.06.026.

Boldt, F. d. A., Rauber, T. W., and ao, F. M. V. (2013) "Feature Extraction and Selection for Automatic Fault Diagnosis of Rotating Machinery." http://www.lbd.dcc.ufmg.br/colecoes/eniac/2013/0011.pdf.

Bornn, L., Farrar, C. R., Park, G., and Farinholt, K. (2009). "Structural Health Monitoring With Autoregressive Support Vector Machines." Journal of Vibration and Acoustics, vol. 131, pp. 021004-021004. DOI:10.1115/1.3025827.

California State Bridge Inspection Manual, 2008.

Cha, Y.-J., and Buyukozturk, O. (2015). "Structural Damage Detection Using Model Strain Energy and Hybrid Multiobjective Optimization." Computer-Aided Civil and Infrastructure Engineering, vol. 30, pp. 347-358. DOI:10.1111/mice.1212.

Chaturvedi, Iti; Erik Cambria, Soujanya Poria, Rajiv Bajpai (2016) "Bayesian Deep Convolutional Belief Networks for Subjectivity Detection", 2016 IEEE 16th International Conference on Data Mining Workshops (ICDMW). DOI: 10.1109/ICDMW.2016.0134.

Chen, Genda Brandon P. Schafer, Zhibin Lin, Ying Huang, Oscar Suaznabar, Jerry Shen and Kornel

Kerenyi. "Maximum scour depth based on magnetic field change in smart rocks for foundation stability evaluation of bridges," *Structural Health Monitoring Journal*, accepted, 2014.

Cho, K., Raiko, T., and Ilin, A. (2013). "Gaussian-Bernoulli deep Boltzmann machine". *The 2013 International Joint Conference on Neural Networks (IJCNN),* DOI:10.1109/ijcnn.2013.6706831.

Chong, J. W., Kim, Y., and Chon, K. H. (2014). "Nonlinear multiclass support vector machine–based health monitoring system for buildings employing magnetorheological dampers." Journal of Intelligent Material Systems and Structures, vol. 25, pp. 1456-1468. DOI:10.1177/1045389x13507343.

Christian, I. (2009). "Contrastive Divergence Learning May Diverge When Training Restricted Boltzmann Machines". *Frontiers in Computational Neuroscience*, 3, DOI:10.3389/conf.neuro.10.2009.14.121.

City-data. 2019. "Bridges in Fargo, ND." Accessed on (add the date here). (http://www.city-data.com/bridges/bridges-Fargo-North-Dakota.html#FRGO03).

Deng Li and Yu Dong, (2014). "Deep learning: methods and applications". Foundations and Trends in Signal Processing, Vol. 7, pp. 197–387.

Dahl, G., Dong Yu, Li Deng, and Acero, A. (2012). "Context-Dependent Pre-Trained Deep Neural Networks for Large-Vocabulary Speech Recognition". *IEEE Transactions on Audio, Speech, and Language Processing*, 20(1), 30-42, DOI:10.1109/tasl.2011.2134090.

Dushyanth, N. D., Suma, M. N., and Latte, M. V. (2016). "Detection and localization of damage using empirical mode decomposition and multilevel support vector machine." Applied Physics A, vol. 122, pp. 1-9. DOI:10.1007/s00339-016-9753-z.

Fahim, A. A., Gallego, R., Bochud, N., and Rus, G. (2013). "Model-based damage reconstruction in composites from ultrasound transmission." Composites Part B: Engineering, vol. 45, pp. 50-62. DOI:http://dx.doi.org/10.1016/j.compositesb.2012.09.003.

Farrar, C. R., and Worden, K. (2007). "An introduction to structural health monitoring." Philosophical Transactions of the Royal Society of London A: Mathematical, Physical and Engineering Sciences, vol. 365, pp. 303-315. DOI:10.1098/rsta.2006.1928.

Farrar, C. R., and Worden, K. (2013). *Structural Health Monitoring: A Machine Learning Perspective*, John Wiley & Sons, Ltd., Chichester, UK.

Figueiredo, E., G.Park, J.Figueiras, C.Farrar, and K.Worden (2009). "Structural Health Monitoring Algorithm Comparisons Using Standard Data Sets." *Technical ReportLA-14393*.

Figueiredo, E., G. Park, C. R. Farrar, K. Worden, and J. Figueiras.(2011). "Machine learning algorithms for damage detection under operational and environmental variability," Structural Health Monitoring, vol. 10, pp. 559-572. DOI:10.1177/1475921710388971.

Figueiredo, E., Figueiras, J., Park, G., Farrar, C. R., and Worden, K. (2011). "Influence of the Autoregressive Model Order on Damage Detection." Computer-Aided Civil and Infrastructure Engineering, vol. 26, pp. 225-238. DOI:10.1111/j.1467-8667.2010.00685.x.

Fischer, A. (2015). "Training Restricted Boltzmann Machines". *KI - Künstliche Intelligenz*, 29(4), 441-444, DOI:10.1007/s13218-015-0371-2.

Florida State Bridge Inspection Manual, 2013.

Furey, T. S., Cristianini, N., Duffy, N., Bednarski, D. W., Schummer, M., and Haussler, D. (2000). "Support vector machine classification and validation of cancer tissue samples using microarray expression data." Bioinformatics, vol. 16, pp. 906-914.

DOI:10.1093/bioinformatics/16.10.906

Ge, R., Pan, H., lin, Z., gong, N., and wang, J. (2016). "RF-Powered Battery-less Wireless Sensor Network." *The 5th International Symposium on Next-Generation Electronics* Hsinchu, Taiwan, 32-33.

Gui, G., Pan, H., Zhibin Lin, Li, Y. and Yuan, Z. (2017). "Data-driven support vector machine with optimization techniques for structural health monitoring and damage detection." KSCE Journal of Civil Engineering, 21(2), 523–534.5.

Gersch, W. (1970). "Estimation of the autoregressive parameters of a mixed autoregressive moving-average time series." IEEE Transactions on Automatic Control, vol. 15, pp. 583-588. DOI:10.1109/TAC.1970.1099560.

Ghiasi, R., Torkzadeh, P., and Noori, M. (2016). "A machine-learning approach for structural damage detection using least square support vector machine based on a new combinational kernel function." Structural Health Monitoring, vol., pp. DOI:10.1177/1475921716639587.

Herrasti, Z., Val, I., Gabilondo, I., Berganzo, J., Arriola, A., and Martínez, F. (2016). "Wireless sensor nodes for generic signal conditioning: Application to Structural Health Monitoring of wind turbines." Sensors and Actuators A: Physical, vol.237, pp. 604-613. DOI: http://dx.doi.org/10.1016/j.sna.2016.06.027.

Hinton, G., Deng, L., Yu, D., Dahl, G., Mohamed, A., Jaitly, N., Senior, A., Vanhoucke, V., Nguyen, P., Sainath, T., and Kingsbury, B. (2012). "Deep Neural Networks for Acoustic Modeling in Speech Recognition: The Shared Views of Four Research Groups". *IEEE Signal Processing Magazine*, 29(6), 82-97, DOI:10.1109/msp.2012.2205597.

Hinton, G., Osindero, S., and Teh, Y. (2006). "A Fast Learning Algorithm for Deep Belief Nets". *Neural Computation*, 18(7), 1527-1554, DOI:10.1162/neco.2006.18.7.1527.

Hinton, G.E., (2010). "A Practical Guide to Training Restricted Boltzmann Machines" (Accessed 12 October 2015) Available at: http://www.cs.toronto.edu/~hinton/absps/guideTR.pdf.

Hofmann, Martin (2006) "Support vector machines-Kernels and the kernel trick", from http://www.cogsys.wiai.uni-bamberg.de/teaching/ss06/hs_svm/slides/SVM_Seminarbericht_Hofmann.pdf.

Holland, J., and ARbor, A. (1975). *Adaptation in natural and artificial systems*, MIT press, Cambrige.

Hou, Z., Noori, M., and Amand, R. S. (2000). "Wavelet-Based Approach for Structural Damage Detection." Journal of Engineering Mechanics, vol. 126, pp. 677-683. DOI: 10.1061/(ASCE)0733-9399(2000)126:7(677).

Hsu, C.-W., Chang, C.-C., and Lin, C.-J. (2010). "A Practical Guide to Support Vector Classification." http://www.csie.ntu.edu.tw/~cjlin/papers/guide/guide.pdf.

Huang, C.-L., and Dun, J.-F. (2008). "A distributed PSO–SVM hybrid system with feature selection and parameter optimization." Applied Soft Computing, vol. 8, pp. 1381-1391. DOI:http://dx.doi.org/10.1016/j.asoc.2007.10.007.

Huang, Q., Tang, B., and Deng, L. (2015). "Development of high synchronous acquisition accuracy wireless sensor network for machine vibration monitoring." Measurement, vol. 66, pp. 35-44. DOI:http://dx.doi.org/10.1016/j.measurement.2015.01.021.

Jiang, M., Liang, Y., Feng, X., Fan, X., Pei, Z., Xue, Y., and Guan, R. (2016). "Text classification based on deep belief network and softmax regression". *Neural Computing and Applications,* DOI:10.1007/s00521-016-2401-x.

Junsheng, C., Dejie, Y., and Yu, Y. (2007). "The application of energy operator demodulation approach based on EMD in machinery fault diagnosis." Mechanical Systems and Signal Processing, Vol. 21, pp. 668-677.

Kaveh, A., Bakhshpoori, T., and Azimi, M. (2015). "Seismic optimal design of 3D steel frames using cuckoo search algorithm." The Structural Design of Tall and Special Buildings, vol. 24, pp. 210-227. DOI:10.1002/tal.1162.

Kennedy, J., and Eberhart, R. C. (1995). "Particle swarm optimization." *In Proceedings of the IEEE international conference on neural networks IV*, IEEE, Piscataway, 1942–1948.

Kim, L. (2017). "DeepX: Deep Learning Accelerator for Restricted Boltzmann Machine Artificial Neural Networks". *IEEE Transactions on Neural Networks and Learning Systems*, 1-13, DOI:10.1109/tnnls.2017.2665555.

Kiwaki, T., and Aihara, K. (2015). "An effect of initial distribution covariance for annealing Gaussian restricted Boltzmann machines". *Artificial Intelligence Research*, 4(1), DOI:10.5430/air.v4n1p53.

Ko, J. M., and Ni, Y. Q. (2005). "Technology developments in structural health monitoring of large-scale bridges." Engineering Structures, Vol. 27, pp. 1715-1725.

Kopsaftopoulos, F. P., and Fassois, S. D. (2013). "A functional model based statistical time series method for vibration based damage detection, localization, and magnitude estimation." Mechanical Systems and Signal Processing, Vol. 39, pp. 143-161.

Larochelle, H.; Bengio, Y. (2008) "Classification using discriminative restricted Boltzmann machines". I*n Proceedings of the 25th International Conference on Machine Learning,* Helsinki, Finland, pp. 536–543.

Li, H., and Zhang, Y. "An algorithm of soft fault diagnosis for analog circuit based on the optimized SVM by GA." *Proc., Electronic Measurement & Instruments, 2009. ICEMI '09. 9th International Conference on*,pp. 4-1023-1024-1027. DOI:10.1109/ICEMI.2009.5274151.

Lin, P., Fu, S., Wang, S., Lai, Y., and Tsao, Y. (2016). "Maximum Entropy Learning with Deep Belief Networks." *Entropy, M*DPI, 18, 251. DOI:10.3390/e18070251.

Lin, Z., Fakhairfar, M., Wu, C., and Chen, G. (2013). "Design, Construction and Load Testing of the Pat Daly Road Bridge in Washington County, MO, with Internal Glass Fiber Reinforced Polymers Reinforcement, Washington County, Missouri." *Final Report NUTC R275*, Washington County Commission and US Department of Transportation.

Lin, Z., Fakharifar, M., Huang, Y., Chen, G., and Wang, Z. (2014). "Damage Detection of a Full-Size Concrete Box Girder Bridge with the Moving-Window Least-Square Fitting Method." *NDE/NDT for Structural Materials Technology for Highway & Bridges*.

Lin, Z., Zhao, J., and Habib, T. (2012). "Impact of Overweight Vehicles (with Heavy Axle Loads) on Bridge Deck Deterioration." *Final Report CFIRE 04-06*, USDOT's RITA by CFIRE and UW-Milwaukee, Wisconsin, http://www.wistrans.org/cfire/documents/FR_0406.pdf.

Liu, C., Harley, J. B., Bergés, M., Greve, D. W., and Oppenheim, I. J. (2015). "Robust ultrasonic damage detection under complex environmental conditions using singular value decomposition." Ultrasonics, vol. 58, pp. 75-86. DOI:http://dx.doi.org/10.1016/j.ultras.2014.12.005.

Magalhães, F., Cunha, A., and Caetano, E. (2012). "Vibration based structural health monitoring of an arch bridge: From automated OMA to damage detection." Mechanical Systems and Signal Processing, vol. 28, pp. 212-228. DOI:http://dx.doi.org/10.1016/j.ymssp.2011.06.011.

Maljaars, J., van Dooren, F., and Kolstein, H. (2012). "Fatigue assessment for deck plates in orthotropic bridge decks." Steel Construction, Vol. 5, pp. 93-100.

Mandic, D. P., Rehman, N. u., Wu, Z., and Huang, N. E. (2013). "Empirical Mode Decomposition-Based Time-Frequency Analysis of Multivariate Signals: The Power of Adaptive Data Analysis." IEEE Signal Processing Magazine, Vol. 30, pp. 74-86.

Masciotta, M. G., Ramos, L. F., Lourenço, P. B., and Vasta, M. (2014). "Damage detection on the Z24 bridge by a spectral-based dynamic identification technique." Dynamics of Civil Structures, Volume 4, Springer, 197-206.

Masri, S. F., Smyth, A. W., Chassiakos, A. G., Caughey, T. K., and Hunter, N. F. (2000). "Application of Neural Networks for Detection of Changes in Nonlinear Systems." Journal of Engineering Mechanics, vol. 126, pp. 666-676. DOI: 10.1061/(ASCE)0733-9399(2000)126:7(666).

Melgani, F., and Bazi, Y. (2008). "Classification of Electrocardiogram Signals With Support Vector Machines and Particle Swarm Optimization." IEEE Transactions on Information Technology in Biomedicine, vol. 12, pp. 667-677. DOI:10.1109/TITB.2008.923147.

Memorandum of the FHWA initiatives from http://www.fhwa.dot.gov/bridge/nbi/120416.cfm, 2013

Melhem H. G and Aturaliya S. "Bridge Condition Rating Using an Eigenvector of Priority Settings." *Computer-Aided Civil and Infrastructure Engineering* 11(6): 421-432, 1996.

Minnesota State Bridge Inspection Manual, 2013.

Mohamed, A., Dahl, G., and Hinton, G. (2012). "Acoustic Modeling Using Deep Belief Networks". *IEEE Transactions on Audio, Speech, and Language Processing*, 20(1), 14-22, doi:10.1109/tasl.2011.2109382.

Neerukatti, R. K., Hensberry, K., Kovvali, N., and Chattopadhyay, A. (2016). "A novel probabilistic approach for damage localization and prognosis including temperature compensation." Journal of Intelligent Material Systems and Structures, vol. 27, pp. 592-607. DOI:10.1177/1045389x15575084.

North Dakota State Bridge Inspection Manual, 2012.

Ohio State Bridge Inspection Manual, 2014.

Oh, C. K., and Sohn, H. (2009). "Damage diagnosis under environmental and operational variations using unsupervised support vector machine." Journal of Sound and Vibration, vol. 325, pp. 224-239. DOI:http://dx.doi.org/10.1016/j.jsv.2009.03.014.

Oshiro N., Ishio M., Okubo M., and Tamakoshi T., "Element level inspection results and accuracy of probabilistic structural condition forecasting for highway bridges", 28th US-Japan Bridge Engineering Workshop, 2012.

Pan, H., Ge, R., Wang, J., Gong, N. and Zhibin Lin (2016). "Integrated Wireless Sensor Networks with UAS for Damage Detection and Monitoring of Bridges and Other Large-Scale Critical Civil Infrastructures." NDE/NDT for Highway and Bridges: Structural Materials Technology Portland, OR, USA.

Pan, H., Azimi, M., Gui, G., Yan, F., and Zhibin Lin (2017). "Vibration-based support vector machine for structural health monitoring." 7th International Conference on Experimental Vibration Analysis for Civil Engineering Structures, San Diego, CA, USA.

Pan, H., Azimi, M., Yan, F., and Zhibin Lin (2018) "Time-Frequency Based Data-Driven Structural Diagnosis and Damage Detection for Cable-Stayed Bridges." ASCE Journal of Bridge Engineering, accepted.

Pan, H. , Zhibin Lin, and Gui, G. (2018) "Enabling Damage Identification of Structures using Time-Series Based Feature Extraction Algorithms." *ASCE Journal of Aerospace Engineering*, accepted.

Pan, H. [+], Yan, C. and Zhibin Lin. (2018) "Data-Driven Structural Diagnosis and Conditional Assessment: From Shallow to Deep Learning." *SPIE Smart Structures + Nondestructive Evaluation,* Denver, Colorado, USA.

Pan, H. [+], Gui, G., Zhibin Lin, and Yan, C. (2018) "Deep BBN Learning for Health Assessment toward Decision-Making on Structures under Uncertainties." *KSCE Journal of Civil Engineering*, In press.

Pavlopoulou, S., Worden, K., and Soutis, C. (2016). "Novelty detection and dimension reduction via guided ultrasonic waves: Damage monitoring of scarf repairs in composite laminates." Journal of Intelligent Material Systems and Structures, vol. 27, pp. 549-566. DOI:10.1177/1045389x15574937.

Rashedi, R., and Hegazy, T. (2015). "Capital renewal optimisation for large-scale infrastructure networks: genetic algorithms versus advanced mathematical tools." Structure and Infrastructure Engineering, Vol. 11, pp. 253-262.

Rashidi, M. & Gibson, P. A methodology for bridge condition evaluation. Journal of Civil Engineering and Architecture, 6 (9), 1149-1157, 2012.

Rashidi M and Lemass B "Holistic decision support for bridge remediation". *The 4 International Conference on Construction Engineering and Project Management"ICCEPM, S2-4,* 2011.

Santos, A. E. Figueiredo, M. F. M. Silva, C. S. Sales, and J. C. W. A. Costa. (2016). "Machine learning algorithms for damage detection: Kernel-based approaches," Journal of Sound and Vibration, vol. 363, pp. 584-599. DOI:http://dx.doi.org/10.1016/j.jsv.2015.11.008.

Sarikaya, R., Hinton, G., and Deoras, A. (2014). "Application of Deep Belief Networks for Natural Language Understanding". *IEEE/ACM Transactions on Audio, Speech, and Language Processing*, 22(4), 778-784, DOI:10.1109/taslp.2014.2303296.

Saaty, T. L "The Analytic Hierarchy Process". New York: McGraw-Hill, 1980.

Seyedpoor, S. M. (2012). "A two stage method for structural damage detection using a model strain energy based index and particle swarm optimization." International Journal of Non-Linear Mechanics, vol. 47, pp. 1-8. DOI:http://dx.doi.org/10.1016/j.ijnonlinmec.2011.07.011.

Shawe-Taylor, John., Shiliang Sun, (2011) A review of optimization methodologies in support vector machines, In Neurocomputing, Volume 74, Issue 17, , pp. 3609-3618, DOI: https://doi.org/10.1016/j.neucom.2011.06.026.

Sharma, A., Amarnath, M., and Kankar, P. (2016). "Feature extraction and fault severity classification in ball bearings." Journal of Vibration and Control, vol. 22, pp. 176-192. DOI:10.1177/1077546314528021.

Silva, M., Santos, A., Figueiredo, E., Santos, R., Sales, C., and Costa, J. C. W. A. (2016). "A novel unsupervised approach based on a genetic algorithm for structural damage detection in bridges." Engineering Applications of Artificial Intelligence, Vol. 52, pp. 168-180.

Sohn, H., Farrar, C. R., Hunter, N. F., and Worden, K. (2001). "Structural Health Monitoring Using Statistical Pattern Recognition Techniques." Journal of Dynamic Systems, Measurement, and Control, vol. 123, pp. 706-711. DOI:10.1115/1.1410933.

South Dakota State Bridge Inspection Manual, 2008.

Suykens, J. A. K., and Vandewalle, J. (1999). "Least Squares Support Vector Machine Classifiers." Neural Processing Letters, vol. 9, pp. 293-300. DOI:10.1023/a:1018628609742.

Tee. A.B , Browman M. D. and Sinha K.C "A fuzzy mathematical approach for bridge condition evaluation" *Journal: Civil engineering systems*, Vol.2, 1988.

Texas State Bridge Inspection Manual, 2012.

Tibaduiza, D. A., Mujica, L. E., Rodellar, J., and Güemes, A. (2015). "Structural damage detection using principal component analysis and damage indices." Journal of Intelligent Material Systems and Structures, vol., 10.1177/1045389x14566520pp. DOI:10.1177/1045389x14566520.

Thompson, P.D., T. Merlo, B. Kerr, A. Cheetham, and R. Ellis, The New Ontario Bridge Management System, in preprints of the 8th International Bridge Management Conference, Denver, available from the Transportation Research Board, 1999.

Thompson, P., Shepard R., AASHTO Commonly-Recognized Bridge Elements-Successful Applications and Lessons Learned, National Workshop on Commonly Recognized Measures for Maintenance, 2000.

Valenzuela et.,al "Proposal of an integrated index for prioritisation of bridge maintenance", Journal of Bridge Engineering, Volume 15, Issue 3, 2010.

Vesely, K., A. Ghoshal, L. Burget, and D. Povey.(2013) Sequence-discriminative training of deep neural networks. In *Proceedings of Interspeech*.

Wang, H., Wang, G., Li, G., Peng, J., and Liu, Y. (2016). "Deep belief network based deterministic and probabilistic wind speed forecasting approach". *Applied Energy*, 182, 80-93. doi:10.1016/j.apenergy.2016.08.108.

Watters, D. G., Jayaweera, P., Bahr, A. J., and Huestis, D. L. "Design and performance of wireless sensors for structural health monitoring." Proc., Review of Progress in Quantitative Nondestructive Evaluation, 29 July-3 Aug. 2001, AIP,pp. 969-976. DOI:10.1063/1.1472901.

Widodo, A., and Yang, B.-S. (2007). "Application of nonlinear feature extraction and support vector machines for fault diagnosis of induction motors." Expert Systems with Applications, vol. 33, pp. 241-250. DOI:http://dx.doi.org/10.1016/j.eswa.2006.04.020.

Worden, K., and Dulieu-Barton, J. M. (2004). "An Overview of Intelligent Fault Detection in Systems and Structures." Structural Health Monitoring, vol. 3, pp. 85-98. DOI:10.1177/1475921704041866.

Worden, K., Farrar, C. R., Manson, G., and Park, G. (2007). "The fundamental axioms of structural health monitoring." Proceedings of the Royal Society A: Mathematical, Physical and Engineering Science, vol. 463, pp. 1639-1664. DOI:10.1098/rspa.2007.1834.

Worden, K., and Lane, A. J. (2001). "Damage identification using support vector machines." Smart Materials and Structures, vol. 10, pp. 540, DOI:http://stacks.iop.org/0964-1726/10/i=3/a=317.

Xia, Y., Nassif, H., Hwang, E.-S., and Linzell, D. (2013). "Optimization of design details in orthotropic steel decks subjected to static and fatigue loads." Transportation Research Record: Journal of the Transportation Research Board, pp. 14-23.

Yan, F., and Lin, Z. (2016). "New strategy for anchorage reliability assessment of GFRP bars to concrete using hybrid artificial neural network with genetic algorithm." Composites Part B: Engineering, vol. 92, pp. 420-433. DOI:http://dx.doi.org/10.1016/j.compositesb.2016.02.008.

Yan, F., Lin, Z., Wang X., Azarmi F., and Sobolev, K. (2016). "Evaluation and prediction of bond strength of GFRP-bar reinforced concrete using artificial neural network optimized with genetic algorithm." Composite Structures, In press. DOI: http://dx.doi.org/10.1016/j.compstruct.2016.11.068.

Yao, R., and Pakzad, S. N. (2012). "Autoregressive statistical pattern recognition algorithms for damage detection in civil structures." Mechanical Systems and Signal Processing, vol. 31, pp. 355-368. DOI:http://dx.doi.org/10.1016/j.ymssp.2012.02.014.

Yeesock, K., Jo Woon, C., Ki, H. C., and JungMi, K. (2013). "Wavelet-based AR–SVM for health monitoring of smart structures." Smart Materials and Structures, vol. 22, pp. 015003. DOI:http://stacks.iop.org/0964-1726/22/i=1/a=015003.

Ying, Y., Jr., J. H. G., Oppenheim, I. J., Soibelman, L., Harley, J. B., Shi, J., and Jin, Y. (2013). "Toward Data-Driven Structural Health Monitoring: Application of Machine Learning and Signal Processing to Damage Detection." Journal of Computing in Civil Engineering, vol. 27, pp. 667-680. DOI: 10.1061/(ASCE)CP.1943-5487.0000258.

Yu, D., Cheng, J., and Yang, Y. (2005). "Application of EMD method and Hilbert spectrum to the fault diagnosis of roller bearings." Mechanical Systems and Signal Processing, Vol. 19, pp. 259-270.

Zang, C., and Imregun, M. (2001). "STRUCTURAL DAMAGE DETECTION USING ARTIFICIAL NEURAL NETWORKS AND MEASURED FRF DATA REDUCED VIA PRINCIPAL COMPONENT PROJECTION." Journal of Sound and Vibration, vol. 242, pp. 813-827. DOI:http://dx.doi.org/10.1006/jsvi.2000.3390.

Zeiler, M.(2014) Hierarchical convolutional deep learning in computer vision. Ph.D. Thesis, New York University.

Zhao, Rui; Ruqiang Yan, Zhenghua Chen, Kezhi Mao, Peng Wang, and Robert X. Gao, "Deep Learning and Its Applications to Machine Health Monitoring: A Survey", JOURNAL OF LATEX CLASS FILES, VOL. 14, NO. 8, AUGUST 2015.

Zou, Y., Tong, L., and Steven, G. P. (2000). "VIBRATION-BASED MODEL-DEPENDENT DAMAGE (DELAMINATION) IDENTIFICATION AND HEALTH MONITORING FOR COMPOSITE STRUCTURES — A REVIEW." Journal of Sound and Vibration, vol. 230, pp. 357-378. DOI:http://dx.doi.org/10.1006/jsvi.1999.2624.